

---

Electronic Thesis and Dissertation Repository

---

7-25-2022 10:00 AM

# Oxygen Speciation in Potassium Silicate and Potassium Aluminosilicate Glasses: Insights From X-Ray Photoelectron Spectroscopy

Ryan Sawyer, *The University of Western Ontario*

Supervisor: Nesbitt, H. Wayne, *The University of Western Ontario*

Co-Supervisor: Secco, Richard A., *The University of Western Ontario*

A thesis submitted in partial fulfillment of the requirements for the Doctor of Philosophy degree in Geophysics

© Ryan Sawyer 2022

Follow this and additional works at: <https://ir.lib.uwo.ca/etd>

 Part of the [Geochemistry Commons](#), [Materials Chemistry Commons](#), and the [Other Earth Sciences Commons](#)

---

## Recommended Citation

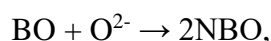
Sawyer, Ryan, "Oxygen Speciation in Potassium Silicate and Potassium Aluminosilicate Glasses: Insights From X-Ray Photoelectron Spectroscopy" (2022). *Electronic Thesis and Dissertation Repository*. 8821. <https://ir.lib.uwo.ca/etd/8821>

This Dissertation/Thesis is brought to you for free and open access by Scholarship@Western. It has been accepted for inclusion in Electronic Thesis and Dissertation Repository by an authorized administrator of Scholarship@Western. For more information, please contact [wlsadmin@uwo.ca](mailto:wlsadmin@uwo.ca).

## Abstract

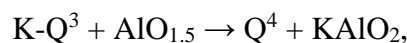
In a geological context, glasses are useful analogues for silicate melts as they are more readily studied in the laboratory using a wide range of techniques that are impractical for molten liquids. Understanding the structure of binary silicate glasses can help us understand more about the magmatic processes that affect terrestrial planetary bodies.

Potassium silicate glasses ranging in composition from 10 mol% to 35 mol% K<sub>2</sub>O were studied using X-ray Photoelectron Spectroscopy (XPS). From high resolution O 1s XPS spectra, Bridging Oxygen (BO) mole fractions were calculated and compared with those of previous <sup>29</sup>Si MAS NMR studies. From 25-35 mol% K<sub>2</sub>O, XPS BO mole fractions were higher resulting in a discrepancy. Thermodynamic analysis indicated the presence of a few mol% of Free Oxygen (O<sup>2-</sup>) in these glasses, which challenges the longstanding assumption that the reaction



goes to completion where NBO is Non-Bridging Oxygen. The uncertainties involving the synthesis of glass samples and the fitting of the XPS spectra were addressed. An attempt was made to resolve the discrepancy with the NMR results by examining the NMR data and reconsidering the assignment of Q-species. The amount of O<sup>2-</sup> in potassium silicate glasses was found to sufficient to affect reactions with CO<sub>2</sub> and other volatile species which suggests that it is more reactive than Non-Bridging Oxygen.

XPS was then used to study oxygen speciation in glasses with 31 mol% K<sub>2</sub>O and 0, 1 and 3 mol% Al<sub>2</sub>O<sub>3</sub>. NBO decreased while BO increased in two contributions representing Q<sup>4</sup> and KAlO<sub>2</sub>. Aluminum was found to dissolve according to the reaction:



At high temperatures the dissociation of Si-O-K moieties results in a process whereby NBO are converted to BO through nucleophilic attack of Si-NBO<sup>-</sup> melt species on surface Al<sub>2</sub>O<sub>3</sub> sites. The conversion of NBO to BO results in a more stable melt. Without the stability that aluminum provides in melts, the composition of the upper mantle and crust and the subsequent evolution of the crust would have been different from what we observe today.

KEYWORDS: Glass, Potassium Silicate Glass, X-ray Photoelectron Spectroscopy, XPS, Alkali Silicate Glass, Alkali Aluminosilicate Glass, Potassium Aluminosilicate Glass, Free Oxygen, Q-Species, Bridging Oxygen, Non-Bridging Oxygen, BO, NBO,  $O^{2-}$ .

## Summary For Lay Audience

Glass is a material that has been used for millennia for a variety of artistic, industrial and scientific purposes. The structure of a glass is essentially a snapshot of the melt structure at the point when it becomes a glass. In the Earth and Planetary Sciences, glasses provide useful analogues for natural melts. Glasses can be studied at room temperature using a wide variety of techniques unavailable to melts which require high temperatures. Glasses with simple compositions provide a basis for modeling the properties and behaviour of melts with more complex compositions.

In this work, X-ray Photoelectron Spectroscopy is used to quantify abundances of BO (e.g., Si-O-Si) and NBO (e.g., Si-O-K) atoms in potassium silicate glasses containing 10-35 mol% K<sub>2</sub>O. XPS results indicate an overabundance of BO atoms if the glasses are assumed to only contain BO and NBO and no O<sup>2-</sup>. Thermodynamic modeling reveals indirect evidence for O<sup>2-</sup> (e.g., K-O-K) being present at levels of several mol%. A discrepancy is found between the XPS results and results from previous Nuclear Magnetic Resonance (NMR) studies. An attempt is made to resolve this discrepancy by carefully considering uncertainties related to XPS analysis and sample preparation and offering a more complete interpretation of the NMR results. It is then shown that there is sufficient O<sup>2-</sup> in these glasses to react with CO<sub>2</sub> and other volatile species, suggesting that it is the reactive species in these glasses and not NBO as is commonly assumed.

Small amounts of Al<sub>2</sub>O<sub>3</sub> (1 and 3 mol%) are added to a glass containing 31 mol% K<sub>2</sub>O to study the dissolution of Al<sub>2</sub>O<sub>3</sub>. NBO is found to decrease, and BO is found to increase in two contributions with an increase in Al. From these results, the chemical reactions that are dominant at the start of dissolution are proposed where Si-NBO<sup>-</sup> melt species attack solid Al<sub>2</sub>O<sub>3</sub> species to produce more BO atoms. The overall result is an increase in melt stability without which the evolution of the crust and mantle may have been much different.

## Co-Authorship Statement

At the core of the scientific process is collaboration. Such is true of this work which is presented in the integrated article format. This thesis is comprised of three papers, two of which are published and one of which is an early draft of a paper that was published only recently. The publication details are given below.

1. Sawyer, R., Nesbitt, H.W. and Secco, R.A., 2012. High resolution X-ray Photoelectron Spectroscopy (XPS) study of K<sub>2</sub>O–SiO<sub>2</sub> glasses: Evidence for three types of O and at least two types of Si. *Journal of Non-Crystalline Solids*, 358(2), pp.290-302. doi:10.1016/j.jnoncrysol.2011.09.027
2. Sawyer, R., Nesbitt, H.W., Bancroft, G.M., Thibault, Y. and Secco, R.A., 2015. Spectroscopic studies of oxygen speciation in potassium silicate glasses and melts. *Canadian Journal of Chemistry*, 93(1), pp.60-73. doi: 10.1139/cjc-2014-0248
3. Sawyer, R., Nesbitt, H.W., Bancroft, G.M., Secco, R.A. and Henderson, G.S., 2022. Congruent dissolution of Al<sub>2</sub>O<sub>3</sub> in a K-disilicate melt, with constraints on the reaction mechanism. *Journal of Non-Crystalline Solids*, 586, p.121565. doi: 10.1016/j.jnoncrysol.2022.121565

In the case of the first paper (Chapter 2), the majority was written by me with editorial contributions by H.W. Nesbitt and R.A. Secco. Chapter 3 in its published form was written largely by H.W. Nesbitt with contributions from myself, G.M. Bancroft, Y. Thibault and R.A. Secco. This was due to time constraints and severe health issues I was experiencing that affected my ability to work and function. As such, that paper has been re-written in my own style so I can claim it in this thesis as a product largely of my own experimental work and interpretation of results. Chapter 4 was written by me with contributions from H.W. Nesbitt, G.M. Bancroft and R.A. Secco and is included here rather than the published manuscript because we were unsure of how long it would take to get published and what changes might have needed to be made. I can also say that the majority of Chapter 4 as it appears here was composed by me.

The preparation of samples was done entirely by me. Collection of XPS spectra was done by me under the supervision of M. Biesinger (Surface Science Western). Spectral fitting was done by me and aided by discussion with H.W. Nesbitt. Data analysis and interpretation were done by me

with helpful contributions from H.W. Nesbitt, G.M. Bancroft, G.S. Henderson, Y. Thibault and R.A. Secco. The EPMA data, analysis and interpretation in Chapter 3 was done by Y. Thibault at Natural Resources Canada.

When the totality of this work is considered, I can state with confidence that it is a work done largely by me aided by contributions from those listed above, but without the work I have done, this thesis and the papers it is composed of would not exist.

## Acknowledgements

If anything can be said about this experience and the concept of a PhD in general, it's that such an undertaking is a test of perseverance and at times a struggle against the odds as much as it is about the work you are doing. I experienced the greatest triumphs and hit the lowest low of my life throughout this project. But I persisted and never gave up. I overcame a lot and emerged stronger. I could not have done this alone. None of this could have been accomplished without the support and guidance of many people through the years.

I owe a great debt of gratitude to my supervisors, Dr. H.W. Nesbitt and Dr. R.A. Secco. Their support of me throughout the years means more to me than words can express. They exhibited a great deal of patience, understanding and empathy for me and I do not think I could have had better mentors. They taught me the importance of careful experimental preparation and rigorous analysis and rekindled my interest in chemistry that had long laid dormant. They never gave up on me and always believed in me, and that helped give me the confidence to succeed during the toughest times. To both of you, I say thank you! I could not have done this without your guidance, teaching and support!

My collaborators G.M. Bancroft, G.S. Henderson and Y. Thibault are also owed many thanks for their helpful discussions and the contributions they made. I am thankful for the help of R. Ho who taught me the glass preparation process and instructed me in conducting XPS analysis. I owe M. Biesinger my thanks for his help and supervision of the XPS analyses. He was always able to help me when I got stuck or encountered issues with the device and his expertise and patience in training me were invaluable.

Thank you to the people I shared lab space with over the years: Marie Burford, Innocent Ezenwa, Sean Funk, Soushyant Kiarasi. Josh Littleton, Tim Officer, Reynold Silber and Wenjun Yong. And thank you to Jon Jacobs in the machine shop. You are all great people and you made things more enjoyable with your thought-provoking discussions.

Over the years I have lived with several people, and they deserve thanks for putting up with me and being fantastic roommates. So, thank you to Amanda Obodovsky, Lise Babcock, Scott Davison, Laura Thomson, Matt Izawa and Mary Kerrigan. Thank you all for the good times and fun discussions about every imaginable topic.

Many people provided me with friendship and support over the years. In particular, I would like to thank Tim Officer, Matt Izawa, Anna Channou, Michael Craig, Paul Graham, Emily Anderson, Lise Babcock, Nicole Ramsay, Scott Davison, Greg and Amanda Obodovsky, Will O'Donnell, Nelson Cho, Laura Thomson, Liane Loiselle, Julia Thysman, Sean Funk, Anji Michalski, Will and Heather Evans and Jan and Jon Evans, Jane Hill, Alyssa Appel, Shiro Drake, Brittany Woodall, Victoria Richey, Dina Tuggle, Avied Rosado, and all the people I played soccer and baseball with over the years. There are many others whose names could fill a volume longer than this thesis and though they are not named here, their friendships and support are not forgotten.

None of this would have been possible without the love and support of my family. My mom Karen, my dad David, my sister Roxanne, my nephew Lucas and all my aunts, uncles and cousins supported me throughout and constantly asked me when I'd be done (my dad was the only one who didn't). My dad passed away in 2018 and I am sad that he could not see me finish this project. Our long discussions about music, science, politics, history, literature and film are missed. It is to his memory that I dedicate this thesis, as he was a constant source of encouragement, love, support and inspiration throughout my life. I would also like to thank my partner Shi'nane's mother Veronica and her aunt Tracy, both of whom welcomed me into their family and gave me a home away from home. I also would like to thank my frequent collaborator of many years, Rage, the most wonderful of all bearded dragons. It's just not the same without him around.

Finally, but in no way the least, I owe a special thanks to my partner of the last seven years, Shi'nane Mina Widow. Her love, support and encouragement have kept me going. Her belief in me has never waned and her unwavering love has sustained me. Thank you, my love, from the bottom of my heart, for all the years you've spent with me, and all the laughs, smiles and happiness we have shared along the way. We have stood with each other always during the good times and the bad. You have brought so much joy to my life. אוהב אותך לנצח



# Table of Contents

Abstract.....	ii
Summary For Lay Audience.....	iv
Co-Authorship Statement.....	v
Acknowledgements.....	vii
Table of Contents.....	ix
List of Tables.....	xiii
List of Figures.....	xiv
List of Appendices.....	xix
List of Nomenclature and Terms Used.....	xx
1.0 INTRODUCTION.....	1
1.1 Glass Structure and Concepts.....	1
1.2. X-Ray Photoelectron Spectroscopy (XPS).....	3
1.3. Free Oxygen (O <sup>2-</sup> ).....	5
1.4. Aluminosilicate Glasses.....	7
1.5. Overview.....	8
1.6. References.....	11
2.0. HIGH RESOLUTION X-RAY PHOTOELECTRON SPECTROSCOPY (XPS) STUDY OF K <sub>2</sub> O-SiO <sub>2</sub> GLASSES: EVIDENCE FOR THREE TYPES OF O AND AT LEAST TWO TYPES OF Si.....	17
2.1 INTRODUCTION.....	17
2.2. EXPERIMENTAL METHOD.....	18
2.2.1. Sample Preparation.....	18
2.2.2. XPS Analysis.....	19
2.3. RESULTS AND INTERPRETATION OF SPECTRA.....	19
2.3.1. Constraints Used to Fit XPS Spectra.....	19
2.3.1.1. Spin-orbit Split Doublets.....	21
2.3.2. Bulk Glass Compositions by XPS and Homogeneity.....	21
2.3.3. K 2p Spectra.....	27

2.3.4. Si 2p Spectra .....	30
2.3.4.1. Relationship to Q-species.....	31
2.3.5. O 1s Spectra .....	33
2.3.5.1. X-ray Beam Effects on O 1s Spectra.....	37
2.3.6. Comparison of O 1s XPS and NMR Results.....	37
2.4. DISCUSSION.....	40
2.4.1. Oxygen Species in Potassium Silicate Glasses .....	40
2.4.2. Two Types of BO From XPS Spectra .....	42
2.4.3. A Third Type of Oxygen, O <sup>2-</sup> .....	43
2.4.4. Calculated Distribution of Oxygen Species .....	44
2.4.5. Equilibrium Distribution Among Oxygen Species.....	45
2.4.6. The Relationship Between O <sup>2-</sup> and Activity of K <sub>2</sub> O.....	46
2.5. CONCLUSIONS .....	47
2.6. REFERENCES .....	48
3.0. SPECTROSCOPIC STUDIES OF OXYGEN IN POTASSIUM SILICATE GLASSES AND MELTS .....	53
3.1. INTRODUCTION .....	53
3.1.1. Constraints on Oxygen Speciation .....	55
3.1.1.1. General Considerations .....	55
3.1.1.2. The Orthosilicate Composition.....	57
3.1.1.3. Oxygen Species Abundances Derived from Experiments.....	57
3.2. EXPERIMENTAL METHOD.....	59
3.2.1. Preparation.....	59
3.2.2. XPS and Electron Probe X-ray Microanalyzer (EPMA) Analytical Considerations.....	60
3.3. RESULTS AND EXPERIMENTAL UNCERTAINTIES.....	61
3.3.1. Homogeneity and the Composition of Glasses .....	61
3.3.2. O 1s XPS Spectral Fits, Assignments and Linewidths .....	61
3.3.3. Analytical Uncertainties in BO%, NBO% and O <sup>2-</sup> .....	64
3.3.4. Other Contributions to Uncertainty .....	66
3.3.5. Oxygen Speciation from O 1s XPS Spectra .....	68
3.4. OXYGEN SPECIATION FROM <sup>29</sup> Si MAS NMR SPECTRA .....	69
3.4.1. Q-species Signals and Lineshapes .....	69
3.4.2. Two Q <sup>2</sup> Species Peaks in Potassium Silicate Glasses .....	74

3.4.3. Test for Two Q <sup>2</sup> Species .....	76
3.4.4. Two Q <sup>3</sup> Peaks in Potassium Silicate Glasses.....	77
3.4.5. Test for Two Q <sup>3</sup> Signals .....	77
3.5. <sup>17</sup> O NMR OF POTASSIUM DISILICATE GLASS .....	78
3.5.1. Standard Interpretation.....	78
3.5.2. Oxygen Coordination and Chemical Shifts .....	78
3.5.3. Search for O <sup>2-</sup> .....	79
3.6. O <sup>2-</sup> ABUNDANCES AND KINETICS OF DISSOLUTION OF GASES IN MELTS.....	80
3.6.1. Oxygen Speciation and Thermodynamic Considerations.....	80
3.6.2. Kinetic and Thermodynamic Aspects of Gas Dissolution in Melts .....	81
3.7. CONCLUSIONS .....	85
3.8. REFERENCES .....	85
4.0 DISSOLUTION OF Al <sub>2</sub> O <sub>3</sub> IN K-SILICATE MELTS, WITH IMPLICATIONS FOR THE STABILITY OF Al-BEARING SILICATE MELTS.....	95
4.1. INTRODUCTION .....	95
4.2. BACKGROUND AND EXPERIMENTAL ASPECTS .....	97
4.2.1. Background .....	97
4.2.2. Lewis Acids and Bases .....	97
4.2.3. Sample Preparation .....	98
4.2.4. XPS Analysis .....	98
4.2.5. XPS Results .....	99
4.3. INTERPRETATION OF DATA.....	100
4.3.1. O 1s XPS Spectra .....	100
4.3.2. Difference Spectra .....	103
4.3.3. Interpretation of Peaks A and B.....	105
4.4. STOICHIOMETRIC DISSOLUTION REACTIONS.....	106
4.4.1. Al <sub>2</sub> O <sub>3</sub> Dissolution Reaction .....	106
4.4.2. Another reaction .....	108
4.5. REACTIONS AT THE MELT-Al <sub>2</sub> O <sub>3</sub> INTERFACE AND IN MELTS.....	111
4.5.1. Al (Lewis Acid) surface sites.....	111
4.5.2. Reactions in melts.....	112
4.6. DISCUSSION.....	114
4.6.1. Stoichiometric and elementary reactions.....	114

4.6.2. Stability of Al-bearing melts .....	116
4.7. CONCLUSIONS .....	117
4.8. REFERENCES .....	117
5.0. CONCLUSIONS .....	124
5.1. Potassium Silicate Glasses.....	124
5.2. Potassium Aluminosilicate Glasses.....	126
5.3. Future Directions and Implications .....	127
5.4. References .....	129
Appendix A: Calculation of $X_{BO}$ and $X_{O_2}$ from Q-species Abundances and from BO%.....	130
Curriculum Vitae.....	132

## List of Tables

Table 2.1: Potassium Silicate Glass Compositions Synthesized and Compared with XPS Analysis .....	28
Table 2.2: Peak Parameters Derived from Fitting XPS Spectra: K 2p and Si 2p (BE and FWHM in eV) .....	29
Table 2.3: Peak Parameters Derived from Fitting XPS Spectra, O 1s (BE and FWHM in eV) ...	39
Table 2.4: Effect of Photon Source on BO Abundance .....	39
Table 3.1: EPMA analyses for samples 35a, 35b and 35c .....	63
Table 3.2: Fitted peak parameters for the potassium silicate glasses of Figure 3.2 .....	65
Table 4.1: Calculation of BO% and NBO% in Al-bearing K silicate melts .....	101

## List of Figures

Figure 1.1: (a) Drawing showing BO and NBO of Si tetrahedra, taken from Calas et al. (2006). (b) The Modified Random Network model of Greaves where large unfilled circles represent BO and small filled circles represent NBO, taken Henderson (2005) from Greaves (1985).....	2
Figure 2.1: Survey scans of (a) vitreous silica and (b) potassium silicate glass with 23 mol % K <sub>2</sub> O. Major spectral lines are labeled. ....	20
Figure 2.2: K 2p spectrum for 23 mol % K <sub>2</sub> O sample. The C 1s peak is also shown. The K 2p <sub>1/2</sub> peak is constrained by the properties of the K 2p <sub>3/2</sub> peak. A Shirley background was used. Fit parameters are given in Table 2.2. ....	22
Figure 2.3: Si 2p spectra of select compositions over the entire range studied fit with one Si 2p <sub>3/2</sub> .....	23
Figure 2.4: Si 2p spectra of vitreous silica and the potassium silicate glass compositions analyzed along with the fit residuals. Each spectrum was fit with two Si 2p <sub>3/2</sub> - Si 2p <sub>1/2</sub> spin-orbit split doublets (solid curves) where the Si 2p <sub>1/2</sub> is constrained by the properties of the Si 2p <sub>3/2</sub> peak. A Shirley background was used, and the fits are represented by solid lines through the data points. Peak fit parameters are listed in Table 2.2.....	24-26
Figure 2.5: Comparison of the abundances of the two Si 2p <sub>3/2</sub> contributions with the abundances of Q <sup>4</sup> and Q <sup>3</sup> species from NMR studies (Maekawa et al., 1991; Malfait et al., 2007; Sen and Youngman, 2003) The filled shapes represent the abundance of the high binding energy Si 2p <sub>3/2</sub> contribution from this study (squares) and the Q <sup>4</sup> NMR abundances from Maekawa et al. (1991) (circles), Malfait et al. (2007) (triangles) and Sen and Youngman (2003) (diamonds). The open shapes represent the abundance of the low binding energy Si 2p <sub>3/2</sub> contribution from this study and the Q <sup>3</sup> abundances from the aforementioned NMR studies. ....	32
Figure 2.6: O 1s spectra of vitreous silica and the potassium silicate glasses studied along with the fit residuals. The BO and NBO peaks were fitted freely with no constraints. A Shirley background was used and the fits are represented by solid lines intersecting the data points. Peak fit parameters are listed in Table 2.3.....	34-36
Figure 2.7: Examples of BO mol % as a function of time of exposure to the X-ray beam for two samples (35 mol % and 17 mol % K <sub>2</sub> O). The BO abundances with analysis time for all samples	

are given in Table 2.4. Data points were fit with a polynomial line and the y-intercept indicates the BO mol % in the glass prior to analysis. This procedure was used to obtain the BO mol % for all glasses studied and the extrapolated values are given in Table 2.3. .... 38

Figure 2.8: Mol fractions of different types of oxygen as a function of composition (given in  $X(K_2O)$ ). XPS data (squares) from this study were obtained from measurements of the BO peaks of the O 1s spectra. The XPS data are compared with the NMR data from studies by Maekawa et al. (1991) (circles), Malfait et al. (2007) (triangles) and Sen and Youngman (2003) (diamonds). The fraction of BO (solid line) was calculated using Eq. 2.2 where  $K_2 = \infty$ . The fractions of BO (dot-dash line), NBO (long dashed line) and  $O^{2-}$  (short dashed line) were calculated assuming  $K_2 = 2.0$ . The squares representing the XPS data are drawn to reflect the estimated errors associated with both  $K_2O$  content and the abundance of BO. .... 41

Figure 3.1: Plot of BO mole fraction versus mole fraction of MO (or  $M_2O$ ) illustrating feasible BO values (clear region between solid curves) and regions where  $X_{BO}$  values are physically impossible to achieve in equilibrated melts (shaded regions). The curve labelled  $K_1 = \infty$  illustrates  $X_{BO}$  where the polymerization equation (Equation 3.1) goes to completion. The curve labelled  $K_1 = 0.0$  illustrates  $X_{BO}$  where the polymerization reaction does not occur (i.e., no NBO is produced). The dashed curve represents BO values for  $K_1 = 8.0$ . The  $X_{BO}$  derived from the free fits of  $^{29}Si$  MAS NMR data (Table 3.1 of Malfait et al., 2007) are plotted as shaded circles. ....56

Figure 3.2: O 1s XPS spectra of six potassium silicate glasses. The nominal compositions of glasses shown in Figures 3.2a, 3.2b and 3.2c are 35 mol%  $K_2O$  but they were melted either three or four times and analyzed by EPMA to yield the corrected compositions (see text for details). The corrected compositions for glasses of Figures 3.2d, 3.2e and 3.2f are 26, 31 and 34 mol% were previously published in Sawyer et al. (2012) and are modified here. ....58

Figure 3.3: The effects of defocusing the electron beam to 40  $\mu m$  for a glass containing 30 mol%  $K_2O$ . With a 40  $\mu m$  beam size, the count rate between 0 and 10 s provides accurate analysis of potassium in the glass. The precise instrumental conditions used to analyze the glass reported here are provided in the text. .... 62

Figure 3.4: (a-d) Plots illustrating the changes to BO% as a function of time of exposure to the X-ray beam. A least squares quadratic fit to each set of data is included in these plots and its extrapolation to zero exposure yields the best estimate of BO% in the glass (see text). (e)

Variation of BO% about the least squares quadratic fits (e.g., those in Figures 3.4a-d). The variations have been plotted in Figure 3.4e as a function of exposure time to obtain an estimate of the uncertainty associated with the BO% quoted in Table 3.2. The dashed curves represent  $\pm 3\sigma$  (see text).....67

Figure 3.5: Plot of BO mole fraction versus mole fraction MO (or  $M_2O$ ) illustrating relationships among the oxygen species and experimentally determined  $X_{BO}$  values from O 1s XPS and  $^{29}Si$  MAS NMR spectra.  $X_{O_2^-}$  values are plotted and have been derived from experimental  $X_{BO}$  values (see text for calculations). The shaded circles represent experimentally determined  $X_{BO}$  values derived from XPS spectra of Figures 3.2a, 3.2b and 3.2c. The corresponding  $X_{O_2^-}$  values are plotted as small, shaded circles and they straddle the dash-dotted curve labelled  $K_1 = 8.0$ . The open circles are  $X_{BO}$  values previously reported (Sawyer et al., 2012) and the corresponding  $X_{O_2^-}$  values are plotted as small open circles. The crosses represent O 1s XPS results obtained from a separate laboratory (Matsumoto et al., 1998) Large open squares and large shaded triangle represent  $X_{BO}$  values derived from  $^{29}Si$  NMR experiments (Maekawa et al., 1991; Malfait et al., 2007) (see Appendix A) and the corresponding  $X_{O_2^-}$  values are plotted as smaller squares and triangles. BO, NBO and  $O^{2-}$  curves labelled  $K_1 = 8.0$  were calculated from mass action Equation 3.2. The short-dashed curve illustrates  $X_{BO}$  where Reaction 3.1 goes to completion (i.e.,  $K_1 = \infty$ ). ..... 70-71

Figure 3.6: Reproduction of the  $^{29}Si$  MAS NMR spectrum of crystalline  $K_2Si_2O_5$  from de Jong et al., (1998) illustrating the Q-species distribution. The spectrum includes seven peaks. A small peak at  $\sim -93.5$  ppm is extraneous (see de Jong et al., (1998) for explanation). The centroids of groups 1 and 2 have been estimated at the half-height for each group and are indicated by the dotted lines. .... 73

Figure 3.7: (a)  $^{29}Si$  MAS NMR spectrum of potassium metasilicate glass after Maekawa et al. (1991) and (b) reproduction of the  $^{29}Si$  MAS NMR spectrum of sodium metasilicate glass from Maekawa et al. (1991) along with their original spectral peak assignments. The differences in the spectra make Q-species assignments uncertain for the potassium metasilicate glass.....75

Figure 4.1: O 1s XPS spectra, fits and residuals for K-silicate glasses containing 0, 1 and 3 mol%  $Al_2O_3$ . All fits were performed using..... 102



Figure 4.2: O 1s XPS spectra of the K-silicate glasses where the BEs have been standardized to a common value and the intensities have been normalized to obtain intensity per mole of O.

Difference spectra are indicated by the solid dots in each diagram. (a) The standardized and normalized KS and KAS1 spectra. The difference spectra obtained by the subtraction of the KS spectrum from the KAS1 spectrum. (b) The standardized and normalized KS and KAS3 spectra. The difference spectrum is obtained by subtracting the KS spectrum from the KAS3 spectrum. The arrows indicate the BEs of vitreous SiO<sub>2</sub> (Nesbitt et al., 2015) and of crystalline NaAlO<sub>2</sub> (Barr, 1991). Both phases contain only BO atoms. .... 104

Figure 4.3: NBO and BO abundances measured and calculated as a function of dissolved AlO<sub>1.5</sub> in K-disilicate glass. The large, filled circles are experimental results from Fig. 4.1 ( $\pm 2\%$  uncertainty). The small, shaded circles represent calculated values of Table 4.1 (columns 12 and 13). The solid lines indicate the trends of the calculated results. The calculations are provided in section 4.4.1. .... 107

Figure 4.4: Schematic diagram showing the reaction between a Q<sup>3</sup> species of the melt and under-coordinated Al<sup>V</sup> and O atoms at the Al<sub>2</sub>O<sub>3</sub> surface. Surface Al sites are strong Lewis acids and surface O sites are strong Lewis bases. (a) illustrates the reaction of a Q<sup>3</sup> melt species (Reactant #1) with a surface Al<sup>V</sup> atom (Reactant #2) to produce a Si-O-Al species attached to the Al<sub>2</sub>O<sub>3</sub> surface. Three Al-O bonds numbered 1, 2 and 5 are labelled. Bonds 3 and 4 are directed along the x-axis and are not shown. (b) illustrates the reaction between a Q<sup>3</sup> species of the melt (Reactant #1) and a surface NBO species (Reactant #2). A surface transition species containing Si<sup>V</sup> is produced. The reactant NBO becomes a BO in the transition species. The transition species may decompose to either the original reactants (double arrow) or to a surface Si-O-Al species and a Q<sup>2</sup> melt species (single arrow). Detachment of the surface species produces a Si-O-Al melt species. .... 109-110

Figure 4.5: The conversion of an Al<sup>III</sup> melt species (Reactant #2) to an Al<sup>IV</sup> species by reaction with a Q<sup>3</sup> species bearing an NBO<sup>-</sup> (Reactant #1). The NBO<sup>-</sup> is converted to BO by the reaction, which increases the number of BOs bonded to the Al moiety by one. The reaction occurs in the melt. .... 113

Figure 4.6: Schematic showing the replacement of NBOs for BOs on the aluminate species by attack of a Q<sup>3</sup> species containing an NBO<sup>-</sup>. The NBO<sup>-</sup> is converted to BO with formation of the

transition species. With successful reaction, the number of BOs on the product moiety ( $\text{AlO}_4$ ) increases by one. When the reaction is repeated, it may yield an  $\text{AlO}_4$  moiety consisting of only BOs. The reaction follows a  $\text{S}_\text{N}$  reaction mechanism with the transition species in which Al is five-fold coordinated..... 115

## List of Appendices

Appendix A: Calculation of  $X_{\text{BO}}$  and  $X_{\text{O}_2}$  from Q-species Abundances and from BO%.....130

## List of Nomenclature and Terms Used

<b>Parameter</b>	<b>Definition</b>
BO	Bridging Oxygen
NBO	Non-Bridging Oxygen
O <sup>2-</sup>	Free Oxygen
MO or M <sub>2</sub> O	Modifier or counter Oxide
Q <sup>n</sup>	Silica tetrahedron bonded to n BO atoms (n = 0, 1, 2, 3, 4)
FWHM	Full Width at Half Maximum
BE	Binding Energy
XPS	X-ray Photoelectron Spectroscopy
MAS NMR	Magic Angle Spinning Nuclear Magnetic Resonance
Broadscan	Scan over a long range of binding energies, ppm etc.
Narrowscan	Scan over a narrow range of binding energy, ppm, etc.
Linewidth	Another term for the FWHM of an XPS spectrum
Lineshape	The function that describes the shape of a peak in a spectrum
EPMA	Electron Probe Micro Analysis/Analyser
K <sub>n</sub>	Equilibrium constant for Reaction n (n = 1, 2, 3.... n)
X <sub>BO,NBO,O<sup>2-</sup>,SiO<sub>2</sub>,etc.</sub>	Mole fraction (subscript denotes specific species)
N <sub>BO</sub>	Number of moles of BO
N <sub>T</sub>	Number of moles total Oxygen
X <sup>*</sup> <sub>BO</sub>	X <sub>BO</sub> remaining after reaction completes (calculated)
X <sup>e</sup> <sub>BO</sub>	X <sub>BO</sub> determined from experiment (measured)
X <sup>X</sup> <sub>BO</sub>	Excess BO caused by incomplete reaction. Equal to the difference between measured (X <sup>e</sup> <sub>BO</sub> ) and calculated (X <sup>*</sup> <sub>BO</sub> ) values.

# Chapter 1

## 1.0 INTRODUCTION

Glasses have been used for millennia for a variety of purposes and are one of the oldest industrial materials (e.g., Mysen and Richet, 2005). The importance of glasses to modern society is reflected in their ubiquity. In the context of earth sciences, glasses are often used as analogues for natural silicate melts since they are more readily studied by a large variety of analytical techniques (e.g., Calas et al., 2006; Henderson, 2005). Glasses with simple compositions, such as binary alkali silicates, can help us extrapolate and model the structure and properties of more complex natural melts. Such results shed light on the magmatic processes that occur on and in terrestrial planetary bodies.

### 1.1 Glass Structure and Concepts

A glass is an amorphous material with no long-range order that exhibits the glass transition (Calas et al., 2006; Henderson, 2005). The glass transition is the range of temperatures over which a rapid but continuous change in second-order thermodynamic properties (e.g., heat capacity and thermal expansivity) from liquid to solid-like values occurs (Calas et al., 2006; Henderson, 2005). The glass transition temperature,  $T_g$ , defines this region. Glasses are solids in the sense that they are rigid materials that do not flow when subjected to moderate stress (Calas et al., 2006; Henderson, 2005). A glass can be considered as an inorganic material that is the product of fusion and has been cooled to a rigid condition without crystallizing (Scholze, 1991). Alternatively, glass can be considered, in the physicochemical sense, as a “frozen-in undercooled liquid” (Scholze, 1991) which exhibits the structure of a melt at  $T_g$  (Calas et al., 2006).

Silicate glasses consist of a network of interconnected silica tetrahedra. In this sense, silicon is a network former (e.g., Calas et al., 2006). Oxygen atoms which link silica tetrahedra together are called Bridging Oxygens (BO). The introduction of oxides comprised of cations such as alkali and alkaline earth elements modifies the structure by bonding with oxygen atoms in the glass network through polymerization reactions. Oxygen atoms that connect a silica tetrahedron to a

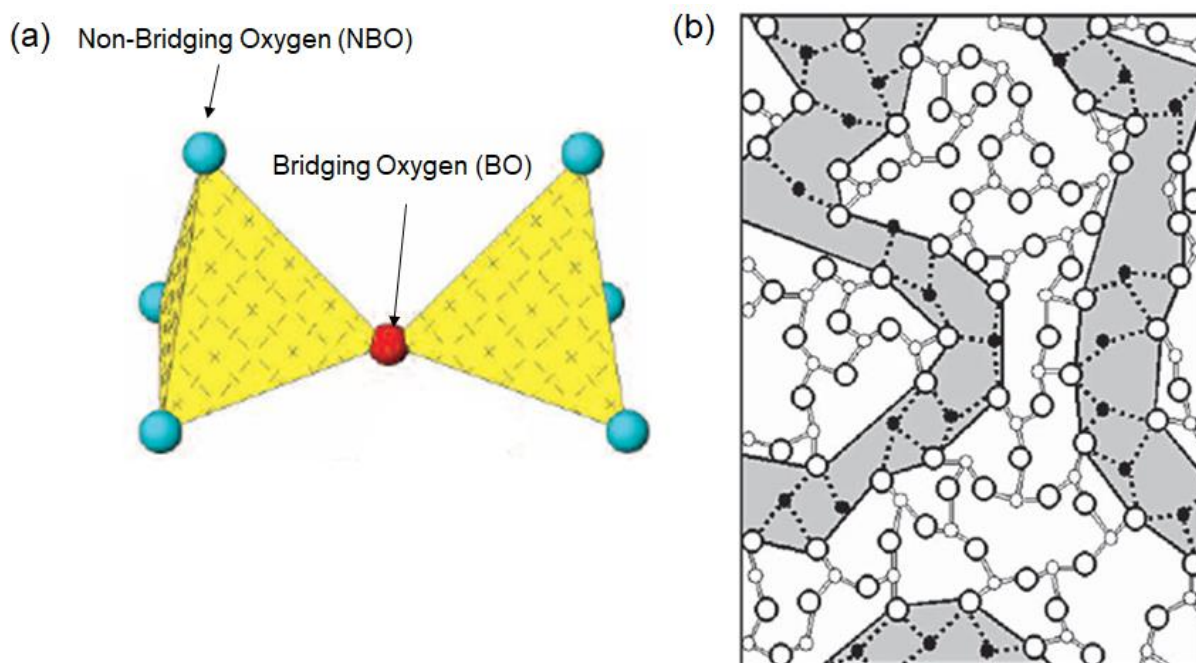


Figure 1.1: (a) Drawing showing BO and NBO of Si tetrahedra, taken from Calas et al. (2006). (b) The Modified Random Network model of Greaves where large unfilled circles represent BO and small filled circles represent NBO, taken from Henderson (2005) after Greaves (1985).

network modifying cation are called Non-Bridging Oxygens (NBO) (see Figure 1.1a). Free Oxygen atoms ( $O^{2-}$ ) are not connected to any network formers and connect only to modifying cations. Q-species are Si tetrahedra distinguished by the number of BO bonded to the central Si atom. They are denoted as  $Q^n$ , where Q represents a silica tetrahedron and n is the number of BO atoms connected to it.

Henderson (2005) notes that glass structure models tend to be categorized as crystallite or continuous random network (CRN) models, but recent studies favour the CRN theory or some modified variation of it. Zachariasen (1932) proposed the CRN model where the structure of glass is made up of a disordered network of silica tetrahedra connected to each other by corner sharing BO atoms. This model found experimental support from Warren (1934). Greaves (1985) developed the modified random network (MRN) model (see Figure 1.1b) where the structure of a glass is made up of two sublattices which are interconnected: one made up of network formers and one made up of network modifiers. In this model, the structure is partly covalent (network formers) and partly ionic (network modifiers), with the modifier sublattice forming percolation channels that facilitate ionic transport (Greaves, 1985). The MRN model is currently the most widely accepted hypothesis of glass structure because it agrees with most recent experimental studies (Henderson 2005).

## 1.2. X-Ray Photoelectron Spectroscopy (XPS)

X-ray Photoelectron Spectroscopy (XPS) is a technique developed in the 1960s that utilizes the photoelectric effect to obtain spectra of materials. High energy photoelectrons from an X-ray source with energy  $h\nu$  bombard a sample. The incident photons impart energy to electrons in core orbitals and if the imparted energy is greater than the binding energy (BE) of an electron, the electron is ejected as a photoelectron possessing kinetic energy (KE). The kinetic energy of the photoelectrons are measured by a detector. The binding energies of the orbitals from which the photoelectrons originated can be found using the equation:

$$BE = h\nu - \phi - KE, \quad (1.1)$$

where BE is the binding energy, KE is the kinetic energy,  $h\nu$  is the energy of the X-ray source and  $\phi$  is the work function of the spectrometer which is typically negligible. Although considered a surface analytical technique, the depth of analysis of XPS is on the order of a few

10s of Å and XPS therefore can be used for bulk analysis provided that the bulk of the sample is homogeneous (Hochella and Brown, 1988; Hochella, 1988; Nesbitt and Bancroft, 2014).

Insulators or non-conductors such as silicate glasses experience a build-up of charge during analysis. Continuous charging occurs when the amount of charging is uniform across a smooth sample surface and results in shifts in the BEs of every peak. Differential charging is caused by variations of charge across the whole surface and is reflected in a range of KE values which result in broadened spectra. Continuous charging poses little issue for spectral analysis and differential charging is often mitigated with the use of electron flood guns that flood the sample with low energy electrons (Nesbitt, 2002). This technique has limited effectiveness on irregular surfaces (e.g., fractured surfaces) due to the directional nature of the electron flood gun. An advanced charge compensation technique using a magnetic confinement system was developed (Nesbitt et al., 2004). Low energy electrons are magnetically confined to 'float' above the sample and neutralize any positively charged regions of the sample, regardless of sample morphology. This has allowed for spectra of insulating materials to be obtained with similar resolutions (linewidths) to spectra of semi-conductors and conductors. The implication of this is that XPS can be considered viable as a tool for geochemical analysis (Nesbitt et al., 2004; Nesbitt and Bancroft, 2014).

XPS spectra presented here are standardized to the C 1s binding energy at 285.0 eV thus allowing comparison of BEs from one sample to another. The reason for this is that adventitious carbon is present in the analysis chamber for any analysis and so it provides an internal standard for all samples studied. XPS peaks have combined Gaussian and Lorentzian contributions to their shape. The Lorentzian shape is inherent to the analytical technique and relates to the exponential decay of the effects of the X-ray source energy on the sample. The Gaussian shape arises from counting statistics due to slight variations in the KE of the photoelectrons. The combined Gaussian-Lorentzian shape is known as a Voigt function. Backgrounds can be fit using Shirley backgrounds. Shirley (1972) recognized that the backgrounds of XPS spectra underneath peaks must be produced in proportion to the peak. The Shirley background is advantageous because of its theoretical basis. It allows for consistently accurate evaluations of areas under peaks and highly reproducible background.



XPS has been used to study glasses for several decades. The sodium silicate system (e.g., Bruckner et al., 1980; Matsumoto et al., 1998; Nesbitt et al., 2011) and lead silicate system (e.g., Smets and Lommen, 1982; Dalby et al., 2007) have been studied in detail. Few XPS studies exist for the potassium silicate system and those that do have focused on sample irradiation with an electron beam (e.g., Zemek et al., 2005; Gedeon et al., 2008), although Matsumoto et al. (1998) included two potassium silicate glasses in their study. In this thesis I present the first comprehensive study of oxygen speciation in potassium silicate glasses using XPS.

### 1.3. Free Oxygen ( $O^{2-}$ )

The three oxygen species ( $BO$ ,  $NBO$  and  $O^{2-}$ ) in silicate glasses are related through the reaction:



where  $O^{\cdot}$  is  $NBO$  and  $O^{\circ}$  is  $BO$  (Fincham and Richardson, 1954; Toop and Samis, 1962; Hess, 1971; Fraser, 1975). Determination of the concentrations of oxygen species in silicate glasses is important for thermodynamic modelling of glasses and melts and understanding the kinetics of reactions involving reagents such as  $CO_2$ ,  $H_2O$  and  $S$ -species. Studies related to the abundance of free oxygen in glasses have been relatively scarce until recently. Presently, the abundance of free oxygen in silicate glasses is a contentious issue (c.f., Nesbitt et al., 2015; Stebbins, 2017).

Maekawa et al. (1991) conducted a comprehensive  $^{29}Si$  MAS NMR study on Li-, Na- and K-silicate glasses over a wide range of compositions. The K-silicate glasses with  $K_2O > 40$  mol% exhibited spectral shapes different from the Na-silicates, showing four contributions instead of three. They assigned the additional peak as a second  $Q^2$  species, while acknowledging that there was no direct experimental evidence to support this claim. This assumption gave an  $[NBO]/[Si]$  ratio that satisfied the stoichiometric value of 2.00 leading to the claim of no free oxygen in glasses more siliceous than the orthosilicate composition (i.e., Reaction 1.2 goes to completion). A study by Malfait et al. (2007) of potassium silicate glasses used the interpretations of Maekawa et al. (1991) in fitting their  $^{29}Si$  NMR spectra and concluded that there was no  $O^{2-}$  present in the glasses above the orthosilicate composition. A  $^{29}Si$  MAS NMR and Raman spectroscopy study by Schaller et al. (1999) found evidence for up to 2.4 mol%  $O^{2-}$  in La-doped Na- and K-silicate glasses. Stebbins and Sen (2013) studied two potassium silicate glasses with compositions 34 mol% and 40 mol%  $K_2O$  with  $^{17}O$  NMR. They concluded that free oxygen was

present in negligible amounts since they were unable to detect a direct signal in the spectra in the region they calculated. Stebbins (2020) came to the same conclusions for a series of high alkali sodium silicate glasses and a high alkali potassium silicate glass.

Advances in charge compensation techniques have allowed for the collection of high resolution XPS spectra from silicates. Studies by Dalby et al. (2007) on Pb-silicate glasses and Nesbitt et al. (2011) on Na-silicate glasses presented spectra of a resolution unseen before from XPS, due primarily to the advances in charge compensation. Dalby et al. (2007) measured the abundances of BO in a series of Pb-silicate glasses. They found that BO was in excess of what was predicted assuming that Reaction 1.2 goes to completion and concluded that  $O^{2-}$  (referred to as Metal Bridging Oxygen or MBO) was present in all compositions. Their models indicated that  $O^{2-}$  was present at ~0.5-3.0 mol% in glasses containing 20-40 mol% PbO. The XPS and NMR data of Nesbitt et al. (2011) found 0.5 mol% in glasses containing 10 mol%  $Na_2O$  to ~3-6 mol% in glasses containing 50 mol%  $Na_2O$  depending on the technique. Both XPS studies indicate that the amount of  $O^{2-}$  is significant in glass compositions where  $SiO_2 > 33.33$  mol%. The  $^{29}Si$  NMR data of Nesbitt et al. (2011) are in general agreement with previous NMR results. Nesbitt et al. (2015) presented an O 1s XPS spectrum for a Pb-silicate glass sample nominally containing 75% PbO. They provided the first accurate measurements of free oxygen in Pb-silicate glasses with a value of 35 mol%  $O^{2-}$ .

Nasikas et al. (2012) presented  $^{17}O$  NMR spectra of a series of  $(Ca_{0.5}Mg_{0.5}) SiO_2$  glasses where  $SiO_2 = 28-33.3$  mol%. They identified a shoulder peak of the main signal at -110 ppm to be free oxygen. This was the first direct experimental evidence for free oxygen to be presented. The experimentally derived values of free oxygen from their  $^{29}Si$  spectra were greater than expected from stoichiometry which, as they note, indicates an excess of free oxygen in the structure of the glasses. However, they did not provide fits to their  $^{17}O$  NMR spectra. Nesbitt et al. (2015) scanned and fit the  $^{17}O$  NMR spectra for the orthosilicate glass and the glass containing 28 mol%  $SiO_2$ . They obtained  $O^{2-}$  values of  $10 \pm 4$  mol% and  $18 \pm 4$  mol% respectively after testing for consistency and applying uncertainties related to scanning the spectra and assuming all peak contributions were Gaussian.

Nasikas et al. (2011) provided Raman spectra for  $CaMgSiO_2$  glasses with  $SiO_2 = 28, 30$  and  $33$  mol% and gave Q-species abundances for the orthosilicate sample. Nesbitt et al. (2015) used

these Q-species abundances and following the calculations in the Appendix A they obtained a value of 8.4 mol%  $O^{2-}$ . The presence of  $O^{2-}$  at the orthosilicate composition indicates that Reaction 1 does not go to completion. The implication is then that free oxygen is present at all possible compositions and is an important, thermodynamically relevant species. These results support the XPS results of Dalby et al. (2007), Nesbitt et al. (2011).

A  $^{29}\text{Si}$  NMR study of a  $\text{CaSiO}_3$  (metasilicate) glass by Zhang et al. (1997) reported  $\sim 1.0$  mol%  $O^{2-}$  from Q-species abundances derived from a 2D  $^{29}\text{Si}$  MAF NMR spectrum. Thompson et al. (2012) studied  $\text{Ca}_{0.56}\text{Si}_{10.44}\text{O}_{1.44}$  glass using 17O MAS NMR. Although they state there is no evidence for  $O^{2-}$  in the glass, their reported BO abundance is in excess of the expected value assuming Reaction 1.2 goes to completion. Nesbitt et al. (2015) calculated  $\sim 3.2$  mol% or  $\sim 1.7$  mol%  $O^{2-}$  in the glass, depending on the method used to obtain BO and NBO abundances. Nesbitt et al. (2015) also note evidence for  $O^{2-}$  in  $\text{MgO-SiO}_2$  glasses from previous X-ray and neutron scattering and  $^{29}\text{Si}$  and  $^{17}\text{O}$  NMR studies.

Measuring the abundances of different structural species of oxygen is an effective way of limiting the possible structural units in a glass and creating constraints on structural models. This thesis is concerned with the measurement of abundances of structural species of oxygen in potassium silicate glasses using X-ray Photoelectron Spectroscopy (XPS) to obtain spectra with high resolutions. Discrepancies between these XPS results and the results from previous Nuclear Magnetic Resonance (NMR) studies for potassium silicate glasses are addressed and an attempt is made to resolve them. The thesis also adds to the evidence that XPS has now become a viable tool for the study of silicate glasses. Once a binary glass system is well characterized, a third component can be added to the glasses. The addition of each new component increases the complexity of the structure. In this regard an exploratory study of potassium aluminosilicate glasses is conducted to examine the reactions that occur during the initial stage of dissolution of  $\text{Al}_2\text{O}_3$  in K-disilicate melts.

#### 1.4. Aluminosilicate Glasses

Approximately 95% of natural magmatic compositions are made up of  $\text{SiO}_2$ ,  $\text{Al}_2\text{O}_3$  and metal oxides (Mysen and Richet, 2005). Furthermore, the minerals plagioclase and K-feldspar, along with quartz make up approximately 75% of all minerals in Earth's crust. Studies have shown that

$\text{Al}_2\text{O}_3$  is the second most abundant oxide (~15 wt.%) in the bulk crust composition (Nesbitt and Young, 1984; Taylor and McLennan, 1981; Wedepohl, 1969; Shaw et al., 1967). The standard model of aluminosilicate glasses states that  $\text{Al}^{3+}$  acts as a network former and is tetrahedrally coordinated where there are enough charge compensating cations to provide charge balance, which are typically alkali and alkaline earths cations.

Several early XPS studies have focused on sodium aluminosilicates (Bruckner et al., 1978; Bruckner et al., 1980; Lam et al., 1980; Kaneko et al., 1983; Onorato et al., 1985, Tasker et al., 1985; Hochella and Brown, 1988, Miura et al., 2000). These studies were performed before the advent of advanced charge compensation techniques. The sodium aluminosilicate O 1s spectra of Onorato et al. (1985) and Tasker et al. (1985) were fit with three contributions (two BO representing Si-O-Al and Si-O-Si, and one NBO). Hochella and Brown (1988) argued that the peak positions of the O 1s contributions are not well defined theoretically or experimentally. Such fitting is arbitrary when done without constraints. They found that the FWHM of the O 1s peak is related to the number of chemically distinct oxygen bonding environments. The previous XPS studies all demonstrate that the addition of aluminum to an alkali silicate glass decreases the NBO contribution and increases the BO contribution in peralkaline glasses.

The dissolution kinetics of refractory oxides, such as  $\text{Al}_2\text{O}_3$ , have been studied extensively, but have primarily focused on the mechanism controlling the rates of dissolution (e.g., Scherdtferger, 1966; Monaghan, 2004; Shaw, 2004; Shaw et al., 2018). Kuo and Kirkpatrick (1985) state that the rate of dissolution is determined by the rates of reactions at the melt-crystal interface or by diffusion of cations through the melt. Generally, the rate of diffusion is thought to be the controlling mechanism in melts of geological interest (e.g., Zhang et al., 1989). However, Shaw (2006; 2012) and Shaw et al., (2018) found that there is a variable period during the initial stages of dissolution where reactions at the interface are the controlling mechanism, after which saturation of the interface melt is reached and diffusion becomes the controlling mechanism. None of the above-mentioned studies discuss how, for instance, Al is incorporated into the melt after removal from the bulk solid surface.

## 1.5. Overview

In Chapter 2, high resolution O 1s, Si 2p and K 2p XPS spectra are presented for nine glasses in the  $\text{K}_2\text{O}$ - $\text{SiO}_2$  system with compositions ranging from 10 mol% - 35 mol%  $\text{K}_2\text{O}$ . The mole

fraction of Bridging Oxygen (BO) atoms is evaluated accurately from the O 1s spectrum for each glass. BO mole fractions from the spectra are compared with those calculated from Q-species distributions previously reported by  $^{29}\text{Si}$  MAS NMR data. The mole fractions are identical for the two techniques (within experimental error) in glasses containing 13 mol% to 25 mol% but in the compositional range between 25 mol% and 35 mol% BO mole fractions obtained by XPS are slightly greater than values derived from NMR data. The slight discrepancies between the two techniques at higher  $\text{K}_2\text{O}$  content are not resolved. The experimental data between 13 mol% and 25 mol%  $\text{K}_2\text{O}$  indicate the presence of free oxygen ( $\text{O}^{2-}$ ) atoms in the glasses. A thermodynamic analysis indicates the presence of  $\text{O}^{2-}$  at a few mol% in the glasses of low  $\text{K}_2\text{O}$  content, which increases monotonically with increased  $\text{K}_2\text{O}$  content.

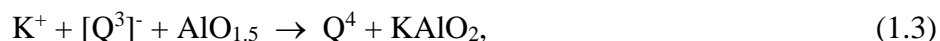
The high variability of the O 1s XPS line widths for the BO peaks may result from two BO contributions. One probably bridges two Si atoms (Si-O-Si) and the second type is an O bonded to two Si atoms and one K atom, similar to the  $\text{Na}_2\text{O}$ - $\text{SiO}_2$  glass system (Nesbitt et al., 2017).

Two contributions are suggested to explain the distinctly non-symmetric Si 2p XPS spectra where low binding energy shoulders are common on the major peak. A strong correlation between the Si 2p peak and shoulder intensities and the abundances of  $\text{Q}^4$  and  $\text{Q}^3$  species in glasses of the same composition from previous NMR studies suggests that, with additional resolution, XPS may be capable of resolving Q-species in the  $\text{K}_2\text{O}$ - $\text{SiO}_2$  system.

Chapter 3 reports a study that attempts to resolve the discrepant results between O 1s XPS and  $^{29}\text{Si}$  and  $^{17}\text{O}$  NMR techniques. Four new glass spectra are presented for three glasses of nominal composition 35 mol%  $\text{K}_2\text{O}$  and one of nominal composition 37 mol%  $\text{K}_2\text{O}$ . The effects of melting on the compositions of the glasses are documented and quantified, as are uncertainties associated with fitting the O 1s spectra. These spectra are well resolved into two symmetric peaks: a narrow peak due to NBO (Si-O-K) plus “free oxide” ( $\text{O}^{2-}$  or K-O-K) and a broader peak due to BO (Si-O-Si). Values of mol% BO (uncertainties of  $\pm 1\%$ ) are obtained from the computed peak areas and indicate 2.2 ( $\pm 0.8$ ) mol%  $\text{O}^{2-}$  for glasses containing 32 ( $\pm 1$ ) mol%  $\text{K}_2\text{O}$ . Reassignment of Q-species for previously published  $^{29}\text{Si}$  NMR spectra leads to BO and  $\text{O}^{2-}$  values in good agreement with the O 1s XPS spectra. A recent  $^{17}\text{O}$  NMR study on potassium silicate glasses concluded that there is  $< 1$  mol%  $\text{O}^{2-}$  in these glasses based mainly on the assumption that the  $^{17}\text{O}$  chemical shift for  $\text{O}^{2-}$  should be similar in the glasses and the oxide in

crystalline  $K_2O$ . This assumption is questionable. Free oxide in these glasses should be highly reactive toward gases such as  $CO_2$  (via  $CO_2 + O^{2-} \rightarrow CO_3^{2-}$ ) and it seems likely that the reactive species in silicate glasses is  $O^{2-}$  rather than NBO as often assumed. The small amounts of  $CO_2$  found in reacted glasses are qualitatively consistent with the abundance of  $O^{2-}$  obtained from these O 1s XPS spectra of silicate glass.

In Chapter 4, I focus on reactions that occur at the melt-solid interface and in the melt during dissolution of  $Al_2O_3$  using data obtained from XPS analyses and taking difference spectra. Chapter 4 is an elementary study of  $K_2O-SiO_2-Al_2O_3$  glasses. High resolution O 1s X-ray Photoelectron Spectroscopy (XPS) has been used to study the dissolution of  $Al_2O_3$  in a  $K_2O$  disilicate melt. The spectra exhibit two well-resolved O 1s peaks one due to bridging oxygen (BO) and the other to non-bridging oxygen (NBO). There are two obvious, well-characterized, changes to the spectra resulting from increased  $Al_2O_3$  content of the melt. The NBO peak decreases in intensity relative to the BO peak, and the breadth (linewidth) of the BO peak increases. Difference spectra indicate that NBOs are converted to two BO-bearing melt species with binding energies (BE) characteristic of vitreous  $SiO_2$  ( $Q^4$  species) and of tetrahedrally coordinated Al ( $KAlO_2$ ) species. The results indicate that  $Al_2O_3$  dissolves in K disilicate melt according to the overall or *stoichiometric* polymerization reaction:



where Q represents a Si tetrahedron and the superscript indicates the number of bridging oxygen atoms (BO) associated with it. Reaction 1.3 is initiated by the presence of a strong Lewis base in the melt (i.e.,  $NBO^-$ ). At the high temperature of the melt, Si-NBO-K moieties dissociate to some extent to produce Si-NBO $^-$  and  $K^+$ , with the former moiety being present on  $Q^0$ - $Q^3$  species. The  $Q^3$  species dominates K-disilicate melt and where it approaches the  $Al_2O_3$  surface the Si-NBO $^-$  moiety attacks under-coordinated Al sites on the surface (Lewis acid sites). Successful attack results in formation of a Si-O-Al moiety attached to the  $Al_2O_3$  surface, with bonding electrons being donated by the base (i.e.,  $NBO^-$ ). Reaction 1.3 converts the attacking  $NBO^-$  to a BO, thereby converting the reactant  $Q^3$  species (i.e.,  $[Q^3]^-$ ) to a  $Q^4$  species. Subsequent detachment of Al from the surface yields a Si-O-Al moiety in the melt. Some surface or near-surface O atoms likely accompany the detached Al, with most being NBOs due to Al-O bond rupture. Reactions within the melt convert the Al-NBOs to Al-BOs, coupled with the reaction with K, produces the  $KAlO_2$  melt species.

Production of  $Q^4$  species during dissolution compensates for production of the less stable  $KAlO_2$  melt species so that dissolution of  $Al_2O_3$  does not affect appreciably melt stability either thermodynamically or kinetically. From a broader perspective, the thermodynamic and kinetic stabilities of alkali-Al-bearing silicate melts result from redistribution of electron densities, originally localized on NBOs, to BO atoms associated with both Si and Al tetrahedra. Without redistribution, Al-bearing melts would be less stable than observed, and the composition of melts produced in the upper mantle, and the composition and evolution of the crust, would be different from what is observed today. For instance, it is likely that feldspars would not be as common and that would have implications for the biosphere.

## 1.6. References

- Bruckner, R., Chun, H. U., and Goretzki, H., (1978) Photoelectron spectroscopy (ESCA) on alkali silicate and soda aluminosilicate glasses. *Glastechnische Berichte – Glass Science and Technology* **1**, 1-7.
- Bruckner, R., Chun, H. U., Goretzki, H., and Sammet, M., (1980) XPS measurements and structural aspects of silicate and phosphate glasses. *Journal of Non-Crystalline Solids* **42**, 49-60.
- Calas, G., Henderson, G. S., and Stebbins, J. F., (2006) Glasses and melts: Linking geochemistry and materials science. *Elements* **2**, 265-268.
- Dalby, K. N., Nesbitt, H. W., Zakaznova-Herzog, V. P., and King, P. L., (2007) Resolution of bridging oxygen signals from O 1s spectra of silicate glasses using XPS: Implications for O and Si speciation. *Geochimica et Cosmochimica Acta* **71**, 4297-4313.
- Fincham, C. F. B., and Richardson, F. D., (1954) The behaviour of sulphur in silicate and aluminate melts. *Proceedings of the Royal Society of London, Series A* **223**, 40-62.
- Fraser, D. G., (1977) Thermodynamic properties in silicate melts. In: *Thermodynamics in Geology* (ed. D. G. Fraser), pp. 301-326. D. Reidel Dordrecht.
- Gedeon, O., Zemek, J., and Jurek, K., (2008) Changes in alkali-silicate glasses induced with electron radiation. *Journal of Non-Crystalline Solids* **354**, 1169-1171.
- Greaves, G.N., (1985) EXAFS and the structure of glass. *Journal of Non-Crystalline Solids* **71**, 203-217.
- Henderson, G. S., (2005) The structure of silicate melts: A glass perspective. *The Canadian*

- Mineralogist* **43**, 1921-1958.
- Hess, P. C., (1971) Polymer model of silicate melts. *Geochimica et Cosmochimica Acta* **35**, 289-306.
- Hochella, M. F., (1988) Chapter 13: Auger electron and X-ray photoelectron spectroscopies. In: *Spectroscopic Methods in Mineralogy and Geology* (ed. F. C. Hawthorne) Reviews in Mineralogy and Geochemistry **18**, pp. 573-637.
- Hochella, M. F. Jr, and Brown, G. E. Jr., (1988) Aspects of silicate surface and bulk structural analysis using X-ray photoelectron spectroscopy (XPS). *Geochimica et Cosmochimica Acta* **52**, 1641-1648.
- Kaneko, Y., Nakamura, H., Yamane, M., Mizoguchi, K., and Suginozawa, Y., (1983) Photoelectron spectra of silicate glasses containing trivalent cations. *Yogyo-Kyokai-Shi* **91** [7], 321-324.
- Kuo, L.-C., and Kirkpatrick, R. J., (1985) Kinetics of crystal dissolution in the system diopside-forsterite-silica. *American Journal of Science* **285**, 51-90.
- Lam, D. J., Paulikas, A. P., and Veal, B. W., (1980) X-ray photoemission spectroscopy studies of soda aluminosilicate glasses. *Journal of Non-Crystalline Solids* **42**, 41-48.
- Maekawa, H., Maekawa, T., Kawamura, K., and Yokokawa, T., (1991) The structural groups of alkali silicate glasses determined from  $^{29}\text{Si}$  MAS-NMR. *Journal of Non-Crystalline Solids* **127**, 53-64.
- Malfait, W. J., Halter, W. E., Morizet, Y., Meier, B. H., and Verel, R., (2007) Structural control on bulk melt properties: Single and double quantum  $^{29}\text{Si}$  NMR spectroscopy on alkali-silicate glasses. *Geochimica et Cosmochimica Acta* **71**, 6002-6018.
- Matsumoto, S., Nanba, T., and Miura, Y., (1998) X-ray photoelectron spectroscopy of alkali silicate glasses. *Journal of the Ceramic Society of Japan* **106**, 415-421.
- Miura, Y., Matsumoto, S., Nanba, T. and Akazawa, T., (2000) X-ray photoelectron spectroscopy of sodium aluminosilicate glasses. *Physics and Chemistry of Glasses* **41**, 24-31.
- Monaghan, B. J., Nightingale, S. A., Chen, L., and Brooks, G. A., (2004) The dissolution behaviour of selected oxides in  $\text{CaO-SiO}_2\text{-Al}_2\text{O}_3$  slags. *VII International Conference on Molten Slags, Fluxes and Salts*, South African Institute of Mining and Metallurgy, 585-594.
- Mysen, B. O., and Richet, P., (2005) *Silicate Glasses and Melts: Properties and Structure*.



- Elsevier, Amsterdam, 544 p.
- Nasikas, N. K., Chrissanthopoulos, A., Bouropoulos, N., Sen, S., and Papatheodorou, G. N., (2011) Silicate glasses at the ionic limit: Alkaline-earth sub-orthosilicates. *Chemistry of Materials* **23**, 3692-3697.
- Nasikas, N. K., Edwards, T. G., Sen, S., and Papatheodorou, G. N., (2012) Structural characteristics of novel Ca-Mg orthosilicate and suborthosilicate glasses: Results from  $^{29}\text{Si}$  and  $^{17}\text{O}$  NMR spectroscopy. *The Journal of Physical Chemistry B* **116**, 2696-2702.
- Nesbitt, H. W., (2002) Interpretation of x-ray photoelectron spectra with applications to mineralogy and geochemistry. In: *Synchrotron Radiation: Earth, Environmental and Materials Sciences Applications* (eds. Henderson, G. S., Baker, D. S.), Mineralogical Association of Canada Short Course 30, 131-158.
- Nesbitt, H. W., and Bancroft, G. M., (2014) Chapter 7: High resolution core- and valence-level XPS studies of the properties (structural, chemical and bonding) of silicate minerals and glasses. In: *Spectroscopic Methods in Mineralogy and Materials Sciences* (eds. G. S. Henderson, D. R. Neuville, R.T. Downs) Reviews in Mineralogy and Geochemistry **78**, pp. 271-330
- Nesbitt, H.W., and Young, G.M., (1984) Prediction of some weathering trends of plutonic and volcanic rocks based on thermodynamic and kinetic considerations. *Geochimica et Cosmochimica. Acta* **48**, 1523-1534.
- Nesbitt, H. W., Bancroft, G. M., Davidson, R., McIntyre, N. S., and Pratt, A. R., (2004) Minimum XPS core-level line widths of insulators, including silicate minerals. *American Mineralogist* **89**, 878-882.
- Nesbitt, H. W., Bancroft, G. M., Henderson, G. S., Ho, R., Dalby, K. N., Huang, Y., and Yan, Z., (2011) Bridging, non-bridging and free ( $\text{O}^{2-}$ ) oxygen in  $\text{Na}_2\text{O-SiO}_2$  glasses: An X-ray Photoelectron Spectroscopic (XPS) and Nuclear Magnetic Resonance (NMR) study. *Journal of Non-Crystalline Solids* **357**, 170-180.
- Nesbitt, H. W., Bancroft, G. M., Henderson, G. S., Sawyer, R., and Secco, R. A., (2015) Direct and indirect evidence for free oxygen ( $\text{O}^{2-}$ ) in MO-silicate glasses and melts (M = Mg, Ca, Pb). *American Mineralogist* **100**, 2566-2578.
- Nesbitt, H.W., Henderson, G.S., Bancroft, G.M., Sawyer, R., and Secco, R.A., (2017) Bridging oxygen speciation and free oxygen ( $\text{O}^{2-}$ ) in K-silicate glasses: Implications for

- spectroscopic studies and glass structure. *Journal of Non-Crystalline Solids* **461**, 13–22.
- Onorato, P. I. K., Alexander, M. N., Struck, C. W., Tasker, G. W., and Uhlmann, D. R., (1985) Bridging and nonbridging oxygen atoms in alkali aluminosilicate glasses. *Journal of the American Ceramic Society* **68** [6], C-148-C-150.
- Schaller, T., Stebbins, J. F., and Wilding, M. C., (1999) Cation clustering and formation of free oxide ions in sodium and potassium lanthanum silicate glasses: Nuclear magnetic resonance and Raman spectroscopic findings. *Journal of Non-Crystalline Solids* **243**, 146-157.
- Scholze, H., (1991) *Glass: Nature, Structure and Properties* (trans. M. J. Lakin). Springer-Verlag, New York, 454 p.
- Schwerdtfeger, K., (1966) Dissolution of solid oxides in oxide melts. The rate of dissolution of solid silica in Na<sub>2</sub>O-SiO<sub>2</sub> and K<sub>2</sub>O-SiO<sub>2</sub> melts. *Journal of Physical Chemistry* **70**, 2131-2136.
- Shaw, C. S., (2004) Mechanisms and rates of quartz dissolution in melts in the CMAS (CaO–MgO–Al<sub>2</sub>O<sub>3</sub>–SiO<sub>2</sub>) system. *Contributions to Mineralogy and Petrology* **148**, 180-200.
- Shaw, C. S. J., (2006) Effects of melt viscosity and silica activity on the rate and mechanism of quartz dissolution in melts of the CMAS and CAS systems. *Contributions to Mineralogy and Petrology* **151**, 665-680.
- Shaw, C. S. J., (2012) The effects of potassium addition on the rate of quartz dissolution in the CMAS and CAS systems. *Contributions to Mineralogy and Petrology* **164**, 839-857.
- Shaw, C. S. J., Klausen, K. B., and Mao, H., (2018) Kinetics of dissolution of sapphire in melts in the CaO–Al<sub>2</sub>O<sub>3</sub>–SiO<sub>2</sub> system. *Geochimica et Cosmochimica Acta* **229**, 129-146.
- Shaw D. M., Reilly G. A., Muysson J. R., Pattenden G. E., and Campbell, F. E., (1967) An estimate of the chemical composition of the Canadian Precambrian Shield. *Canadian Journal of Earth Sciences* **4**, 829-853.
- Shaw D.M., Reilly G.A., Muysson J.R., Pattenden G.E. and Campbell, F.E., (1967) An estimate of the chemical composition of the Canadian 645 Precambrian Shield. *Can. Jour. Earth Sci.* **4**, 829-853.
- Shirley, D. A., (1972) High resolution x-ray photoelectron spectrum of the valence band of gold. *Physical Review B* **5** [12], 4709-4714.
- Smets, B. M. J., and Lommen, T. P. A., (1982) The structure of glasses and crystalline

- compounds in the system PbO-SiO<sub>2</sub>, studied by X-ray Photoelectron Spectroscopy. *Journal of Non-Crystalline Solids* **48**, 423-430.
- Stebbins, J. F., (2020) Anionic speciation in sodium and potassium silicate glasses near the metasilicate ([Na,K]<sub>2</sub>SiO<sub>3</sub>) composition: <sup>29</sup>Si, <sup>17</sup>O and <sup>23</sup>Na MAS NMR. *Journal of Non-Crystalline Solids: X* **6**, 100049.
- Stebbins, J. F., and Sen, S., (2013) Oxide ion speciation in potassium silicate glasses: New limits from <sup>17</sup>O NMR. *Journal of Non-Crystalline Solids* **368**, 17-22.
- Stebbins, J. F., (2017) “Free” oxide ions in silicate melts: Thermodynamic considerations and probably effects of temperature. *Chemical Geology* **461**, 2-12.
- Tasker, G., Uhlmann, D., Onorato, P., Hoole, A., and Struck, C., (1985) Structure of sodium aluminosilicate glasses: X-ray photoelectron spectroscopy. *Journal de Physique Colloques* **46** [C8], C8-273-C8280.
- Taylor S. R., and McLennan S. M., (1981) The composition and evolution of the continental crust: rare earth element evidence from sedimentary rocks. *Philosophical Transactions of the Royal Society of London* **A301**, 381-399.
- Thompson, L. M., McCarty, R. J., and Stebbins, J. F., (2012) Estimating accuracy of <sup>17</sup>O NMR measurements in oxide glasses: Constraints and evidence from crystalline and glassy calcium and barium silicates. *Journal of Non-Crystalline Solids* **358**, 2999-3006.
- Toop, G. W., and Samis, C. S., (1962) Activities of ions in silicate melts. *Transactions of the Metallurgical Society of America* **224**, 878-887.
- Warren, B. E., (1934) The diffraction of X-rays in glass. *Physical Review* **45**, 657-661.
- Wedepohl, K. H., (1969) The handbook of Geochemistry. v. 1, (ed. K. H. Wedepohl), pp. 247-248, Springer-Verlag.
- Zachariasen, W. H., (1932) The atomic arrangement in glass. *Journal of the American Chemical Society* **54**, 3841-3850.
- Zemek, J., Jiricek, P., Gedeon, O., Lesiak, B., Jozwik, A., (2005) Electron irradiated potassium-silicate glass surfaces investigated by XPS. *Journal of Non-Crystalline Solids* **351**, 1665-1674.
- Zhang, P., Grandinetti, P. J., and Stebbins, J. F., (1997) Anionic species determination in CaSiO<sub>3</sub> glass using two-dimensional <sup>29</sup>Si NMR. *Journal of Physic Chemistry B* **101**, 4004-4008.
- Zhang, Y., Walker, D., and Lesher, C. E., (1989) Diffusive crystal dissolution. *Contributions to*

*Mineralogy and Petrology* **102**, 492-513.

## Chapter 2

### 2.0. HIGH RESOLUTION X-RAY PHOTOELECTRON SPECTROSCOPY (XPS) STUDY OF $K_2O-SiO_2$ GLASSES: EVIDENCE FOR THREE TYPES OF O AND AT LEAST TWO TYPES OF Si<sup>1</sup>

#### 2.1 INTRODUCTION

The recent use of effective charge compensation methods for XPS has allowed for the collection of high-resolution spectra and chemical state information of insulators. Line widths for insulators, comparable to those of semi-conductors, can now be obtained on a routine basis (Nesbitt et al., 2004). XPS is just now becoming a useful tool for the study of silicate glasses. XPS is a powerful technique due to its sensitivity and ability to obtain bulk chemical state information and it is providing new insights into the structural species within glasses (Nesbitt, 2002). Previous thermodynamically based models on the activities of metal oxides in silicate glasses have been proposed (Fraser, 1977; Hess, 1975; Nesbitt and Fleet, 1981; Nesbitt and Dalby, 2005). Those relating specifically to Pb (Hess, 1975; Nesbitt and Fleet, 1981; Nesbitt and Dalby, 2005), have been found to agree with a recent experimental XPS study of  $Pb_2O-SiO_2$  glasses (Dalby et al., 2007). XPS studies of Pb-silicate (Dalby et al., 2007) and Na-silicate (Nesbitt et al., 2011) glasses have shown evidence for three types of oxygen species within the glass network. The study of Na silicate glass by XPS has also provided evidence for the presence of two types of BO atoms (Nesbitt et al., 2011); in agreement with other experimental studies (Ching et al., 1983; Ching et al., 1985; Lee and Stebbins, 2009) and computational models which predict the same (Uchino and Yoko, 1998; Du and Cormack, 2004; Mountjoy, 2007; Tilocca and de Leeuw, 2006). XPS has been used to study potassium silicate glasses as well. However, previous XPS studies have focused on the effects of irradiation with an electron beam and the XPS spectra were of low resolution (Zemek et al., 2005; Gedeon et al., 2008). The presence of free oxygen ( $O^{2-}$ ) in small quantities has been noted from  $^{29}Si$  MAS NMR studies of Na- and K-

---

<sup>1</sup> This chapter is a modified version of the publication "Sawyer, R., Nesbitt, H.W. and Secco, R.A., 2012. High resolution X-ray Photoelectron Spectroscopy (XPS) study of  $K_2O-SiO_2$  glasses: Evidence for three types of O and at least two types of Si. *Journal of Non-Crystalline Solids*, 358(2), pp.290-302. doi:10.1016/j.jnoncrysol.2011.09.027"

silicate glasses containing lanthanum (~3% O<sup>2-</sup>) (Schaller et al., 1999) and <sup>29</sup>Si NMR studies of CaSiO<sub>3</sub> glasses (~3% O<sup>2-</sup>) (Zhang et al., 1997). A recent XPS and <sup>29</sup>Si MAS NMR study by Nesbitt et al. (2011) has shown O<sup>2-</sup> to be present in small quantities in Na-silicate glasses (between 2% and 6% in Na-silicate glasses containing 40–50 mol% Na<sub>2</sub>O); corroborating the finding of the aforementioned NMR studies. Molecular dynamic simulations of Al<sub>2</sub>O<sub>3</sub>–MgO glasses (Jahn, 2008), Yttrium–Aluminum–Silicon glasses (Christie and Tilocca, 2010) and Li silicate glasses (Prasada Rao et al., 2010) have also indicated the presence of O<sup>2-</sup>. In this work we report a core level XPS study of K<sub>2</sub>O–SiO<sub>2</sub> glasses, emphasizing the O 1s, Si 2p and K 2p spectral lines. The XPS data provide evidence for two types of BO atoms and the presence of O<sup>2-</sup>; an oxygen atom not bonded to a silicon atom. Additionally, the XPS Si 2p data indicate at least two Q-species whose abundances correlate with measurements of Q<sup>4</sup> and Q<sup>3</sup> species from previous NMR studies (Maekawa et al., 1991; Sen and Youngman, 2003; Malfait et al., 2007).

## 2.2. EXPERIMENTAL METHOD

### 2.2.1. Sample Preparation

Preparation follows the procedures outlined in Nesbitt et al. (2011). Nine compositions of K<sub>2</sub>O–SiO<sub>2</sub> glasses were prepared using K<sub>2</sub>CO<sub>3</sub> and SiO<sub>2</sub> powders as starting materials. The compositions were crushed in anhydrous ethanol, sintered at temperatures 200 °C below their melting points, crushed again and melted at temperatures 200 °C above their melting points. Samples were sintered and melted in a platinum crucible. All glasses were clear with no inhomogeneities present when observed under a binocular microscope. Compositions were prepared at 10, 15, 17, 20, 23, 27, 30 and 35 mol% K<sub>2</sub>O with two separate preparations and analyses carried out on the 15 mol% K<sub>2</sub>O composition to check for reproducibility. Several attempts were made to synthesize a glass at 25 mol% K<sub>2</sub>O but a homogenous sample could not be obtained. Samples were quenched in air. Pellets for analysis were cut with a diamond saw and notched to facilitate their fracture in the XPS transfer chamber. Glass pellets were fractured under the vacuum conditions (~10<sup>-8</sup> Torr) of the XPS transfer chamber in order to obtain a clean surface for analysis. The pellets were then immediately transferred to the XPS analysis chamber. All glass samples were stored in a sealed desiccator containing desiccant in order to minimize exposure to atmospheric moisture.

### 2.2.2. XPS Analysis

Analyses were conducted using a Kratos Ultra Axis X-ray Photoelectron Spectrometer with an Al K- $\alpha$  source operating at 210 W. Vacuum pressures in the sample introduction and transfer chambers were on the order of  $10^{-8}$  Torr whereas pressures in the analysis chamber were on the order of  $10^{-9}$  Torr. Survey scans (e.g., Figure 2.1) for the compositions at 10, 15 and 20 mol% K<sub>2</sub>O were collected over a range of binding energies from 0 eV to 1100 eV with a step size of 0.7 eV and a dwell time of 76 ms. Similar scans for the compositions at 15, 17, 23, 27, 30 and 35 mol% K<sub>2</sub>O were collected over a binding energy range of 0 eV to 600 eV with a step size of 0.3 eV and a dwell time of 60 ms. The narrower binding energy range and decreased step size were used to obtain higher resolution survey scans in order to more precisely evaluate sample compositions. All survey scans were completed in 3 sweeps of 2 min each with pass energies of 160 eV. Narrowscans were collected over a 10–15 eV binding energy range with step sizes of 0.025 eV, dwell times of 100 ms and pass energies of 10 eV. For narrow scans, the spectral resolution is approximately 0.4 eV (Nesbitt et al., 2004). A magnetic confinement charge compensation system was used during analysis in order to obtain the narrowest possible spectral linewidths (Nesbitt et al., 2004). Three or four survey scans were collected for each sample at the beginning, middle and end of analysis. Four to six sequential narrow scans of the O 1s, Si 2p and K 2p/C 1s signals were collected for each composition.

## 2.3. RESULTS AND INTERPRETATION OF SPECTRA

### 2.3.1. Constraints Used to Fit XPS Spectra

The CASAXPS software program was used to fit all XPS spectra. Spectral fits were made using Gaussian–Lorentzian line shapes with a constant 30% Lorentzian component. The broad and narrow scan backgrounds were fit using Shirley backgrounds (Shirley, 1972). All spectra were calibrated to the standard energy of 285 eV for the C 1s peak.

The O 1s and C 1s signals are each composed of a singlet and one peak was used to fit these spectra where peak positions (or binding energies, BE), linewidths and intensities (areas) were treated as fit parameters. The K 2p and Si 2p signals are composed of a spin-orbit doublet; the 2p<sub>3/2</sub> and 2p<sub>1/2</sub> peaks, and the constraints used to fit these spectra are noted at the beginning of Sections 2.3.3 and 2.3.4. Peak areas were used as the measure of the intensity of all peaks.

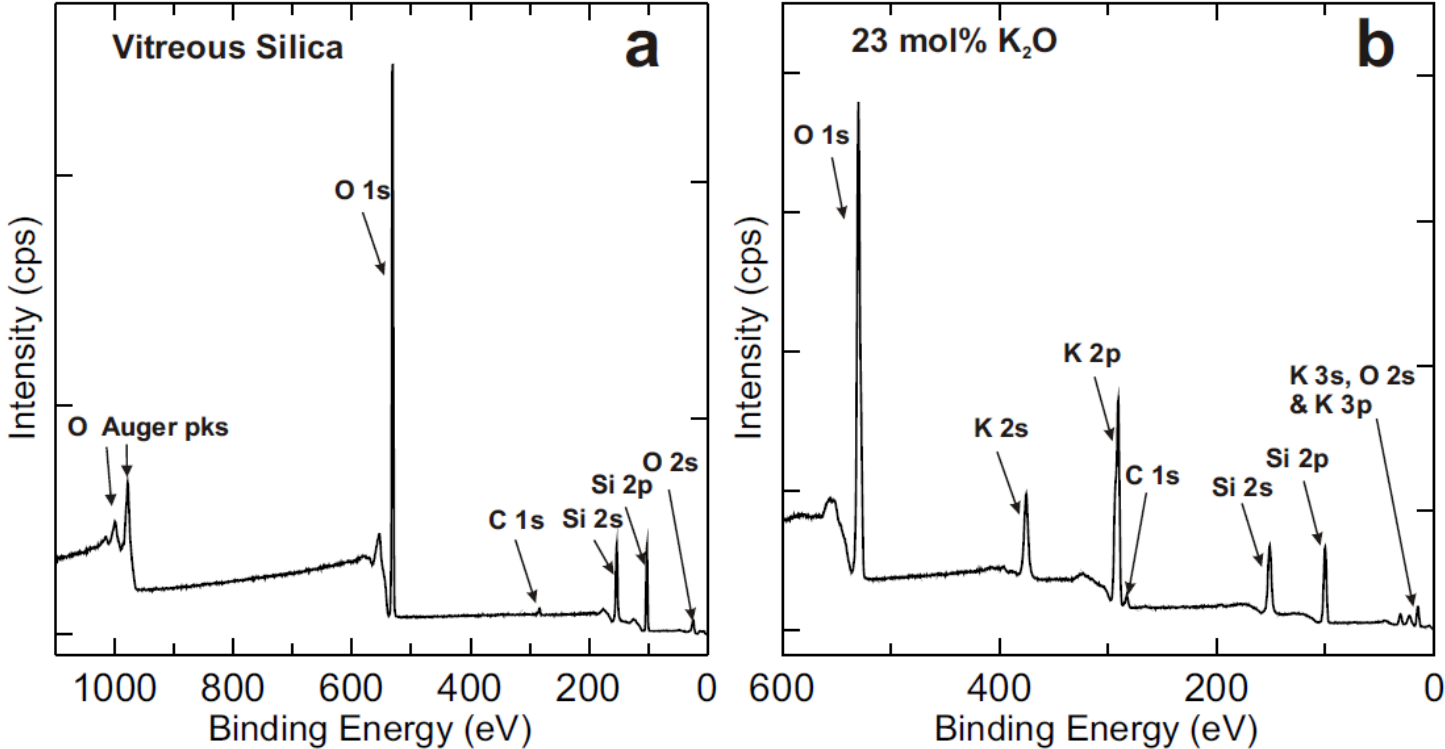


Figure 2.1: Survey scans of (a) vitreous silica and (b) potassium silicate glass with 23 mol % K<sub>2</sub>O. Major spectral lines are labeled.



### 2.3.1.1. Spin-orbit Split Doublets

The K 2p spectrum of Figure 2.2 consists of a spin-orbit split doublet composed of two peaks: a K 2p<sub>3/2</sub> component and a K 2p<sub>1/2</sub> component. The binding energy separating the K 2p<sub>3/2</sub> and K 2p<sub>1/2</sub> peaks obtained from our experiments is 2.77 eV. This energy splitting is constant for all K 2p doublets with the K 2p<sub>3/2</sub> peak located at the lower BE. The K 2p<sub>1/2</sub> peak intensity is constrained by theory to be half the intensity of the K 2p<sub>3/2</sub> peak and these K 2p spectra indicate that the two peaks also have the same FWHM within the precision of the measurements. These three constraints are applied to all K 2p spectral signals so that the K 2p<sub>1/2</sub> peak is completely constrained by the spectral properties of the K 2p<sub>3/2</sub> peak.

Si 2p spectra are illustrated in Figs. 2.3 and 2.4. Each Si 2p contribution to these spectra is, from theoretical considerations, composed of two peaks (spin-orbit split doublets) separated by 0.617 eV (Southerland et al., 1992). The intensity of the Si 2p<sub>1/2</sub> peak is constrained by theory to be half the intensity of the Si 2p<sub>3/2</sub> peak and studies of other silicates have shown that the Si 2p<sub>3/2</sub> and Si 2p<sub>1/2</sub> peaks have similar FWHM (Nesbitt et al., 2004; Zakaznova-Herzog et al., 2006). These constraints were applied to all Si 2p signals so that the Si 2p<sub>1/2</sub> peaks were completely constrained by the properties of the Si 2p<sub>3/2</sub> peaks.

### 2.3.2. Bulk Glass Compositions by XPS and Homogeneity

As illustrated in the broadscans of Figure 2.1a and b, K, Si and O are the dominant elements. There is a small C 1s peak at 285.0 eV which represents adventitious carbon adsorbed to the surface. The adventitious carbon is derived from the residual gasses in the analytical chamber and is present at less than 3 at.% (sub-monolayer coverage) at the commencement of analyses. Its surface character was proved in separate experiments from those reported here where a 35 mol% K<sub>2</sub>O glass sample contaminated with chlorine was sputtered. Upon sputtering, only the K, Si and O signals remained, demonstrating the surface origin of the C 1s signal and the Cl contaminant. There was no indication of CO<sub>2</sub> in the XPS spectra. The CO<sub>2</sub> signal has a binding energy value between about 290 eV and 292 eV in the C 1s spectrum and no such peak was present in any of the broadscans. The bulk compositions of the glasses were determined by

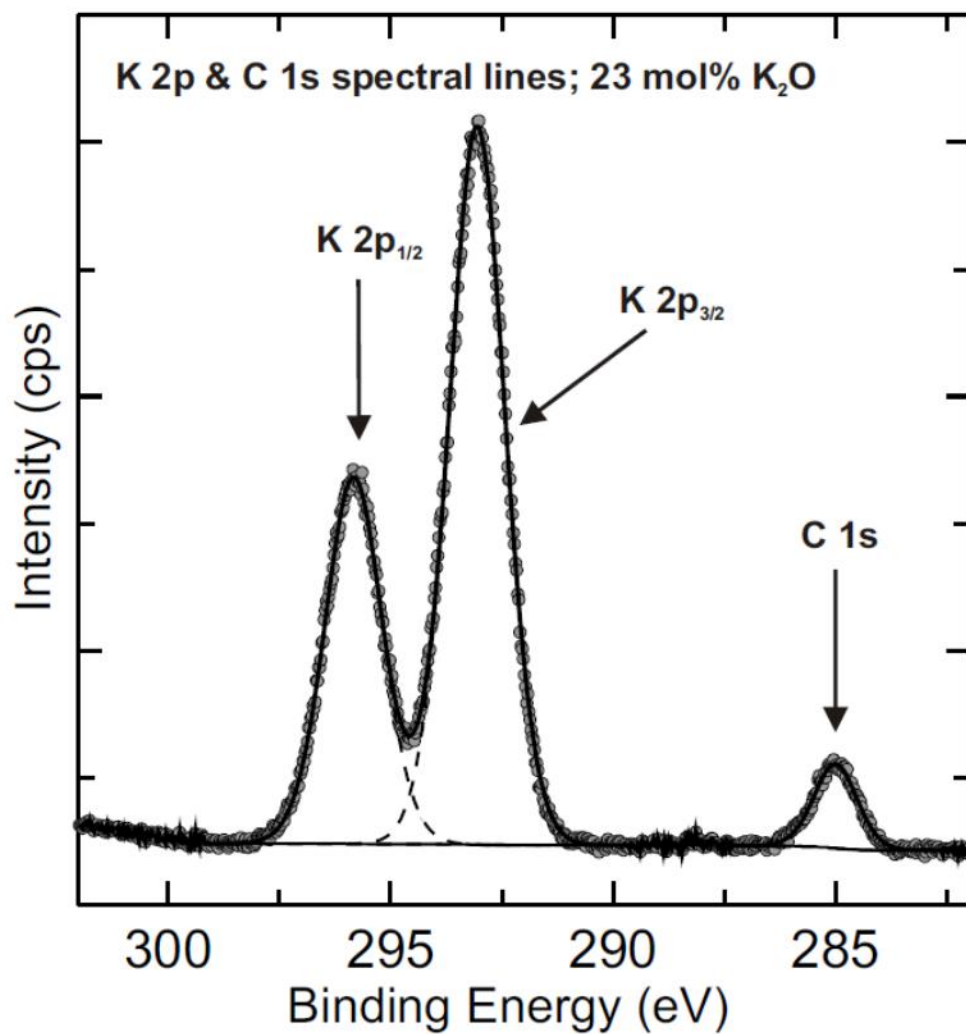


Figure 2.2: K 2p spectrum for 23 mol % K<sub>2</sub>O sample. The C 1s peak is also shown. The K 2p<sub>1/2</sub> peak is constrained by the properties of the K 2p<sub>3/2</sub> peak. A Shirley background was used. Fit parameters are given in Table 2.2.

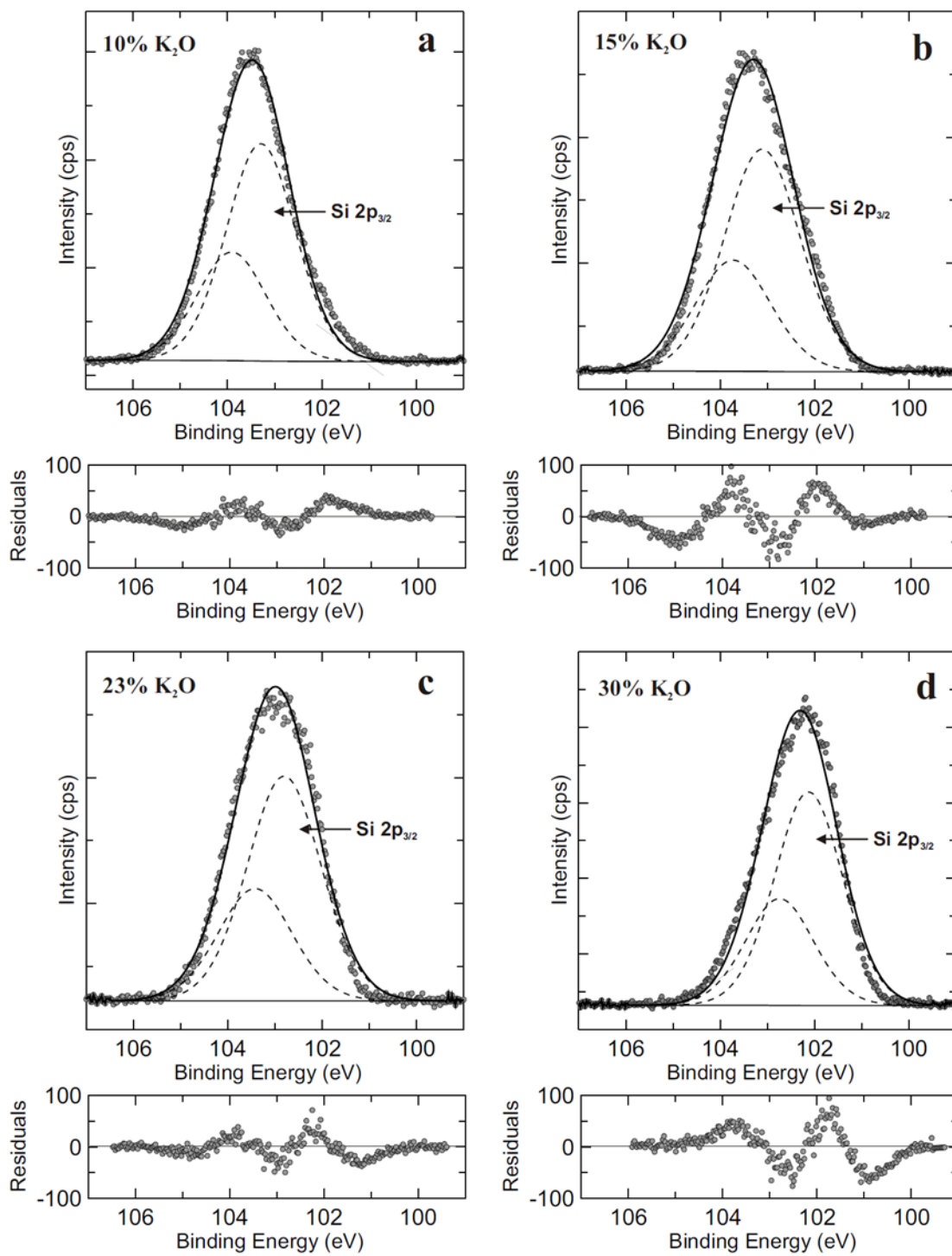
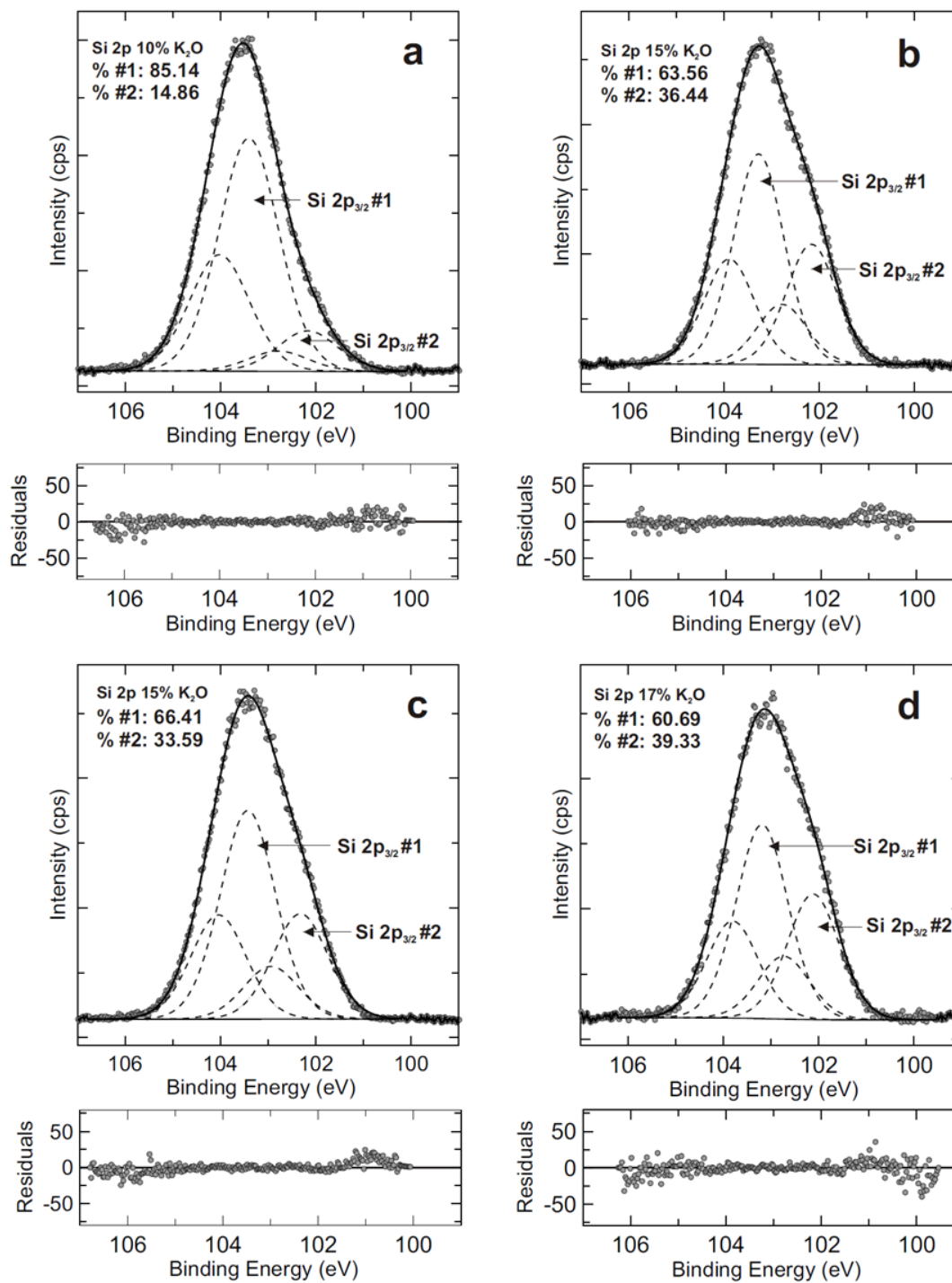
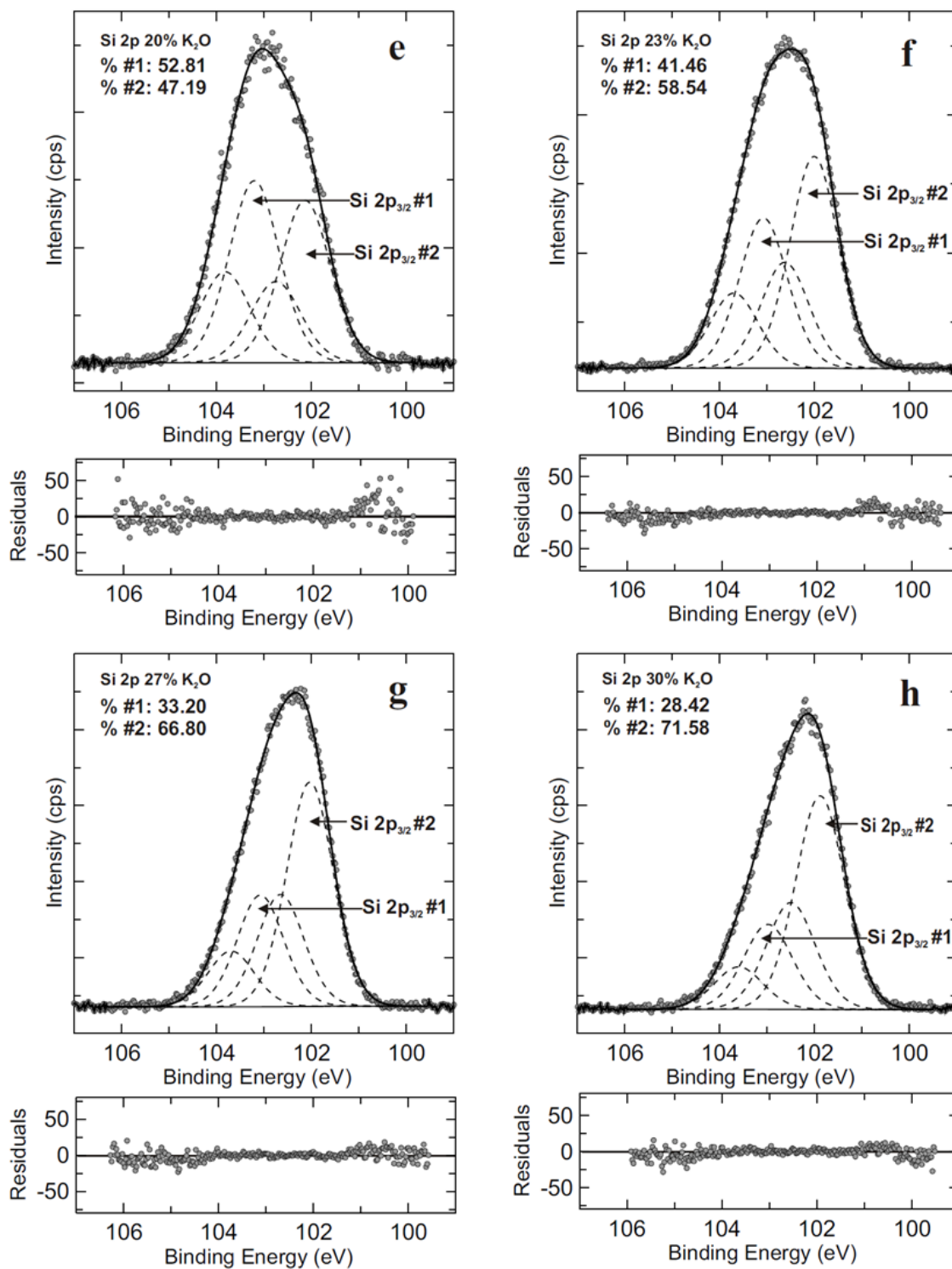


Figure 2.3: Si 2p spectra of select compositions over the entire range studied fit with one Si 2p<sub>3/2</sub>





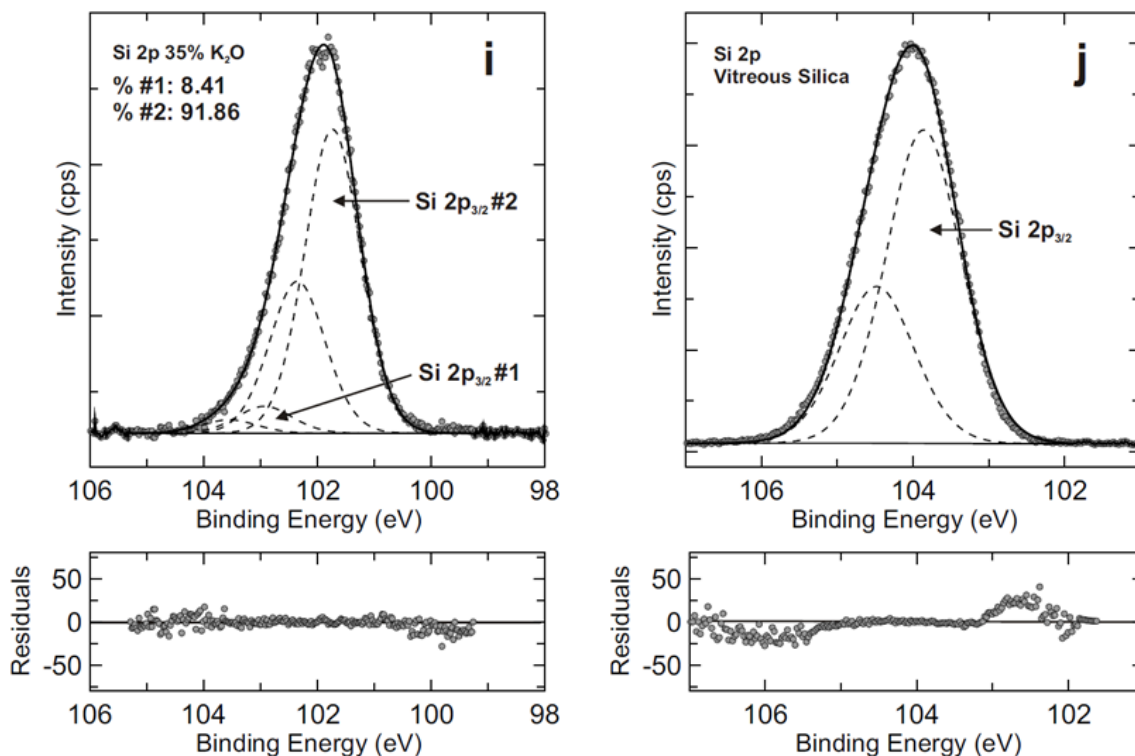


Figure 2.4: Si 2p spectra of vitreous silica and the potassium silicate glass compositions analyzed along with the fit residuals. Each spectrum was fit with two Si 2p<sub>3/2</sub> - Si 2p<sub>1/2</sub> spin-orbit split doublets (solid curves) where the Si 2p<sub>1/2</sub> is constrained by the properties of the Si 2p<sub>3/2</sub> peak. A Shirley background was used, and the fits are represented by solid lines through the data points. Peak fit parameters are listed in Table 2.2.

quantifying the XPS broadscan spectra. The atomic percentages of the K 2p and Si 2s lines were used to obtain the atomic proportions of the two elements in each glass. These proportions were recast to represent mol%  $K_2O$  and  $SiO_2$  and these results are compared with the synthetic compositions (Table 2.1). The XPS results are necessarily approximate because elemental sensitivity factors (based on X-ray capture cross sections in elemental form) were used to convert signal intensity to atomic proportions. The XPS analyses are all within 3 mol% of the synthetic compositions with six being within 2 mol%. The O 1s signal was not used to evaluate oxygen atomic percent because its B.E. (hence kinetic energy of O 1s photoelectrons) is appreciably different from those of K 2p and Si 2s signals. The kinetic energies of the K 2p and Si 2s photoelectrons are similar indicating that they were derived from a similar depth in the solid. Including the O 1s signal in calculations of compositions would degrade the results since its kinetic energy is different meaning the O 1s photoelectrons were derived from a different depth. Zemek et al. (2005) state that compositional variations can occur along the path of glass surface fractures. Though this may seem problematic, only 5%–15% of the total O 1s spectral signal is due to surface contributions with the remainder 85%–95% being derived from the bulk of the glass. Thus, surface contributions have minimal effect on our O 1s and other spectra. Furthermore, great care was taken to analyze smooth fracture surfaces and if a fractured surface was not smooth, no spectra were collected.

To test the ability of XPS to detect phase separated regions, separate samples of 20, 25 and 30 mol% were prepared according to the same procedures described above. Up to three spots on each sample were analyzed to check assumptions of homogeneity. All glasses were within 3 mol% of the synthetic compositions and the results for each spot were consistent with each other (Table 2.1).

### 2.3.3. K 2p Spectra

A K 2p spectrum of the 23 mol% glass is illustrated in Figure 2.2 and the fit parameters to the K 2p spectrum of this and other glasses are provided in Table 2.2. The BE of the K  $2p_{3/2}$  peak shifts to lower binding energy with increasing potassium content, ranging from 293.49 eV at 10 mol%  $K_2O$  to 292.89 eV at 35 mol%  $K_2O$  (Table 2.2). Each glass was analyzed a minimum of three

Table 2.1: Potassium Silicate Glass Compositions Synthesized and Compared with XPS Analysis

Sample	Position <sup>a</sup>	Synthesized (mol%)		Calculated <sup>b</sup> (mol%)		XPS Abundances (at%)		
		SiO <sub>2</sub>	K <sub>2</sub> O	SiO <sub>2</sub>	K <sub>2</sub> O	Si	O	K
<b>1</b>	<b>1</b>	90	10	91.3	8.7	33.1	60.6	6.3
<b>2</b>	<b>1</b>	85	15	81.9	18.1	24.4	64.8	10.8
<b>3</b>	<b>1</b>	85	15	83.6	16.4	27.3	62.0	10.7
<b>4</b>	<b>1</b>	83	17	82.1	17.9	27.9	59.9	12.2
<b>5</b>	<b>1</b>	80	20	78.9	21.1	27.7	57.5	14.8
<b>6</b>	<b>1</b>	77	23	74.2	25.8	23.8	59.7	16.5
<b>7</b>	<b>1</b>	73	27	70.9	29.1	23.3	57.5	19.2
<b>8</b>	<b>1</b>	70	30	71.2	28.8	24.5	55.7	19.8
<b>9</b>	<b>1</b>	65	35	62.4	37.6	21.2	53.2	25.6
<b>10</b>	<b>1</b>	80	20	79.8	20.2	25.9	61.0	13.1
	<b>2</b>	80	20	78.3	21.7	25.2	60.9	13.9
	<b>3</b>	80	20	80.6	19.4	25.4	62.3	12.2
<b>11</b>	<b>1</b>	75	25	73.1	26.9	23.7	58.8	17.4
	<b>1</b>	75	25	72.6	27.4	23.0	59.5	17.4
	<b>2</b>	75	25	72.5	27.5	23.4	58.9	17.7
	<b>2</b>	75	25	72.3	27.7	23.0	59.4	17.6
	<b>3</b>	75	25	72.5	27.5	22.9	59.7	17.4
	<b>3</b>	75	25	73.0	27.0	23.3	59.6	17.2
<b>12</b>	<b>1</b>	70	30	68.7	31.3	22.4	57.2	20.4
	<b>1</b>	70	30	68.5	31.5	22.7	56.4	20.9
	<b>2</b>	70	30	68.0	32.0	22.6	56.2	21.2
	<b>2</b>	70	30	67.5	32.5	22.2	56.4	21.4
	<b>3</b>	70	30	67.3	32.7	21.6	57.4	21.0
	<b>3</b>	70	30	67.0	33.0	21.5	57.4	21.1

<sup>a</sup>“Position” indicates that analyses were taken from certain positions on the sample

<sup>b</sup> Values are calculated from XPS abundanc



Table 2.2: Peak Parameters Derived from Fitting XPS Spectra: K 2p<sup>a</sup> and Si 2p<sup>a</sup> (BE<sup>b</sup> and FWHM in eV)

mol % K <sub>2</sub> O	K 2p <sub>3/2</sub>		Si 2p <sub>3/2</sub> #1		%	Si 2p <sub>3/2</sub> #2		
	BE (±2σ <sup>d</sup> )	FWHM	BE (±2σ)	FWHM		BE (±2σ)	FWHM	%
10(n <sup>c</sup> =6)	293.49(0.10)	1.71	103.41(0.10)	1.48	85.14	102.17(0.17)	1.48	14.86
15(n=4)	293.18(0.10)	1.53	103.27(0.11)	1.25	63.56	102.17(0.10)	1.25	36.44
15(n=6)	293.35(0.05)	1.61	103.43(0.10)	1.37	66.41	102.32(0.10)	1.37	33.59
17(n=6)	293.17(0.04)	1.50	103.19(0.12)	1.28	60.69	102.11(0.10)	1.28	39.33
20(n=5)	293.12(0.03)	1.51	103.20(0.10)	1.25	52.81	102.13(0.10)	1.25	47.19
23(n=6)	293.06(0.11)	1.48	103.08(0.13)	1.20	41.46	102.01(0.14)	1.20	58.54
27(n=6)	292.90(0.10)	1.40	103.08(0.14)	1.16	33.20	102.03(0.14)	1.16	66.80
30(n=6)	292.90(0.14)	1.51	102.98(0.14)	1.22	28.42	101.88(0.14)	1.22	71.58
35(n=6)	292.89(0.10)	1.37	102.93(0.22)	1.15	8.14	101.73(0.12)	1.15	91.86

<sup>a</sup>K 2p<sub>1/2</sub> and Si 2p<sub>1/2</sub> peaks were fit from K 2p<sub>3/2</sub> and Si 2p<sub>3/2</sub> peak parameters

<sup>b</sup>BE values indicate the binding energy of the peak at maximum intensity of fitted peak

<sup>c</sup>“n=...” refers to the number of spectra collected

<sup>d</sup>Indicates the standard deviation of the peak maximum for collected spectra

times and over the period of data collection the BE of the K 2p<sub>3/2</sub> peak was found to deviate by less than 0.2 eV at the 95% confidence interval.

The Full Width at Half Maximum (FWHM) of the K 2p<sub>3/2</sub> peaks fitted to the spectra are variable but generally decrease with increasing potassium content from 1.71 eV at 10 mol% K<sub>2</sub>O to 1.37 eV at 35 mol% K<sub>2</sub>O. Analogy with the Na<sub>2</sub>O–SiO<sub>2</sub> glasses (Nesbitt et al., 2011) suggests that K, like Na, may reside in two (or more) sites in the glass just as observed in Na-silicate crystalline phases (Ching et al., 1983), although this aspect requires further study. Residence of K on two different energetic sites should result in different electron densities over K in each site, thus giving rise to slightly different binding energies. The breadth of the K 2p peaks is likely related to final state vibrational contributions rather than to different types of K contributing to the K 2p signal. The discussion concerning the siting of K in these glasses is speculative in nature and aspects such as agglomeration cannot be proved or disproved using the properties of the K 2p spectra given current instrumental resolutions.

#### 2.3.4. Si 2p Spectra

Si 2p experimental results are illustrated in Figures 2.3 and 2.4. In Figure 2.3 the spectra are fitted with one Si 2p spin-orbit split doublet (the Si 2p<sub>3/2</sub> and Si 2p<sub>1/2</sub> peaks) and as is apparent from inspection of the residuals plots (located below each spectrum) the least squares best fits are poor. Good fits to the spectra can be obtained only by including a second Si 2p spin-orbit split doublet. The least squares best fits to the data using two Si 2p doublets are illustrated in Figure 2.4. The fit parameters are summarized in Table 2.2.

Considering only the spin-orbit split doublet located at the highest binding energy (Table 2.2, labeled Si 2p<sub>3/2</sub> #1), the Si 2p<sub>3/2</sub> peak BE ranges from 103.41 eV to 102.93 eV (Table 2.2) and BE decreases with increased K<sub>2</sub>O content. The BE peak maximum for vitreous silica is 103.85 eV (Nesbitt et al., 2011). A quadratic least squares fit to the BE of the peak maximum vs. mole fraction of K<sub>2</sub>O yields  $BE_{\max} = 0.0003(X_{K_2O})^2 - 0.0343X_{K_2O} + 103.75$  (n=9, R<sup>2</sup>=0.90 where n represents the first scan of each composition and R<sup>2</sup> is the goodness of fit). The relationship is slightly non-linear as indicated by the coefficient of the quadratic term. The strong correlation indicates that charge compensation is consistent across the compositional range studied, and that standardization with the C 1s line is reasonable. The shift of Si 2p<sub>3/2</sub> BE to lower values indicates

increased valence electron density on the Si nuclei with increased  $K_2O$  content, as observed for the  $Na_2O-SiO_2$  suite of glasses (Nesbitt et al., 2011). The linewidths for both Si 2p contributions were constrained to be equal. This constraint was applied to limit uncertainty and there is good reasoning for it. The breadth of the Si 2p signal is determined by final state vibrational contributions. A previous study by Bancroft et al. (2009) showed that Si-O bonding yields similar vibrational envelopes for all Q-species so that each Q-species should have about the same FWHM.

The binding energies separating the two Si  $2p_{3/2}$  peaks fitted to the spectra of Figure 2.4 (Table 2.2, Si  $2p_{3/2}$  #1 and Si  $2p_{3/2}$  #2 columns) range between 1.24 eV to 1.05 eV for the nine glasses studied. The average value for the BE separation is 1.11 eV ( $\pm 0.12$  eV at a 95% confidence interval). This near-constant value of 1.11 eV separating the two doublets in the Si 2p spectra of all glasses warrants an explanation and one is offered by reference to Q-species.

#### 2.3.4.1. Relationship to Q-species

Each Q-species may give rise to a separate signal in XPS spectra because the electron density over the central, tetrahedrally coordinated Si atom should be affected by the number of bridging and non-bridging oxygen atoms bonded to it. The electronegativity of K is much less than that of Si so that there should be a greater electron density over the NBO atoms than over BO atoms bonded only to Si atoms because K effectively relinquishes its 3s electron to the NBO. Ergo, the greater the number of NBO atoms bonded to a Si atom, the greater the electron density over the central Si atom, and the lower the binding energy of the peak.

Some common minerals contain only one type of Q-species. The Si  $2p_{3/2}$  signal for olivine (containing  $Q^0$  only) is 101.7 eV (Zakaznova-Herzog et al., 2008) whereas the Si  $2p_{3/2}$  signal for orthopyroxene (containing  $Q^2$  only) and vitreous silica (containing  $Q^4$  only) are located respectively at 102.7 eV and 103.85 eV. These results demonstrate that the binding energies of the Q-species are strongly affected by the number of NBO bonded to the central Si atom, with BE decreasing systematically from  $Q^4$  to  $Q^0$  species. The strongly asymmetric nature of the Si 2p spectra of the potassic glasses may result from two or more Q-species contributions to the Si 2p spectra (e.g., Figure 2.4). Each Si 2p peak was fit with two Si  $2p_{3/2}$ -Si  $2p_{1/2}$  spin orbit split doublets (Si  $2p_{3/2}$  #1 and #2; Si  $2p_{1/2}$  #1 and #2).

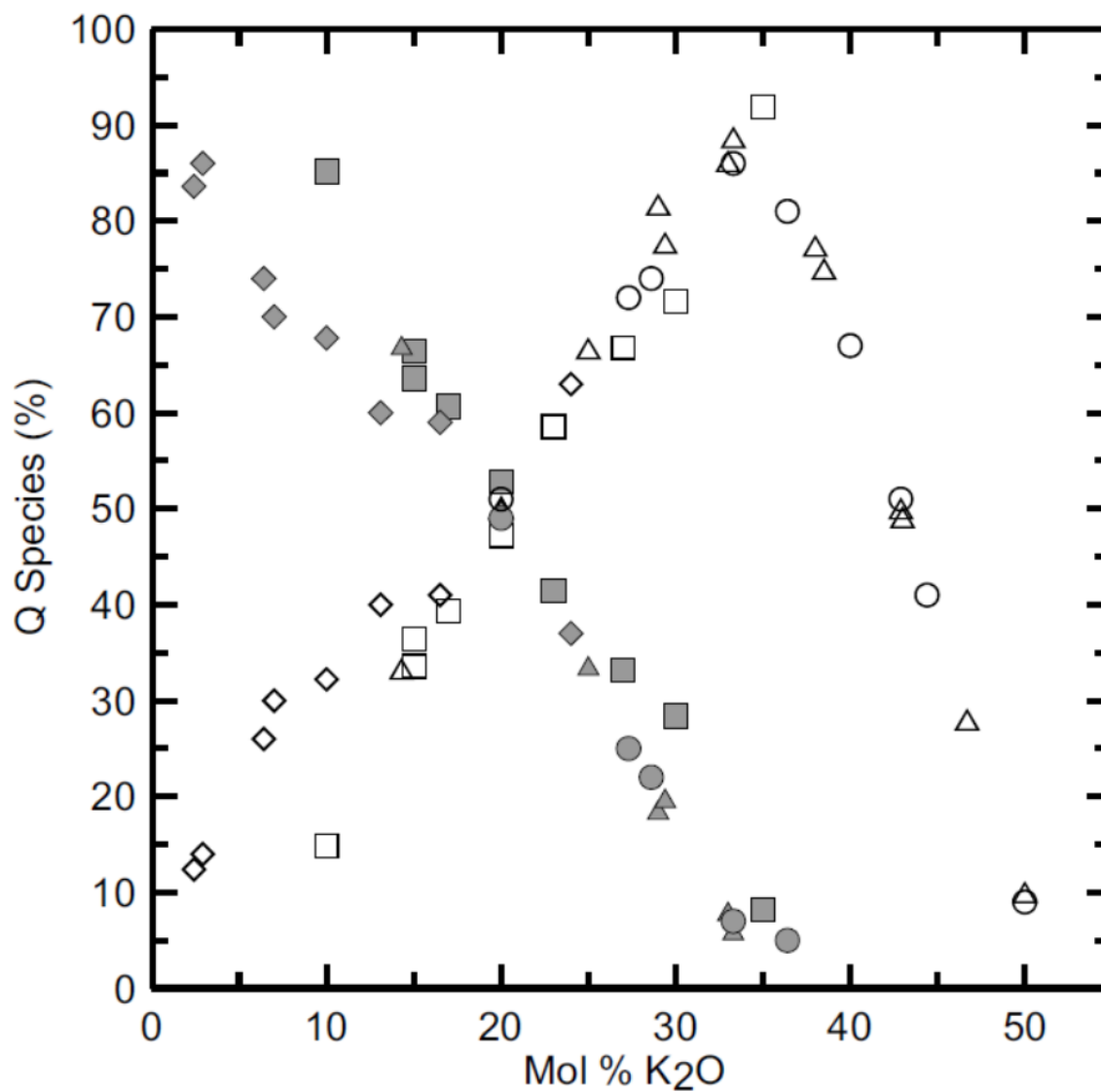
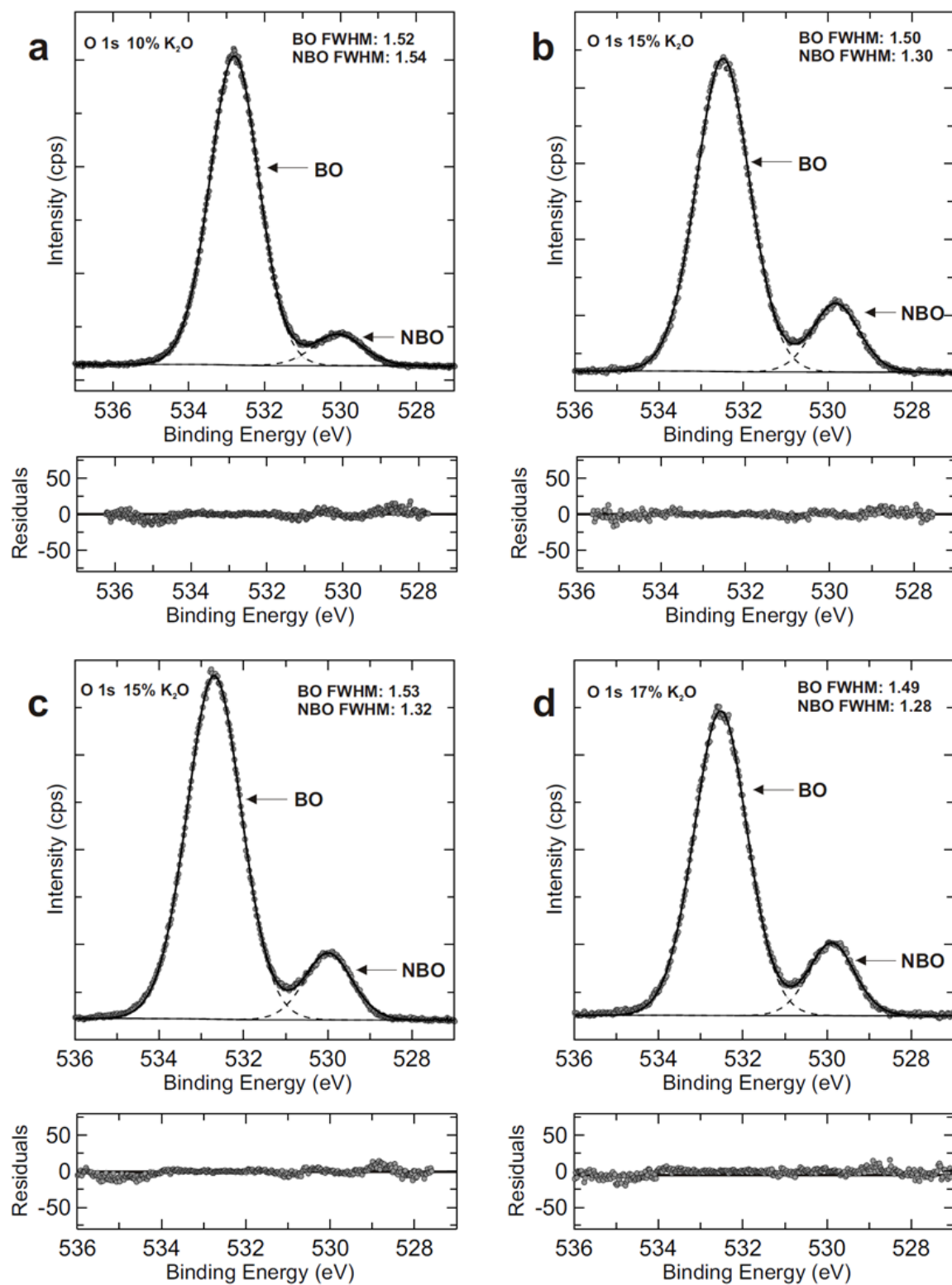


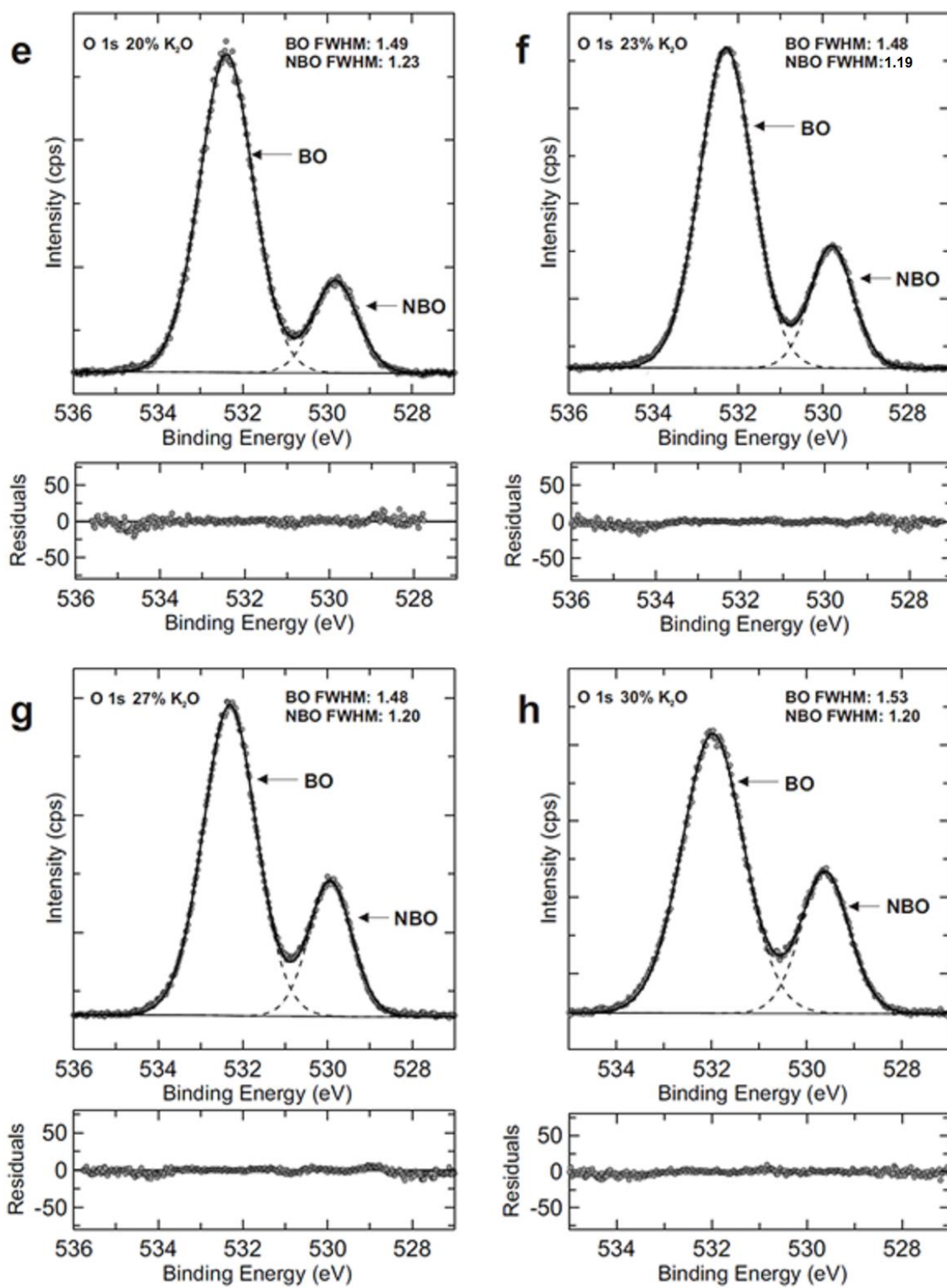
Figure 2.5: Comparison of the abundances of the two Si  $2p_{3/2}$  contributions with the abundances of  $Q^4$  and  $Q^3$  species from NMR studies (Maekawa et al., 1991; Malfait et al., 2007; Sen and Youngman, 2003) The filled shapes represent the abundance of the high binding energy Si  $2p_{3/2}$  contribution from this study (squares, uncertainty of  $\pm 2$  mol%  $K_2O$ ) and the  $Q^4$  NMR abundances from Maekawa et al. (1991) (circles), Malfait et al. (2007) (triangles) and Sen and Youngman (2003) (diamonds). The open shapes represent the abundance of the low binding energy Si  $2p_{3/2}$  contribution from this study and the  $Q^3$  abundances from the aforementioned NMR studies.

The high binding energy doublet of the glass containing 10 mol% K<sub>2</sub>O (Figure 2.4a, labeled #1) has much higher intensity than the low energy doublet (Figure 2.4a, labeled #2). An increase in K<sub>2</sub>O to 15 mol% (Figure 2.4b) results in a decrease in the intensity of the high binding energy doublet (Figure 2.4b, #1) and an increase in intensity of the lower BE doublet (Figure 2.4b, #2). The overall trend is that the contribution at higher binding energy decreases in intensity with increased potassium abundance whereas the contribution at lower binding energy increases. This behavior is consistent with an increase in Q<sup>3</sup> species relative to Q<sup>4</sup> species as K content of the glass increases as demonstrated by NMR studies (Maekawa et al., 1991; Sen and Youngman, 2003; Malfait et al., 2007). In Figure 2.5, the Si 2p<sub>3/2</sub> abundances of the two contributions (Table 2.2, Si 2p<sub>3/2</sub> #1 and Si 2p<sub>3/2</sub> #2) were normalized to 100%, assigned to Q<sup>4</sup> and Q<sup>3</sup> species abundances, and plotted on Figure 2.5 as filled and open squares, respectively. Also shown in Figure 2.5 are the abundances of Q<sup>4</sup> and Q<sup>3</sup> species obtained from three NMR studies (Maekawa et al., 1991; Sen and Youngman, 2003; Malfait et al., 2007). Although the results of Sen and Youngman (2003) for low K<sub>2</sub>O glasses (X<sub>K<sub>2</sub>O</sub> < 13 mol%) are discrepant relative to these XPS results, there is a remarkable correspondence among all data over the compositional range 12 to 37 mol% K<sub>2</sub>O. From this we conclude that changes to the shapes and breadth of the XPS Si 2p spectra result from changed proportions of Q-species in the glasses. Two of the NMR studies (Maekawa et al., 1991; Malfait et al., 2007) show small amounts (~3%) of Q<sup>2</sup> species present in the glass starting at ~30 mol% K<sub>2</sub>O. Our spectra are of too low resolution to resolve a Q<sup>2</sup> species peak at small quantities.

### 2.3.5. O 1s Spectra

Two peaks constitute the O 1s spectra of Figures 2.6a–j and two unconstrained peaks were used to fit each O 1s spectrum. Results of the fits are listed in Table 2.3. Inspection of the residuals (illustrated below the spectra) indicates that the two-peak fit reproduces well the experimental data. The O 1s spectra include contributions from all oxygen spectra in the glass. As demonstrated by previous studies (e.g., Nesbitt et al., 2011 and references therein), the higher binding energy peak in sodic glasses is attributed to oxygen bridging two Si atoms (BO peak) and the second, lower BE peak, is derived from other types of oxygen bridging Na and Si atoms (e.g., NBO peak).





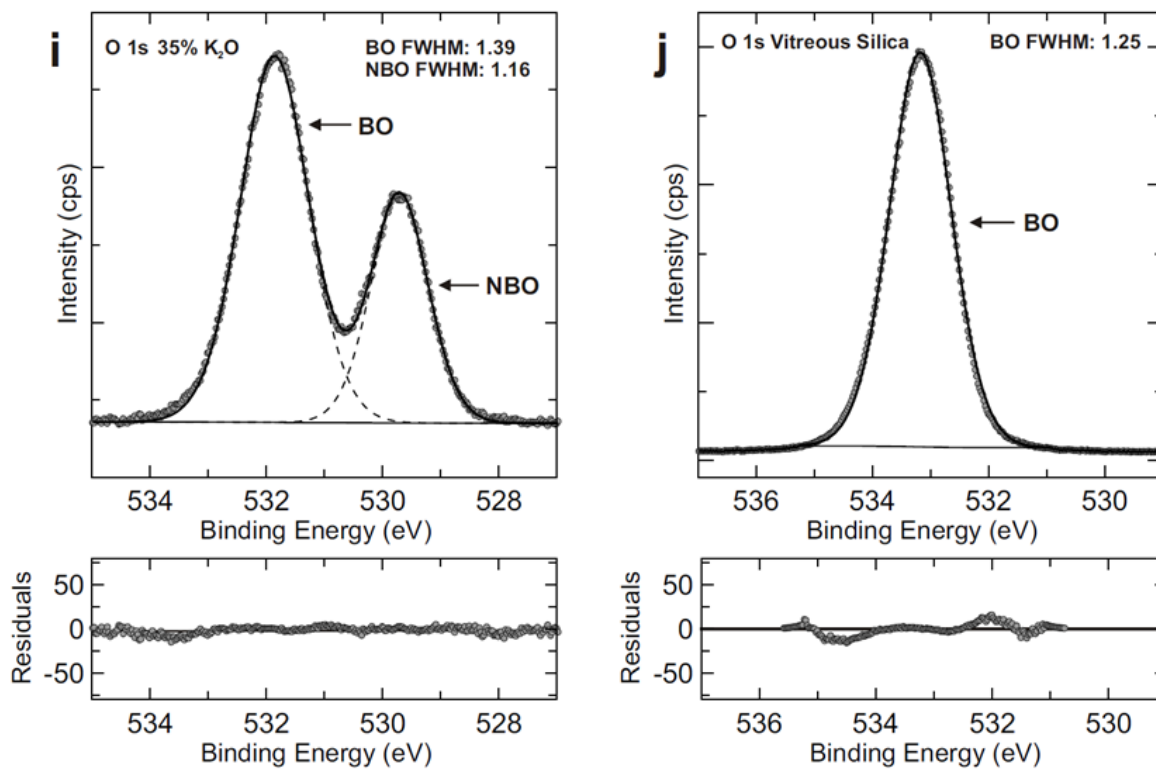


Figure 2.6: O 1s spectra of vitreous silica and the potassium silicate glasses studied along with the fit residuals. The BO and NBO peaks were fitted freely with no constraints. A Shirley background was used, and the fits are represented by solid lines intersecting the data points. Peak fit parameters are listed in Table 2.3.



### 2.3.5.1. X-ray Beam Effects on O 1s Spectra

Exposure to the X-ray beam causes the ratio of the two O 1s peaks to change with time of exposure. Following the approach of Nesbitt et al. (2011), O 1s spectra were collected as a function of time, with 4 to 6 spectra collected during each XPS analytical session (typically about 600 min). Two examples of changing O 1s BO peak percentages are illustrated in Figure 2.7. A polynomial fit to the data was used to extrapolate to zero time from which was obtained the BO at.% of the glass before exposure to the X-ray beam. These values are quoted in Table 2.4. Abundances of BO increased or decreased depending on the composition of each glass. This behavior requires further investigation and could be related to the size of the  $K^+$  cation and mobility over the course of analysis.

### 2.3.6. Comparison of O 1s XPS and NMR Results

The percentages of BO listed in Table 2.3 are plotted on Figure 2.8 (shaded squares, size of the squares represents an uncertainty of  $\pm 2$  mol%  $K_2O$ ) as are percentages of BO calculated from experimental NMR data (Maekawa et al., 1991; Sen and Youngman, 2003; Malfait et al., 2007) (Figure 2.8 circles, triangles, diamonds). The XPS and NMR data are consistent between about  $0.13 < X_{K_2O} < 0.25$  (Figure 2.8), demonstrating that the two techniques can yield similar results. The XPS and NMR results diverge, however, at the extremes of the compositions studied. It should be noted that none of the NMR studies used for comparison provided uncertainties for their data.

Sen and Youngman (2003) measured Q-species abundances at  $X_{K_2O}$  values  $< 0.10$  (Figure 2.8, shaded diamonds). These data fall within the miscibility gap in the  $K_2O-SiO_2$  system and two-phase domains or segregations may exist in these samples (Kracek et al., 1929). However, Sen and Youngman (2003) contend that no phase separation was present in their glasses due to the lack of any characteristic differential relaxation in the  $^{29}Si$  NMR signals. Nevertheless, their data for low  $K_2O$  glasses are inconsistent with the other NMR studies mentioned and our XPS data. Their data for glasses containing greater than 15%  $K_2O$  are, however, consistent with the other NMR and XPS data (Figure 2.8).

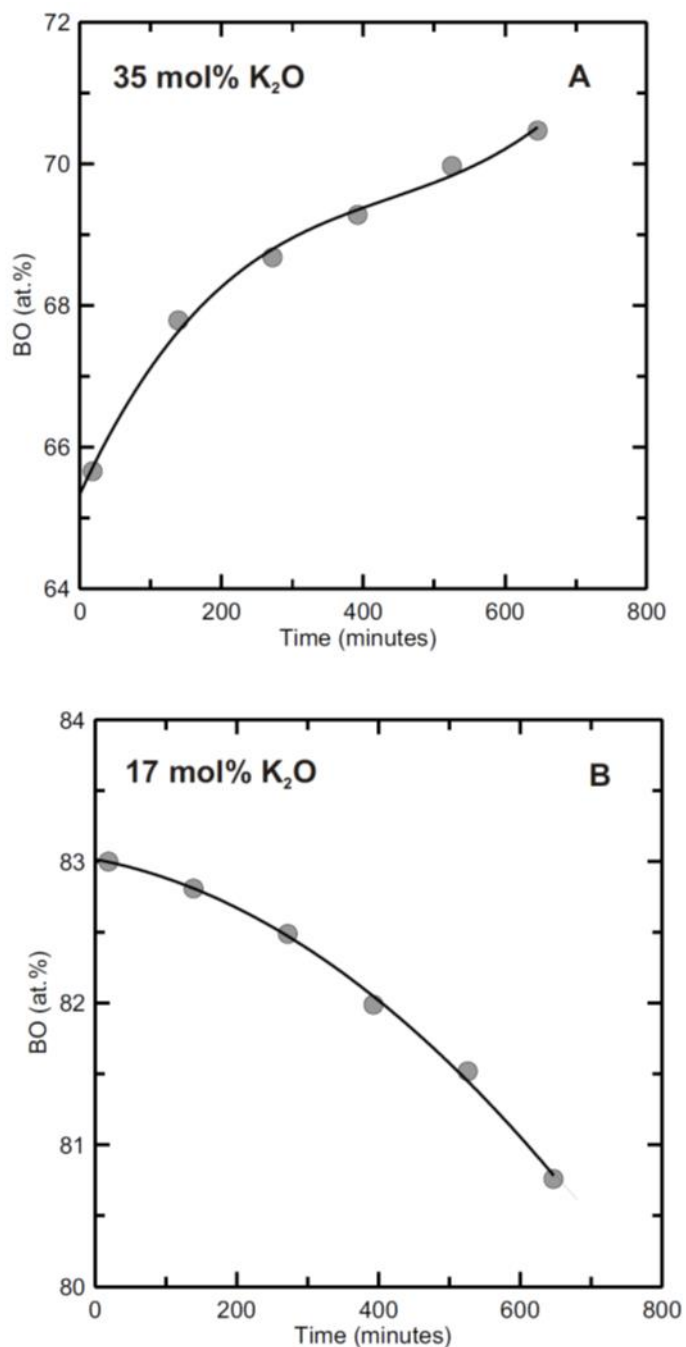


Figure 2.7: Examples of BO mol % as a function of time of exposure to the X-ray beam for two samples (35 mol % and 17 mol % K<sub>2</sub>O). The BO abundances with analysis time for all samples are given in Table 2.4. Data points were fit with a polynomial line and the y-intercept indicates the BO mol % in the glass prior to analysis. This procedure was used to obtain the BO mol % for all glasses studied and the extrapolated values are given in Table 2.3.

Table 2.3: Peak Parameters Derived from Fitting XPS Spectra, O 1s (BE and FWHM in eV)

mol % K <sub>2</sub> O	BO			NBO		
	BE ( $\pm 2\sigma^c$ )	FWHM	% Signal	BE ( $\pm 2\sigma$ )	FWHM	% Signal
10(n <sup>b</sup> =6)	532.80(0.10)	1.52	90.66	530.06(0.12)	1.54	9.34
15(n=4)	532.48(0.10)	1.50	83.98	529.81(0.12)	1.30	16.02
15(n=6)	532.69(0.10)	1.53	85.63	529.99(0.10)	1.32	14.37
17(n=6)	532.53(0.10)	1.49	83.00	529.89(0.11)	1.28	17.00
20(n=5)	532.38(0.10)	1.49	80.60	529.80(0.10)	1.23	19.40
23(n=6)	532.28(0.14)	1.48	76.40	529.78(0.14)	1.19	23.60
27(n=6)	532.31(0.14)	1.48	73.94	529.93(0.12)	1.20	26.06
30(n=6)	531.97(0.21)	1.53	71.61	529.61(0.16)	1.20	28.39
35(n=6)	531.86(0.16)	1.39	65.66	529.71(0.10)	1.16	34.34

<sup>a</sup>BE values indicate the binding energy of the peak at maximum intensity of fitted peak

<sup>b</sup>“n=...” refers to the number of spectra collected

<sup>c</sup>Indicates the standard deviation of the peak maximum for collected spectra

Table 2.4: Effect of Photon Source on BO Abundance

10% K <sub>2</sub> O		15% K <sub>2</sub> O		15% K <sub>2</sub> O		17% K <sub>2</sub> O		20% K <sub>2</sub> O	
BO%	t(min)	BO%	t(min)	BO%	t(min)	BO%	t(min)	BO%	t(min)
90.66	18	83.98	18	85.63	19	83.00	19	80.60	23
91.03	192	83.86	104	85.99	140	82.81	139	79.94	33
90.73	366	82.63	202	86.49	273	82.49	272	79.53	151
90.20	552	81.88	301	86.04	393	81.99	393	79.10	283
90.61	726			86.00	526	81.52	526	78.87	402
90.33	899			86.06	647	80.76	647		
23% K <sub>2</sub> O		27% K <sub>2</sub> O		30% K <sub>2</sub> O		35% K <sub>2</sub> O			
BO%	t(min)	BO%	t(min)	BO%	t(min)	BO%	t(min)		
76.40	19	73.94	18	71.61	18	65.66	18		
76.47	140	74.82	138	72.46	139	67.79	139		
76.93	273	75.19	271	73.36	272	68.85	272		
76.99	393	75.82	392	73.85	393	69.46	392		
76.97	526	75.66	524	74.01	526	70.15	525		
76.69	647	76.33	645	75.58	706	70.78	646		

Between  $0.25 < X_{K_2O} < 0.35$ , the XPS data plot at slightly greater BO values than do the NMR data. The reason for this is uncertain but a similar observation was observed in the  $Na_2O-SiO_2$  glass system (Nesbitt et al., 2011). Nesbitt et al. (2011) attributed the discrepancies to different conditions of synthesis of the glasses in each study. The same explanation may pertain to the  $K_2O-SiO_2$  results because the synthesis conditions are different for the XPS and NMR experiments here compared. Maekawa et al. (1991) prepared all glasses at 1267 °C and melted each for 3 h regardless of composition which in some instances might lead to alkali loss for high-alkali samples. On the other hand, Malfait et al. (2007) melted sample mixtures three times for 1 hour each (less for samples containing high alkali concentrations) at 100 K above their respective melting points. The issue is not primarily one of alkali loss, but that slightly different melt structures may be “frozen” into the glass due to different synthesis conditions and quench rates. Additional study is required to resolve these discrepancies in glasses of high  $K_2O$  content.

## 2.4. DISCUSSION

### 2.4.1. Oxygen Species in Potassium Silicate Glasses

Zachariasen (1932) developed the Continuous Random Network (CRN) model to explain properties of silicate glass. A premise of the model is that the addition of 1 mol of each oxide network modifier (e.g.,  $K_2O$ ,  $Na_2O$ ,  $CaO$ ) to  $SiO_2$  glass (or melt), produces two moles of NBO at the expense of one mole of BO. The reaction may be written using neutral entities:



or using oxygen species and simplified:



where  $O^{2-}$  is here referred to as ‘free oxygen’. Where Reaction (2.1a) goes to completion, there can be only two oxide species, BO and NBO, at compositions more siliceous than the orthosilicate composition and the mole fraction of BO calculated from that premise is illustrated in Figure 2.8 by the solid curve representing BO ( $K_2=\infty$ ). In addition, the premise of the CRN model requires NBO alone to be present at the orthosilicate composition, and the two species

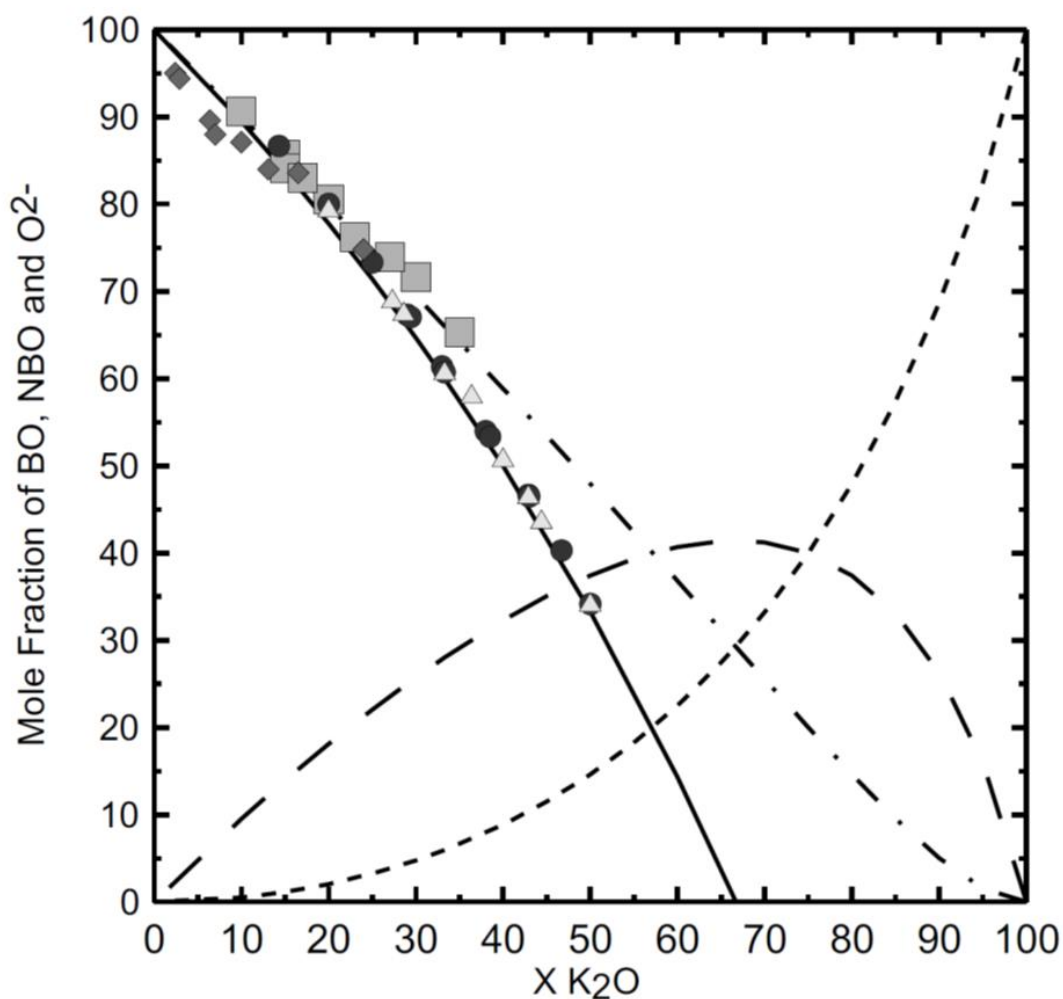


Figure 2.8: Mol fractions of different types of oxygen as a function of composition (given in  $X(K_2O)$ ). XPS data (squares) from this study were obtained from measurements of the BO peaks of the O 1s spectra. The XPS data are compared with the NMR data from studies by Maekawa *et al.* (1991) (circles), Malfait *et al.* (2007) (triangles) and Sen and Youngman (2003) (diamonds). The fraction of BO (solid line) was calculated using Eq. 2.2 where  $K_2 = \infty$ . The fractions of BO (dot-dash line), NBO (long dashed line) and  $O^{2-}$  (short, dashed line) were calculated assuming  $K_2 = 2.0$ . The squares representing the XPS data are drawn to reflect the estimated errors associated with both  $K_2O$  content and the abundance of BO.

NBO and  $O^{2-}$  to be present in compositions less siliceous than the orthosilicate composition (BO is absent).

An early diffraction study of sodium silicate glasses by Warren and Biscoe (1938) found that some oxygen atoms were bonded to two silicon atoms (BO) whereas others were bonded only to one (NBO). The sodium atoms were coordinated to six oxygen atoms and were found in random pockets within the glass network. They also found that the number of NBO increases with the addition of network modifiers. All findings were consistent with the CRN model.

The Modified Random Network (MRN) model (Greaves et al., 1981; Greaves, 1985) considered the structure of alkali silicate glass to be an extension of crystalline silicates with two interconnected sub lattices. One sub-lattice is a continuous, disordered  $SiO_2$  network. It is penetrated by a second sublattice containing modifying cations (e.g., Na, K) where NBO atoms link the two sub-lattices. The cations form clusters around the NBO atoms leading to the formation of percolation channels. Ionic and channel diffusion measurements are consistent with the MRN model (Ingram, 1987).

Molecular dynamic simulations (Huang and Cormack, 1990; Huang and Cormack, 1991; Smith et al., 1995; Du and Cormack, 2004; Meyer et al., 2004; Pedone et al., 2008) show inhomogeneous distributions of elements at high silica compositions. That is to say, there are  $SiO_2$  rich regions and regions rich with network modifiers. As more network modifiers are added, the modifier-rich regions extend and form NBO rich channels, which is again consistent with the MRN model. The MRN also allows for the existence of more than two types of oxygen species in glasses more siliceous than the orthosilicate composition.

#### 2.4.2. Two Types of BO From XPS Spectra

For all potassic glasses studied, the FWHM of the BO peaks are consistently broader and more variable than the associated NBO peaks, ranging from 1.39 eV to 1.53 eV (Table 2.3) just as observed for sodium silicate glasses (Nesbitt et al., 2011). They differ, however, from the results reported for the lead silicate system by Dalby et al. (2007), where both BO and NBO line widths were similar at about 1.23 eV.

It is true that K will have many different sites in the glasses that will likely change with composition, given changes in coordination number. For the sake of brevity, the following

discussion is concerned with only two types of K sites: one in which K is bonded to a BO atom affecting its binding energy, and one where it is not. Na- and Li-disilicate crystalline phases (e.g.,  $\text{Na}_2\text{Si}_2\text{O}_5$ ) include two types of bridging oxygen atoms (Ching et al., 1983; Ching et al., 1985). One type has oxygen bonded only to two Si atoms (Si-O-Si). The second type again bridges two Si atoms, but it is also bonded to a Na atom where the Na-BO bond length is similar to Na-NBO bond lengths. Ab initio molecular orbital calculations on a cluster of atoms modeling the structure of sodium disilicate glass (Uchino and Yoko, 1998) demonstrate that sodium is coordinated to both BOs and NBOs. Molecular dynamic simulations (Du and Cormack, 2004; Mountjoy, 2007) also show that network modifiers bond to both BO and NBO. Additionally, Car-Parrinello molecular dynamic simulations on sodium silicate and soda-lime silicate glasses (Tilocca and de Leeuw, 2006) have shown that the coordination environments of Na and Ca are similar and that the local structural sites of the different modifiers are similar when comparing parameters such as bond angles and distances. They also found evidence for two types of bridging oxygen atoms. Recent  $^{17}\text{O}$  NMR spectra of Lee and Stebbins (2009) show changes to both BO and NBO peaks with changes in  $\text{Na}_2\text{O}$  content, suggesting that network modifiers interact with more than one type of oxygen species.

#### 2.4.3. A Third Type of Oxygen, $\text{O}^{2-}$

Two types of oxygen atoms exist at the compositional extremes of the  $\text{K}_2\text{O}$ - $\text{SiO}_2$  system: BO at 100 mol%  $\text{SiO}_2$  (fused silica), and  $\text{O}^{2-}$  at the 100 mol%  $\text{K}_2\text{O}$  (an ionic melt). Within the binary system an additional anionic species, NBO, is present (Figure 2.6) and the question arises concerning the abundance of the three species BO, NBO and  $\text{O}^{2-}$  within the binary system  $\text{K}_2\text{O}$ - $\text{SiO}_2$ .

The three species BO, NBO and  $\text{O}^{2-}$  are required in Na- and Pb-silicate glasses to explain the fractions of BO observed (Dalby et al., 2007; Nesbitt et al., 2011).  $^{17}\text{O}$  NMR experiments on  $\text{CaSiO}_3$  glass (Zhang et al., 1997) have demonstrated that BO and NBO alone could not provide charge balance to the system suggesting that small amounts of  $\text{O}^{2-}$  atoms were present. Other NMR experiments have indicated small amounts of  $\text{O}^{2-}$  in sodium and potassium silicate glasses containing lanthanum (Schaller et al., 1999). Molecular dynamic simulations in the  $\text{Al}_2\text{O}_3$ - $\text{MgO}$  system (where Al acts as a network former and Mg as a network modifier) have shown that, as the amount of network modifiers increases, so too does the amount of  $\text{O}^{2-}$  (Jahn, 2008). Recent

molecular dynamic simulations of Yttrium–Aluminum–Silicate (Christie and Tilocca, 2010) and Li-silicate (Prasada Rao et al., 2010) glasses indicated the presence of small amounts of  $O^{2-}$ .

The  $O^{2-}$  signal itself cannot be resolved in the XPS spectra but its general location can be determined from electronegativity arguments. To summarize, the  $O^{2-}$  signal is located within the NBO peak. The BO peak has a high binding energy due to the low electron density on the oxygen atom bridging two silicon atoms. The NBO peak is at a lower binding energy because the NBO has a greater electron density due to the presence of K in the Si-O-K moiety. The  $O^{2-}$  contribution is bonded to two K atoms (K-O-K moiety) and it too will have a greater electron density than the BO contribution. The  $O^{2-}$  peak is located at a binding energy similar to the NBO peak and it cannot be resolved due to the low abundance of  $O^{2-}$  and its close proximity to the NBO contribution.

#### 2.4.4. Calculated Distribution of Oxygen Species

The XPS data consistently plot at higher  $X_{BO}$  than the solid curve of Figure 2.8. The NMR data, between 13 mol% and 25 mol%  $K_2O$ , also plot at  $X_{BO}$  values greater than indicated by the solid curve. It is important to note that within this compositional range all data plot consistently above the model curve. The XPS and NMR data are therefore consistent indicating a greater fraction of BO in the glasses than predicted from the CRN model of Zachariasen (1932). A thermodynamic analysis provides insight into, and an explanation for, the high BO abundance.

As previously noted, the distribution of BO, NBO and  $O^{2-}$  in alkali silicate glasses may be evaluated using a thermodynamic approach. Halving Reaction (2.1a) yields:



The mass action equation for this reaction is:

$$K_3 = [NBO]^2 / \{[O^{2-}][BO]\}, \quad (2.3)$$

where square brackets denote activities of the oxygen species. The CRN model (Zachariasen, 1932) requires Reaction (2.2) to proceed to completion (i.e., one of the reactants is completely consumed) and the equilibrium constant,  $K_3$  of Reaction (2.3), to be infinite (i.e., either  $O^{2-}$  or  $BO=0$ ). If Reaction (2.2) does not go to completion, then some  $O^{2-}$  remains unconsumed by the reaction and there will be a greater concentration of BO and lower concentration of NBO in the



glass than calculated from the CRN model. In addition, NBO will not be balanced by K; there will be more K than there will be NBO in glasses more siliceous than the orthosilicate composition. The CRN model fails this stringent experimental test and the thermodynamic analysis provides a simple explanation for the failure; Reaction (2.2) does not go to completion (as required by the CRN model). Instead, some  $O^{2-}$  and excess BO is found in the potassic silicate glasses of composition ranging between 10 mol% and 35 mol%  $K_2O$ .

#### 2.4.5. Equilibrium Distribution Among Oxygen Species

Just as equilibrium among Q-species is assumed to exist in alkali silicate glasses (Stebbins, 1987; Maekawa et al., 1991), equilibrium among oxygen species is likely. Following Stebbins (1987) and applying the same approach to oxygen species, a conditional equilibrium constant may be evaluated from the experimental data using mole fraction of BO determined from the experimental data and two compositional constraints. The two equations constraining the concentrations of the oxygen species are Reaction (2.2) and the sum of the mole fractions of the three species=1.0. With these equations and using  $X_{BO}$  as measured by XPS or NMR, the mole fractions of the two other species can be evaluated. The average mole fraction of BO measured at  $X_{K_2O}=0.17$  (Table 2.3) was used to calculate the equilibrium constant,  $K_2=2.0$ , and this value was used to calculate the BO, NBO and  $O^{2-}$  mole fractions for the entire binary system as shown in Figure 2.8 (dash-dot curve represents BO, long dashed curve, NBO and short dashed curve  $O^{2-}$ ).

The calculated BO mole fractions are consistent with both XPS and NMR data in the compositional range 13 mol% to 25 mol%  $K_2O$ . At greater  $K_2O$  concentrations the BO values determined from the NMR data plot below the calculated values (Figure 2.8, dash-dot curve) whereas the XPS data plot close to the equilibrium values (within experimental error as indicated by the size of the square symbols). The observation that some NMR data plot close to the calculated BO abundance (between 13 mol% and 25 mol%  $K_2O$ ) and those greater than 25 mol%  $K_2O$  plot below the calculated abundance is puzzling and requires explanation. Additional experimental studies are required, however, to resolve this apparent discrepancy. A similar discrepancy was noted in the  $Na_2O-SiO_2$  glass system (Nesbitt et al., 2011).

The O 1s XPS results and the NMR results between 13 mol% and 25 mol%  $K_2O$  indicate the presence of at least three oxygen species in K-silicate glasses and the thermodynamic analysis

indicates that  $O^{2-}$  is present due to Reaction (2.2) failing to go to completion. With  $K_2=2.0$ , approximately 0.5% of total oxygen is  $O^{2-}$  at the 10 mol%  $K_2O$  and this increases to about 6%  $O^{2-}$  at the 35 mol%  $K_2O$  composition. Apparently, there is more  $O^{2-}$  in K-silicate glasses than in Na-silicate glasses at the same concentration of alkali component (Nesbitt et al., 2011). Nesbitt et al. (2011) report values ranging from about 0.1%  $O^{2-}$  at 10 mol%  $Na_2O$  to 3% to 6%  $O^{2-}$  at 50 mol%  $Na_2O$ . Prasada Rao et al. (2010) report about 0.3%  $O^{2-}$  at unspecified high alkali concentrations in their simulations of lithium silicate glasses. We suggest that the abundance of  $O^{2-}$  in alkali silicate glasses is likely affected by the type of alkali cation present and that larger alkali cations (i.e., K, Rb, Cs) produce more  $O^{2-}$  atoms than smaller alkali cations.

Nesbitt et al. (2011) suggest that the  $O^{2-}$  atoms are sited in percolation channels and that their abundance is related to the degree of alkali cation clustering in the channels. Clustering of K in percolation channels may be more pronounced than clustering of Na in glasses of equivalent alkali content if the larger K atom is excluded from the silica network to a greater extent than is Na. Percolation channels then would form at lower concentrations of K than Na in their respective silicate glasses and the channels would be more abundant in K-silicate glasses. These suggestions, however, are speculative because the Na and K glasses were synthesized at somewhat different temperatures which would affect values of the conditional equilibrium constants for the glasses.

#### 2.4.6. The Relationship Between $O^{2-}$ and Activity of $K_2O$

Maekawa et al. (1991) calculated activities of  $Na_2O$  in sodium silicate glasses based on Q-species distributions and compared them to measured activities. As they stated, the agreement was semi-quantitative. An equivalent calculation cannot yet be performed whereby the mole fraction of  $O^{2-}$  is related to activity of the alkali oxide (e.g.,  $Na_2O$  or  $K_2O$ ) because they are related through a dissociation reaction (Equation 2.4) as emphasized by Fraser (1977) who addressed this specific problem. Using the Na-silicate glass system as an example, the appropriate dissociation reaction is:



for which the mass-action equation is:

$$K_4 = \{[Na^+]^2[O^{2-}]\} / [Na_2O], \quad (2.4a)$$

where  $K_4$  is the dissociation constant and square brackets indicate activities. Rearrangement of (Equation 2.4a) yields:

$$[\text{Na}_2\text{O}] = \{[\text{Na}^+]^2[\text{O}^{2-}] / K_4\}^{1/2}. \quad (2.5)$$

Assuming ideal mixing (i.e., mol fractions can be substituted for activities), the activity of  $\text{Na}_2\text{O}$  is related to  $X_{\text{O}_2^-}$  through the activity of  $\text{Na}^+$  and the dissociation constant,  $K_4$  but neither is known. The same development applies to the potassium silicate system where the dissociation reaction is:



and the rearranged mass-action equation for Reaction 2.6 is:

$$[\text{K}_2\text{O}] = \{[\text{K}^+]^2[\text{O}^{2-}] / K_6\}^{1/2}. \quad (2.7)$$

The activity of  $\text{K}_2\text{O}$  can be experimentally evaluated by electrochemical or other means and the  $X_{\text{O}_2^-}$  now has been measured. With measurement or assessment of  $[\text{K}^+]$  in these glasses the dissociation constant can be evaluated and the activity of  $\text{K}_2\text{O}$  then can be related to  $X_{\text{O}_2^-}$ .

## 2.5. CONCLUSIONS

Potassium silicate glasses were studied using XPS and high-resolution O 1s, K 2p and Si 2p spectra are reported. BO abundances obtained from O 1s XPS analysis are consistent with  $^{29}\text{Si}$  MAS NMR studies of K-silicate glasses within the compositional range 13 mol% to 25 mol%  $\text{K}_2\text{O}$ . These experimentally determined BO abundances are greater than predicted by the CRN model of Zachariassen (1932), a basic premise of which is that each K atom is associated with one NBO in K-silicate glasses. Although these experimental data prove the premise to be incorrect, it nevertheless provides a first order estimate of NBO and BO in K-silicate glasses.

As with Q-species, oxygen species (O-species) distribution can be calculated by assuming equilibrium among the species in K-silicate glasses. A conditional equilibrium constant ( $K_3$  of Equation 3) of 2.0 reproduces the BO abundances measured by XPS and reproduces the BO abundances of all  $^{29}\text{Si}$  MAS NMR data within the compositional range 13 mol% to 25 mol%  $\text{K}_2\text{O}$ . From a thermodynamic perspective the CRN model requires the equilibrium constant to be infinite so that Reaction (2.2) goes to completion and one or other of the reactants is completely consumed. A finite value for  $K_2$  requires that each reactant, BO and  $\text{O}^{2-}$  of Reaction (2.2) is present in finite amount within the binary system and by implication the reaction does not go to completion. The XPS and NMR experimental data and the thermodynamic treatment all require

that some  $O^{2-}$  (free oxygen) is present in K-silicate melts and glasses within the binary system, and with its abundance increasing in glasses and melts of progressively increasing  $K_2O$  content.

At equivalent alkali content, however, the experimental data indicate that abundance of  $O^{2-}$  is greater in K-silicate glasses than in Na-silicate. The size of the modifying cation may affect the abundance of  $O^{2-}$  in alkali glasses by promoting formation of percolation channels in which  $O^{2-}$  resides. The establishment of more and larger percolation channels creates an 'ionic environment' which should favor the formation and stability of  $O^{2-}$  over that of BO.

The breadth of the O 1s XPS BO peak is highly variable and wider than that of the NBO peak, whose width remains relatively constant at  $1.21 \text{ eV} \pm 0.07 \text{ eV}$ . The variable width may result from the presence of two types of BO atoms with somewhat different binding energies; one type bridges two Si atoms whereas the second type is bonded to three atoms, two Si and one K atom. Their abundances are similar to the abundances of  $Q^4$  and  $Q^3$  species of previous NMR studies. These findings indicate that XPS has the potential to resolve  $Q^n$  species.

An unresolved aspect, and one that requires additional experimental study, is the discrepancy in BO contents in glasses more potassic than 25 mol%  $K_2O$ . The XPS data yield slightly greater BO contents than the  $^{29}\text{Si}$  MAS NMR results. In this regard, all BO values obtained from O 1s XPS spectra are consistent with the O-species distribution calculated from the conditional equilibrium constant. The BO values obtained from NMR studies for glasses ranging from 13 mol% to 25 mol%  $K_2O$  are also consistent with the thermodynamic treatment. The BO contents obtained from NMR results on glasses containing more than 25 mol%  $K_2O$  are, however, inconsistent with the thermodynamic treatment.

## 2.6. REFERENCES

- Bancroft, G. M., Nesbitt, H. W., Ho, R., Shaw, D. M., Tse, J. S., and Biesinger, M. C., (2009) Toward a comprehensive understanding of solid-state core-level XPS linewidths: Experimental and theoretical studies on the Si 2p and O 1s linewidths in silicates. *Physical Review B* **80**, 075405-1-13.
- Ching, W. Y., Murray, R. A., Lam, D. G., and Veal, B. W., (1983) Comparative studies of electronic structures of sodium metasilicate and  $\alpha$  and  $\beta$  phases of sodium disilicate. *Physical Review B* **28** (8), 4724-4735.

- Ching, W.Y., Li, Y.P., Veal, B.W., and Lam, D.J., (1985) Electronic structures of lithium metasilicate and lithium disilicate. *Physical Review B* **32**, 1203-1207.
- Christie, J.K., and Tilocca, A., (2010) Aluminosilicate Glasses as yttrium vectors for in situ radiotherapy: Understanding composition-durability effects through molecular dynamics simulations. *Chemistry of Materials* **22**, 3725–3734.
- Dalby, K. N., Nesbitt, H. W., Zakaznova-Herzog, V. P., and King, P. L., (2007) Resolution of bridging oxygen signals from O 1s spectra of silicate glasses using XPS: Implications for O and Si speciation. *Geochimica et Cosmochimica Acta* **71**, 4297-4313.
- Du, J., and Cormack, A. N., (2004) The medium range structure of sodium silicate glasses: A molecular dynamics simulation. *Journal of Non-Crystalline Solids* **349**, 66-79.
- Fraser, D. G., (1977) Thermodynamic properties in silicate melts. *In: Thermodynamics in Geology* (ed. D. G. Fraser), pp. 301-326. D. Reidel Dordrecht, Germany
- Gedeon, O., Zemek, J., and Jurek, K., (2008) Changes in alkali-silicate glasses induced with electron radiation. *Journal of Non-Crystalline Solids* **354**, 1169-1171.
- Greaves, G.N., (1985) EXAFS and the structure of glass. *Journal of Non-Crystalline Solids* **71**, 203-217.
- Greaves, G.N., Fontaine, A., Lagarde, P., Raoux, D., and Gurman, S.J., (1981) Local structure of silicate glasses. *Nature* **293**, 611-616.
- Hess, P. C., (1971) Polymer model of silicate melts. *Geochimica et Cosmochimica Acta* **35**, 289-306.
- Huang, C., and Cormack, A.N., (1990) The structure of sodium silicate glass. *Journal of Chemical Physics* **93**, 8180-8186.
- Huang, C., and Cormack, A.N., (1991) Structural differences and phase separation in alkali silicate glasses. *Journal of Chemical Physics* **95**, 3634-3642.
- Ingram, M.D., (1987) Ionic conductivity in glass. *Physics and Chemistry of Glasses* **28**, 215-234.
- Jahn, S., (2008) Atomic structure and transport properties of MgO-Al<sub>2</sub>O<sub>3</sub> melts: A molecular dynamics simulation study. *American Mineralogist* **93**, 1486-1492.
- Kracek, F.C., Bowen, N.L., and Morey, G.W., (1929) The system potassium metasilicate-silica. *Journal of Physical Chemistry* **33**, 1857-1879.
- Lee, S. K. and Stebbins, J. F., (2009) Effects of the degree of polymerization on the structure of

- sodium silicate and aluminosilicate glasses and melts: An  $^{17}\text{O}$  NMR study. *Geochimica et Cosmochimica Acta* **73**, 1109-1119.
- Maekawa, H., Maekawa, T., Kawamura, K., and Yokokawa, T., (1991) The structural groups of alkali silicate glasses determined from  $^{29}\text{Si}$  MAS-NMR. *Journal of Non-Crystalline Solids* **127**, 53-64.
- Malfait, W. J., Halter, W. E., Morizet, Y., Meier, B. H., and Verel, R., (2007) Structural control on bulk melt properties: Single and double quantum  $^{29}\text{Si}$  NMR spectroscopy on alkali-silicate glasses. *Geochimica et Cosmochimica Acta* **71**, 6002-6018.
- Meyer, A., Horbach, J., Kob, W., Kargl, F., and Schober, H., (2004) Channel formation and intermediate range order in sodium silicate melts and glasses. *Physical Review Letters* **93**, 027801-1-4.
- Mountjoy, G., (2007) The local atomic environment of oxygen in silicate glasses from molecular dynamics. *Journal of Non-Crystalline Solids* **353**, 1849-1853.
- Nesbitt, H. W., (2002) Interpretation of x-ray photoelectron spectra with applications to mineralogy and geochemistry. In: *Synchrotron Radiation: Earth, Environmental and Materials Sciences Applications* (eds. Henderson, G. S., Baker, D. S.), Mineralogical Association of Canada Short Course 30, 131-158.
- Nesbitt, H.W., and Dalby, K.N., (2007) High resolution O 1s XPS spectral, NMR, and thermodynamic evidence bearing on anionic silicate moieties (units) in  $\text{PbO-SiO}_2$  and  $\text{Na}_2\text{O-SiO}_2$  glasses. *Canadian Journal of Chemistry* **85**, 782-792.
- Nesbitt, H.W., and Fleet, M., (1981) An ion-associated model for  $\text{PbO-SiO}_2$  melts: Interpretation of thermochemical, conductivity and density data. *Geochimica et Cosmochimica Acta* **45**, 235-244.
- Nesbitt, H.W., Bancroft, G.M., Davidson, R., McIntyre, N.S., and Pratt, A.R., (2004) Minimum XPS core-level line widths of insulators, including silicate minerals. *American Mineralogist* **89**, 878-882.
- Nesbitt, H. W., Bancroft, G. M., Henderson, G. S., Ho, R., Dalby, K. N., Huang, Y., and Yan, Z., (2011) Bridging, non-bridging and free ( $\text{O}^{2-}$ ) oxygen in  $\text{Na}_2\text{O-SiO}_2$  glasses: An X-ray Photoelectron Spectroscopic (XPS) and Nuclear Magnetic Resonance (NMR) study. *Journal of Non-Crystalline Solids* **357**, 170-180.
- Pedone, A., Malavasi, G., Cormack, A.N., Segre, U., and Menziani, M.C., (2008) Elastic and

- dynamical properties of alkali-silicate glasses from computer simulations. *Theoretical Chemistry Accounts* **120**, 557-564.
- Prasada Rao, R., Tho, T.D., and Adams, S., (2010) Ion transport pathways in molecular dynamics simulated alkali silicate glassy electrolytes. *Solid State Ionics* **181**, 1–6.
- Schaller, T., Stebbins, J. F., and Wilding, M. C., (1999) Cation clustering and formation of free oxide ions in sodium and potassium lanthanum silicate glasses: Nuclear magnetic resonance and Raman spectroscopic findings. *Journal of Non-Crystalline Solids* **243**, 146-157.
- Sen, S., and Youngman, R.E., (2003) NMR study of Q-speciation and connectivity in K<sub>2</sub>O-SiO<sub>2</sub> glasses with high silica content. *Journal of Non-Crystalline Solids* **331**, 100–107.
- Shirley, D. A., (1972) High resolution x-ray photoelectron spectrum of the valence band of gold. *Physical Review B* **5** (12), 4709-4714.
- Smith, W., Greaves, G.N., and Gillan, M.J., (1995) The structure and dynamics of sodium disilicate glass by molecular dynamics simulation. *Journal of Non-Crystalline Solids* **192–193** 267-271.
- Stebbins, J., (1987) Identification of multiple structural species in silicate glasses by <sup>29</sup>Si NMR. *Nature* **330**, 465–467.
- Sutherland, D.G.J., Bancroft, G.M., and Tan, K.H., (1992) Vibrational splitting in Si 2p core-level photoelectron spectra of silicon molecules. *Journal of Chemical Physics* **97**, 7918-7931.
- Tilocca, A. and de Leeuw, N. H., (2006) Structural and electronic properties of modified sodium and soda-lime silicate glasses by Car-Parrinello molecular dynamics. *Journal of Materials Chemistry* **16**, 1950-1955.
- Uchino, T., and Yoko, T., (1998) Structure and vibrational properties of sodium disilicate glass from ab initio molecular orbital calculations. *Journal of Physical Chemistry B* **102**, 8372-8378.
- Warren, B.E., and Biscoe, J., (1938) Fourier analysis of x-ray patterns of soda-silica glass. *Journal of the American Ceramic Society* **21**, 259-265.
- Zachariasen, W. H., (1932) The atomic arrangement in glass. *Journal of the American Chemical Society* **54**, 3841-3850.
- Zakaznova-Herzog, V.P., Nesbitt, H.W., Bancroft, G.M., and Tse, J.S., (2006) High resolution

- core and valence band XPS spectra of non-conductor pyroxenes. *Surface Science* **600**, 3175-3186.
- Zakaznova-Herzog, V.P., Nesbitt, H.W., Bancroft, G.M., and Tse, J.S., (2008) Characterization of leached layers on olivine and pyroxenes using high-resolution XPS and density functional calculations. *Geochimica et Cosmochimica Acta* **72**, 69-86.
- Zemek, J., Jiricek, P., Gedeon, O., Lesiak, B., Jozwik, A., (2005) Electron irradiated potassium-silicate glass surfaces investigated by XPS. *Journal of Non-Crystalline Solids* **351**, 1665-1674.
- Zhang, P., Grandinetti, P. J., and Stebbins, J. F., (1997) Anionic species determination in  $\text{CaSiO}_3$  glass using two-dimensional  $^{29}\text{Si}$  NMR. *Journal of Physic Chemistry B* **101**, 4004-4008.

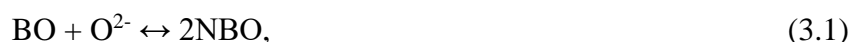


## Chapter 3

### 3.0. SPECTROSCOPIC STUDIES OF OXYGEN IN POTASSIUM SILICATE GLASSES AND MELTS<sup>2</sup>

#### 3.1. INTRODUCTION

Much progress has been made with regards to understanding the structure and properties of silicate glasses and melts using various spectroscopic techniques. Of particular importance are the chemical forms of oxygen atoms in glasses and the role they play in determining the physical and chemical properties of glasses and melts of geochemical and metallurgical significance (Stebbins, 1995; Brown et al., 1995; Mysen, 2003; Henderson, 2005; Henderson et al., 2006; Stebbins et al., 2013; Dingwell, 2006; Park and Rhee, 2001). There is much debate and controversy about the chemical forms of oxygen in alkali (Maekawa et al., 1991; Malfait et al., 2007; Lee and Stebbins, 2009; Matsumoto et al., 1998; Nesbitt et al., 2011; Sawyer et al., 2012; Stebbins and Sen, 2013) and alkaline earth (Zhang et al., 1997; Sen and Tangeman, 2008; Sen et al., 2009; Davis et al., 2011; Nasikas et al., 2012; Cormier and Cuello, 2013; Park, 2013a; Park, 2013b; Retsinas et al., 2014; Lee and Stebbins, 2006; Thompson et al., 2012) silicate glasses, specifically regarding the presence and abundance of the “free oxide” species (oxygen bound only to alkali or alkaline earth cations). For over 60 years, it has been recognized that three species of oxygen are present in silicate melt described by the following polymerization-depolymerization reaction (Fincham and Richardson, 1954):



where BO is bridging oxygen (Si-O-Si), NBO is non-bridging oxygen (Si-O-K, for example) and  $\text{O}^{2-}$  is free oxygen (K-O-K, for example). The mass action equation is:

$$K_1 = [\text{NBO}]^2 / \{[\text{BO}][\text{O}^{2-}]\}, \quad (3.2)$$

where square brackets denote activities and  $K_1$  is the equilibrium constant. The presence of  $\text{O}^{2-}$  was acknowledged in early studies which suggested a finite value for  $K_1$  (Fincham and Richardson, 1954; Toop and Samis, 1962; Pearce, 1964; Fine and Stopler, 1985; Fine and

---

<sup>2</sup> This chapter is modified from the original publication “Sawyer, R., Nesbitt, H.W., Bancroft, G.M., Thibault, Y. and Secco, R.A., 2015. Spectroscopic studies of oxygen speciation in potassium silicate glasses and melts. *Canadian Journal of Chemistry*, 93(1), pp.60-73. doi: 10.1139/cjc-2014-0248”

Stopler, 1986). However, mention of  $O^{2-}$  is absent from recent reviews (Stebbins, 1995; Brown et al., 1995; Mysen, 2003; Henderson, 2005; Henderson et al., 2006; Stebbins et al., 2013). Recent studies have reported the presence of free oxide in alkaline earth silicate glasses with compositions between the metasilicate (50% mol% modifier oxide (MO), e.g.,  $MgSiO_3$ ) and the orthosilicate (66.7 mol% MO, e.g.,  $Mg_2SiO_4$ ). Free oxide abundances from 1 to 5 mol% for the metasilicates and from 5 to 7 mol% for the orthosilicates have been reported from  $^{29}Si$  NMR studies of Mg-Ca-Si glasses (Zhang et al., 1997; Sen and Tangeman, 2008; Sen et al., 2009; Davis et al., 2011), a  $^{17}O$  NMR study of  $(Ca,Mg)_2SiO_4$  glasses (Nasikas et al., 2012) and an X-ray and neutron diffractions study of  $(Ca,Mg)SiO_3$  glasses (Cormier and Cuello, 2013). Additionally, several Raman spectroscopic studies in the metallurgical and glass literature have reported similar or larger amounts of free oxide in Mg-Ca silicates in the compositional range between the metasilicate and orthosilicate (Park, 2013a; Park, 2013b; Retsinas et al., 2014). Free oxide must be present at compositions where  $MO > 66.7$  mol% from the stoichiometry of Reaction 3.1. Free oxide is not mentioned or is implied to exist only in smaller amounts ( $<1$  mol%) below the orthosilicate according to  $^{17}O$  and  $^{29}Si$  NMR studies of a 56 mol% CaO glass (Lee and Stebbins, 2006; Thompson et al., 2012). Thompson et al. (2012) concluded that there was “no evidence of free oxide in detectable quantities” in a 56 mol% CaO glass despite their most accurate measurements of Q-species indicating 3 mol%  $O^{2-}$  and up to 4 mol%  $O^{2-}$  when uncertainties are accounted for.

There is more controversy regarding the presence of free oxide in alkali silicates where its abundances are thought to be smaller than in alkaline earth silicates owing to differences in ionization potential and cation field strength (Stebbins and Sen, 2013). A recent XPS study of potassium silicate glasses has stirred controversy with claims of several mol %  $O^{2-}$  for glasses containing 30 mol%  $K_2O$  (Sawyer et al., 2012). This is in sharp contrast to early Raman studies of potassium silicate glasses with  $<33.3$  mol%  $K_2O$  that did not even mention the possibility of free oxide and  $^{29}Si$  NMR studies of potassium silicate glasses with up to 50 mol%  $K_2O$  that did not indicate any free oxide in their interpretations of their spectra (Matson et al., 1983; Maekawa et al., 1991; McMillan et al., 1992; Malfait et al., 2007). The  $^{29}Si$  NMR spectra of the 50 mol%  $K_2O$  glass were fit with two  $Q^2$  species to constrain the amount of free oxide to 0 so that Reaction 3.1 goes to completion. This interpretation was made without any evidence as noted by Henderson (2005) and to date there is still no evidence for two  $Q^2$  species to our knowledge. A

more recent  $^{17}\text{O}$  and  $^{29}\text{Si}$  NMR study by Stebbins and Sen (2013) of two potassium silicate glasses with 34 and 40 mol%  $\text{K}_2\text{O}$  indicated “negligible free oxide contents” (non-zero, however) and found substantial disagreement with the results from the XPS study. Their  $^{17}\text{O}$  NMR spectra had a very high signal to noise ratio and their conclusions were largely based on the assumption that the  $^{17}\text{O}$  chemical shifts in potassium silicate glasses and crystalline  $\text{K}_2\text{O}$  should be similar. Their  $^{29}\text{Si}$  NMR spectra were constrained in the manner previously mentioned to yield no  $\text{O}^{2-}$  (Stebbins and Sen, 2013).

Several new XPS spectra of potassium silicate glasses are reported with compositions containing ~27-35 mol%  $\text{K}_2\text{O}$ . Novel experimental methods are used to evaluate the compositions of the glasses and the reproducibility of the O 1s spectra. Given that there is agreement between the  $^{29}\text{Si}$  NMR and O 1s spectra for lead silicates (Dalby et al., 2007) and sodium silicates (Nesbitt et al., 2011), this work is necessary since there is no reason why there should be disagreement with the potassium silicates. An attempt is made to resolve these discrepancies by examining the O 1s XPS results (Sawyer et al., 2012) and the  $^{29}\text{Si}$  and  $^{17}\text{O}$  NMR results (Maekawa et al., 1991; Malfait et al., 2007; Stebbins and Sen, 2013). Regarding the  $\text{O}^{17}$  NMR results of Stebbins and Sen (2013), the use of crystalline  $\text{K}_2\text{O}$  as a model for free oxide in glasses is questioned because the oxygen chemical environments may differ greatly. The accuracy of the  $^{17}\text{O}$  NMR results is also examined. A discussion of the importance of free oxide in the uptake of  $\text{CO}_2$ , water, and sulfur species in glasses and magmas concludes this chapter (Stöpler, 1982; Fine and Stöpler, 1985; Fine and Stöpler, 1986; Xue and Kanzaki, 2004; Cody et al., 2005; Baker and Moretti, 2011; Iacovino et al., 2013; Le Losq et al., 2012; Le Losq et al., 2013; Morizet et al., 2013a,b; Seifert et al., 2013; Duncan and Dasgupta, 2014).

### 3.1.1. Constraints on Oxygen Speciation

#### 3.1.1.1. General Considerations

An advantage to XPS is that BO abundances can be determined directly from the peak areas of O 1s spectra. NBO and  $\text{O}^{2-}$  abundances must be determined with calculations which are described in this section after an introduction to the concepts. The relationships between oxygen species for a binary system  $\text{SiO}_2\text{-MO}$  are shown in Figure 3.1. BO species are solely present where  $X_{\text{SiO}_2} = 1$  (or  $X_{\text{MO}} = 0$ ) and  $\text{O}^{2-}$  is solely present where  $X_{\text{MO}} = 1$ .  $\text{O}^{2-}$  is entirely consumed if Reaction 3.1

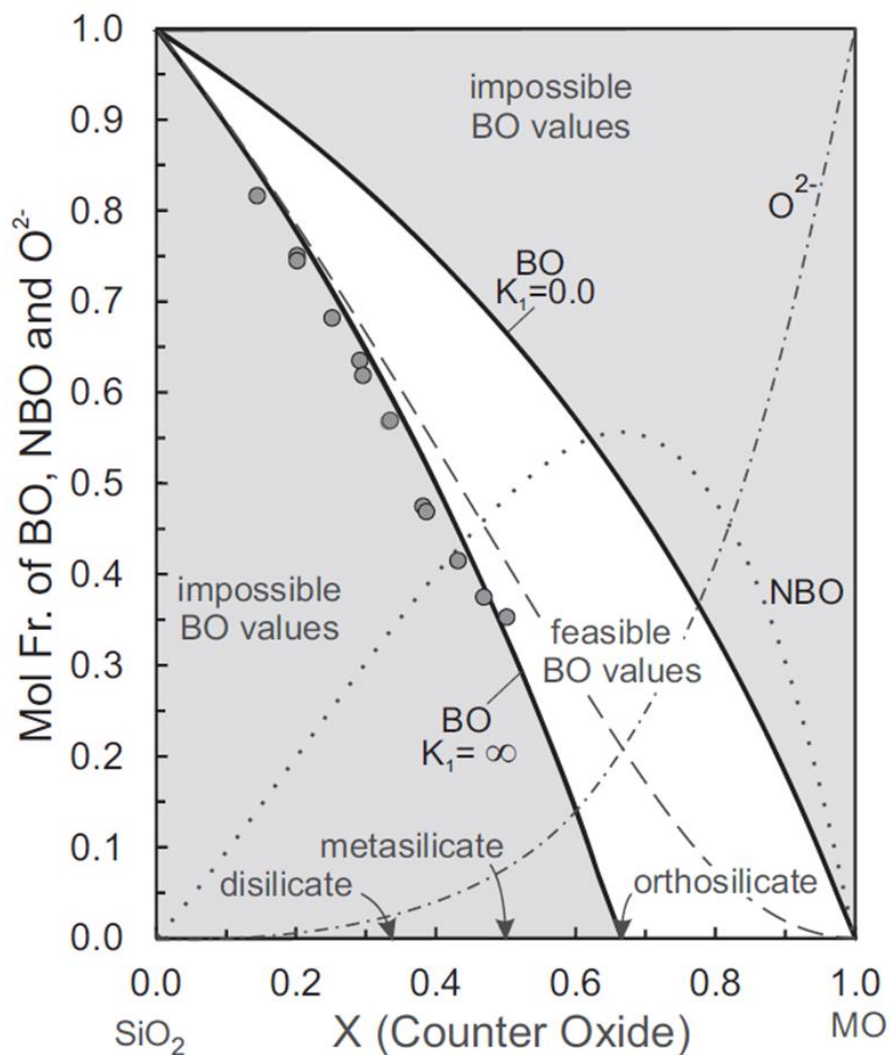


Figure 3.1: Plot of BO mole fraction versus mole fraction of MO (or M<sub>2</sub>O) illustrating feasible BO values (clear region between solid curves) and regions where  $X_{BO}$  values are physically impossible to achieve in equilibrated melts (shaded regions). The curve labelled  $K_1 = \infty$  illustrates  $X_{BO}$  where the polymerization equation (Equation 3.1) goes to completion. The curve labelled  $K_1 = 0.0$  illustrates  $X_{BO}$  where the polymerization reaction does not occur (i.e., no NBO is produced). The dashed curve represents BO values for  $K_1 = 8.0$ . The  $X_{BO}$  derived from the free fits of <sup>29</sup>Si MAS NMR data (Table 3.1 of Malfait et al., 2007) are plotted as shaded circles.

goes to completion (i.e.,  $K_1 = \infty$ ) and exists only where  $X_{MO} > 0.667$ . The solid curve on Figure 3.1 illustrates BO abundances if  $K_1 = \infty$  for Reaction 3.1. Mass balances prevent  $X_{BO}$  from plotting below this curve. The upper limit on  $X_{BO}$  values is where Reaction 1 does not proceed at all (i.e.,  $K_1 = 0.0$ ) and is shown on Figure 3.1 as the solid curve labelled BO  $K_1 = 0.0$  (Figure 3.1). The region between the two curves represents all possible  $X_{BO}$  values. Where  $K_1$  is finite, all three species of oxygen are present in a manner that satisfies the Equation 3.2. The dashed curve in Figure 3.1 represents a feasible range of BO values for  $K_1 = 8.0$ . The dotted and dash-dotted curves are also calculated for this value. A finite value for  $K_1$  requires all three oxygen species to be present across the entire binary to satisfy conditions of equilibrium in a homogeneous medium like a melt. One or more species of oxygen may be difficult to detect directly due to low abundances, such as  $O^{2-}$  at highly siliceous compositions. The presence of  $O^{2-}$  is not due to defects.

### 3.1.1.2. The Orthosilicate Composition

If  $K_1 = \infty$  at the orthosilicate composition ( $X_{MO} = 0.667$ ), BO and  $O^{2-}$  are completely consumed so that NBO is the only species present. If  $K_1 = 0$  then  $X_{BO} = X_{O^{2-}}$ . If  $K_1$  is finite (e.g.,  $K_1 = 8.0$  in Figure 3.1), then all three species are present with BO and  $O^{2-}$  having equal abundances. Figure 3.1 shows that  $X_{O^{2-}}$  increases exponentially with  $X_{MO}$  and that  $X_{NBO}$  increases effectively linearly with  $X_{MO}$  up to the orthosilicate. The free oxide peak is ~2% of the total O 1s intensity but is ~6% of the NBO intensity at the disilicate composition ( $X_{MO} = 0.333$ ).

### 3.1.1.3. Oxygen Species Abundances Derived from Experiments

The O 1s XPS spectra (Figure 3.2) display two prominent peaks: a BO peak at higher BE and a peak at lower BE that is a combination of the NBO and  $O^{2-}$  signals which overlap (Nesbitt et al., 2011; Sawyer et al., 2012; Dalby et al., 2007). The BO peak is resolved well enough to calculate its mol% or mol fraction ( $X_{BO} = \text{area under BO peak} / (\text{area under BO peak} + \text{area under NBO} + O^{2-} \text{ peak}) = N_{BO} / N_T = \text{Total mols BO} / \text{Total mols O}$ ). Values for  $X_{O^{2-}}$  and  $X_{NBO}$  can be calculated once  $X_{BO}$  is known. It is first necessary to calculate  $X_{BO}$  assuming that  $K_1 = \infty$  for Reaction 3.1. In this scenario all  $O^{2-}$  is consumed in the reaction and converted to NBO (where  $X_{SiO_2} \geq 0.666$ ) along with an equal amount of BO being converted to NBO. Thus, the number of moles of BO is  $N_{BO} = 2X_{SiO_2} - X_{K_2O}$  after the reaction is complete. The total number of moles of oxygen in the

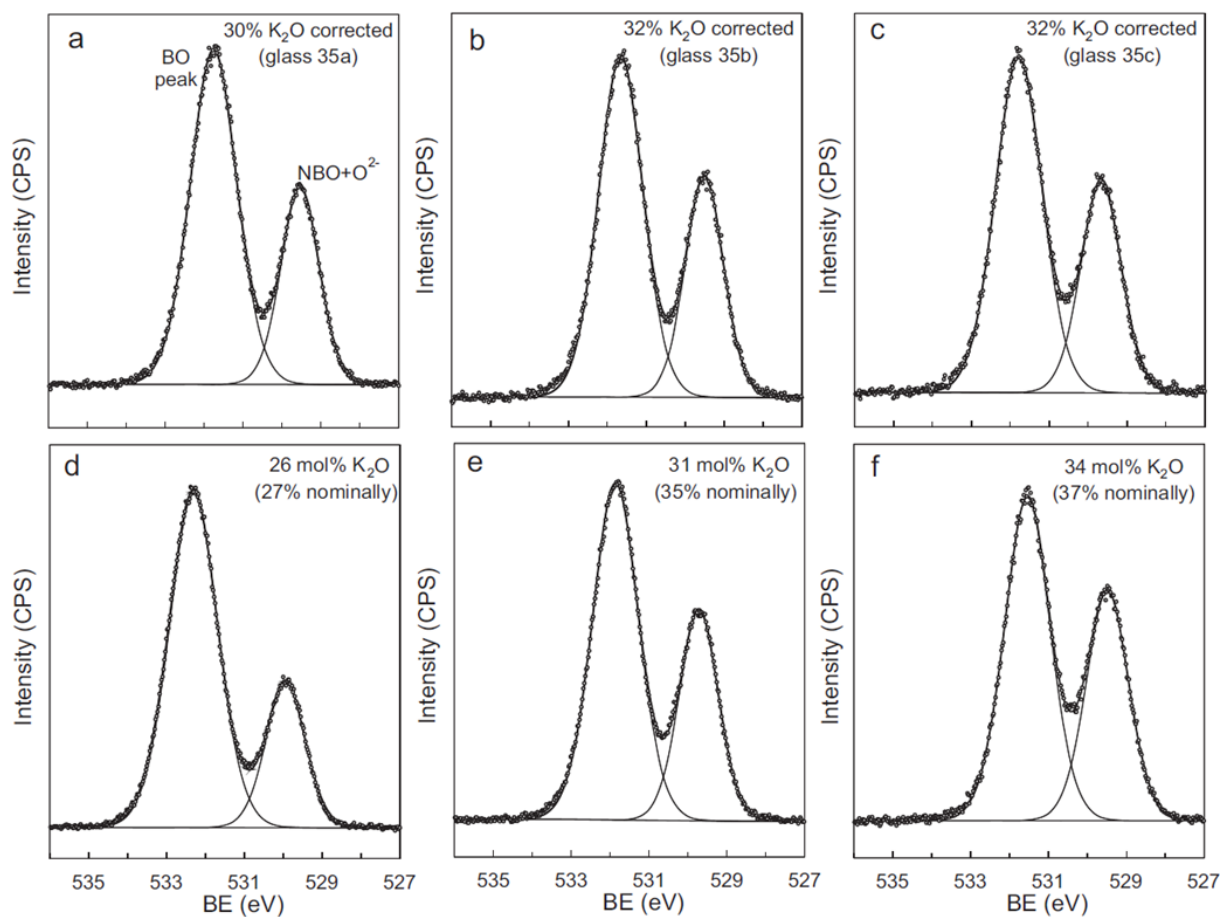


Figure 3.2: *O 1s* XPS spectra of six potassium silicate glasses. The nominal compositions of glasses shown in Figures 3.2a, 3.2b and 3.2c are 35 mol%  $K_2O$  but they were melted either three or four times and analyzed by EPMA to yield the corrected compositions (see text for details). The corrected compositions for glasses of Figures 3.2d, 3.2e and 3.2f are 26, 31 and 34 mol% were previously published in Sawyer et al. (2012) and are modified here.

glass is  $N_T = 2X_{SiO_2} + X_{K_2O}$ , so  $X_{BO}$  remaining after the reaction completes ( $X_{BO}^*$ ) is  $(2X_{SiO_2} - X_{K_2O}) / (2X_{SiO_2} + X_{K_2O})$ . If, however,  $K_1$  is finite for Reaction 3.1, then  $X_{BO}$  must be determined experimentally ( $X_{BO}^e$ ). This value will be greater than  $X_{BO}^*$  and the difference between the two represents an excess of BO ( $X_{BO}^X$ ) caused by an incomplete reaction. This difference is also equal to the amount of  $O^{2-}$  in the glass by the stoichiometry of Reaction 3.1. So  $X_{BO}^X = X_{O_2-} = (X_{BO}^e - X_{BO}^*)$ . For example,  $X_{BO}^X$  and  $X_{O_2-}$  are both equal to 0.07 at the metasilicate composition in Figure 3.1. This illustrates how the easy and direct calculation of  $O^{2-}$  is facilitated by the determination of  $X_{BO}^e$  and calculation of  $X_{BO}^*$  at identical compositions. The error associated with  $X_{O_2-}$  depends on the error associated with determining  $X_{BO}^e$  through experiment and with the error associated with the composition of the glass.  $X_{NBO}$  is determined by the difference  $1.0 = X_{BO}^e + X_{NBO} + X_{O_2-}$ .

Q-species can also be used to determine the mol% (or mole fractions) of oxygen species. The general notation is  $Q^n$  ( $n = 0$  to  $4$ ) where  $n$  denotes the number of BO atoms bonded to each silicon center. This notation is used primarily in  $^{29}Si$  NMR and Raman spectroscopies which are used to derive Q-species abundances. The calculation of  $X_{O_2-}$  from Q-species is uncomplicated and the formulae are presented in Appendix A.

## 3.2. EXPERIMENTAL METHOD

### 3.2.1. Preparation

Four new glasses were prepared: three of nominally 35 mol%  $K_2O$  (subsequently referred to as 35a, 35b and 35c) and one of nominally 37 mol%  $K_2O$ . The O 1s XPS spectra of these four glasses are presented in Figures 3.2a, 3.2b, 3.2c and 3.2f. Samples were prepared from starting materials  $K_2CO_3$  and  $SiO_2$ . The starting materials were carefully mixed and ground at least once under anhydrous ethanol for a minimum of 1 h and dried under an infrared (IR) lamp. The mixtures were then sintered at 830 °C for at least 20 h, reground and then melted in a platinum crucible at a temperature 200 °C above the liquidus based on the phase diagram of Kracek et al., (1937). Each fusion took approximately 6 h where the temperature was increased in steps of 20 °C from 200 °C below the liquidus up to the desired temperature. The melts were quenched immediately by dipping the bottom of the platinum crucible into ice water. Sample 35a was ground and melted four times and samples 35b and 35c were ground and melted three times. The

nominally 37 mol% K<sub>2</sub>O sample was sintered twice at 800 °C for 3 h and melted, crushed and remelted three times: once at 1150 °C and twice at 1200 °C for 1 h each time. The glass samples were immediately placed into a desiccator. Although spectra of glasses with nominal compositions of 27 mol% K<sub>2</sub>O (Figure 3.2d) and 35 mol% K<sub>2</sub>O (Figure 3.2e) were reported by Sawyer et al., (2012), they are presented here because their melting histories require clarification. The 27 mol% K<sub>2</sub>O sample was crushed and sintered at 750 °C for 6 h and melted once at 1200 °C for 1 h so that its corrected composition (as will be subsequently discussed) was 26 mol% K<sub>2</sub>O (Figure 3.2d). The 35 mol% K<sub>2</sub>O sample previously reported was sintered at 825 °C for 3 h and a second time at 800 °C for 2.5 h. That sample was melted, crushed and remelted four times at temperatures between 1150 °C and 1230 °C and its composition was corrected to 31 mol% K<sub>2</sub>O (Figure 3.2e). These two spectra are included in Figure 3.2 in order to highlight the systematic change in O 1s XPS spectra with respect to composition.

### 3.2.2. XPS and Electron Probe X-ray Microanalyzer (EPMA) Analytical Considerations

After glass preparation and prior to EPMA analyses, each sample was notched and placed in the introduction chamber of the XPS instrument. Samples were fractured under vacuum in the transfer chamber where pressures were on the order of 10<sup>-9</sup> – 10<sup>-10</sup> Torr. After fracture, the sample was moved to the analytical chamber (~10<sup>-10</sup> Torr) and analyzed. The analytical conditions were identical to those described by Sawyer et al. (2012). The O 1s spectra were collected with a step size of 0.025 eV, a dwell time of 100 ms and a pass energy of 10 eV. All the data were collected using a Kratos Axis Ultra XPS instrument. The magnetic confinement charge compensation system was used to mitigate the effects of surface charging (Nesbitt et al., 2011; Sawyer et al., 2012). After analysis, samples were removed from the XPS instrument and placed in a desiccator prior to chemical analysis.

EPMA was used to analyze glasses 35a, 35b and 35c. The glass fragments were removed from the desiccator immediately before analysis. They were ground and polished dry (without lubricants) and transferred directly to a high vacuum evaporator for carbon coating. A JOEL JXA 8900 EPMA was used for sample analyses. It was operated at an accelerating voltage of 20 kV, a probe current of 8 nA, a beam defocused at 40 μm, and 8 s counting time (on both peak and background). These were considered the best analytical conditions for obtaining accurate compositions (Fig. 3.3). The characteristic K $\alpha$  X-ray line and an orthoclase standard were used



for both potassium and silicon. Abundances of oxygen were based on stoichiometry. The  $K\alpha$  X-ray intensities of potassium and silicon were monitored as a function of time to make sure that there was no detectable potassium mobility. Table 3.1 shows the individual analyses for glass 35a. Glasses 35b and 35c were analyzed 25 times as well and Table 3.1 provides their average compositions and one standard deviation unit for them.

### 3.3. RESULTS AND EXPERIMENTAL UNCERTAINTIES

#### 3.3.1. Homogeneity and the Composition of Glasses

The EPMA data from Table 3.1 indicates that glasses 35a, 35b and 35c are homogenous. Prepared with a nominal composition of 35 mol%  $K_2O$ , their analyzed compositions are 30, 32 and 32 mol%  $K_2O$  (Table 3.1). It is apparent that each melting during sample preparation decreased the  $K_2O$  content by about 1 mol%. This information has been used to correct the compositions of all potassium silicate glasses studied in this laboratory. The nominally 27 mol%  $K_2O$  glass (Table 3.2) was corrected to 26 mol%  $K_2O$ , the 37 mol%  $K_2O$  glass was corrected to 34 mol%  $K_2O$  and the 35 mol%  $K_2O$  glass reported by Sawyer et al. (2012) was corrected to 31 mol%  $K_2O$ .

For glasses 35a, 35b and 35c, the standard deviations ( $\sigma$ ) of Table 3.1 average to about 0.15 mol%. A conservative uncertainty of  $3\sigma$  ( $\pm 0.45$  mol%) is assigned to  $K_2O$  mol% and  $SiO_2$  mol% for the error in their compositions. A greater uncertainty of  $5\sigma$  ( $\pm 0.75$  mol%) was assigned to the glasses with nominal compositions of 27, 35 and 37 mol%  $K_2O$  which were not analyzed by EPMA. The previously reported results of Sawyer et al. (2012) assigned an error of  $\pm 2$  mol%  $K_2O$  and those uncertainties can now be refined based on these results. All previously reported glasses by Sawyer et al. (2012) were corrected to lower values by 1 or 2 mol%  $K_2O$  depending on the number of fusions the sample underwent during preparation. The same uncertainty ( $\pm 0.75$  mol%) for the nominally 27, 35 and 37 mol%  $K_2O$  compositions was assigned to the glasses reported by Sawyer et al. (2012).

#### 3.3.2. O 1s XPS Spectral Fits, Assignments and Linewidths

Figure 3.2 shows a BO peak located at  $\sim 532$  eV and an NBO +  $O^{2-}$  peak near 529.5 eV. Spectra were fit with a Shirley background (Shirley, 1972) and a 30% Lorentzian – 70% Gaussian line

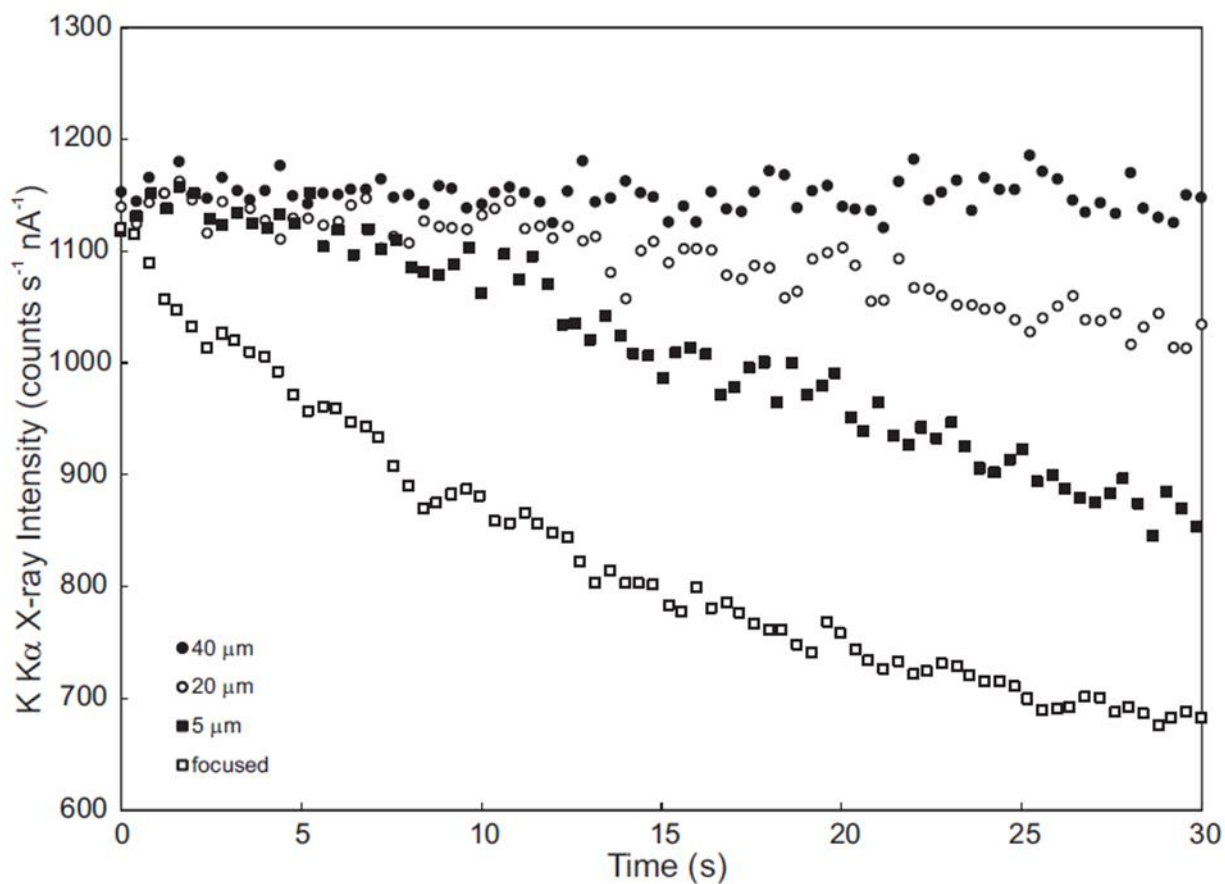


Figure 3.3: The effects of defocusing the electron beam to 40  $\mu$ m for a glass containing 30 mol%  $K_2O$ . With a 40  $\mu$ m beam size, the count rate between 0 and 10 s provides accurate analysis of potassium in the glass. The precise instrumental conditions used to analyze the glass reported here are provided in the text.

Table 3.1: EPMA analyses for samples 35a, 35b and 35c

Analysis No.	SiO <sub>2</sub> wt.%	K <sub>2</sub> O wt.%	Total wt.%	SiO <sub>2</sub> mol%	K <sub>2</sub> O mol%
<b>Glass 35a (nominally 35% K<sub>2</sub>O)</b>					
1	59.70	39.56	99.26	70.29	29.71
2	59.48	39.73	99.21	70.12	29.88
3	59.79	39.83	99.62	70.18	29.82
4	59.55	39.52	99.07	70.26	29.74
5	60.19	39.60	99.79	70.44	29.56
6	59.50	39.47	98.97	70.27	29.73
7	60.15	39.55	99.70	70.45	29.55
8	59.23	39.84	99.07	69.98	30.02
9	59.91	39.82	99.73	70.23	29.77
10	59.84	39.75	99.59	70.24	29.76
11	60.22	39.92	100.14	70.28	29.72
12	59.37	39.64	99.01	70.13	29.87
13	59.43	39.69	99.12	70.13	29.87
14	59.71	39.86	99.57	70.13	29.87
15	60.00	39.64	99.64	70.35	29.65
16	60.02	39.48	99.50	70.44	29.56
17	59.76	39.67	99.43	70.25	29.75
18	59.83	39.59	99.42	70.32	29.68
19	60.03	39.53	99.56	70.42	29.58
20	59.93	39.31	99.24	70.50	29.50
21	59.67	39.63	99.30	70.24	29.76
22	59.85	39.55	99.40	70.35	29.65
23	59.98	39.69	99.67	70.32	29.68
24	59.71	39.51	99.22	70.32	29.68
25	59.78	39.62	99.40	70.29	29.71
Average	59.79	39.64	99.43	70.28	29.72
1σ	0.26	0.14		0.12	0.12
<b>Glass 35b (n = 25, nominally 35% K<sub>2</sub>O)</b>					
Average	57.48	42.02	99.50	68.20	31.80
1σ	0.25	0.19		0.12	0.12
<b>Glass 35c (n = 25, nominally 35% K<sub>2</sub>O)</b>					
Average	57.09	42.76	99.85	67.67	32.33
1σ	0.27	0.17		0.16	0.16

shape, which allows for excellent fits to the O 1s spectra. These parameters were used for all least squares fits shown in Figure 3.2. All spectra were fit using the CasaXPS software (CasaXPS Software Ltd.). Peak intensities and consequently oxygen abundances were determined by area. Table 3.2 lists the parameters derived from the best fits. The NBO + O<sup>2-</sup> (low BE) peaks of Figure 3.2 have full widths at half maxima (FWHM) averaging about 1.2 eV (Table 3.2). These values are comparable to the average O 1s FWHM of quartz (Q<sup>4</sup> species only) which is 1.23 (±0.05) eV, of vitreous silica (Q<sup>4</sup> only) which is 1.25 eV (Nesbitt et al., 2011), and of olivine (Q<sup>0</sup> only) which is 1.26 (±0.05) eV (Bancroft et al., 2009; Nesbitt and Bancroft, 2014; Zakaznova-Herzog et al., 2005; Nesbitt et al., 2004). A FWHM value of 1.22 eV was obtained for the BO peaks for lead silicate glasses (Dalby et al., 2007). These FWHM values are remarkably consistent and are the result of a combination of final state vibrational broadening and phonon broadening (Bancroft et al., 2009; Nesbitt and Bancroft, 2014; Zakaznova-Herzog et al., 2005; Nesbitt et al., 2004). The FWHM for all BO peaks are broader (~1.4 eV) than the NBO peaks as shown in Figure 3.2 (Nesbitt et al., 2011; Sawyer et al., 2012). This breadth is likely due to two overlapping BO signals, one from the Si-O-Si moiety and the other from a BO species bonded to two silicon atoms and a modifying cation such as potassium or sodium (the BO-K or BO-Na moiety) (Nesbitt et al., 2011; Sawyer et al., 2012; Ching et al., 1983; Cormack et al., 2003; Du and Cormack, 2004; Mead and Mountjoy, 2005; Mead and Mountjoy, 2006; Tilocca and de Leeuw, 2006; Kargl et al., 2006; Machacek et al., 2010; Mountjoy, 2007; de Jong et al., 1998; Nesbitt et al., 2015). Figure 3.2 shows that the BO peaks are sufficiently separated from the NBO + O<sup>2-</sup> and symmetric that they have been fit with only one unconstrained peak. Using two peaks to fit the same BO signal provides almost identical results. In Figure 3.2b a free fit using one BO contribution gives 64.0% BO and a free fit using two BO contributions gives 63.9% BO.

### 3.3.3. Analytical Uncertainties in BO%, NBO% and O<sup>2-</sup>

Three to six O 1s spectra were collected for each sample during the analysis and their BO abundances were plotted as a function of time of exposure to the X-ray beam. Some of these results are shown in Figure 3.4a – 4d. Quadratic least squares fits were performed on the data for each sample. The intercepts indicating BO% at zero exposure time were obtained from the fits for each glass. These are shown in Table 3.2 under the “corrected BO%” column. “Corrected

Table 3.2: Fitted peak parameters for the potassium silicate glasses of Figure 3.2

K <sub>2</sub> O% nominal <sup>a</sup>	K <sub>2</sub> O% corrected	Spectrum of Fig.:	BE (eV)		FWHM (eV)		Corrected <sup>b</sup>		
			NBO	BO	NBO	BO	NBO+O <sup>2-</sup> %	BO%	Calculated O <sup>2-</sup> % <sup>c</sup>
27	26 (±0.75%)	2d	529.9	532.3	1.18	1.48	26.1	73.9	3.5 (±1.0)
35a	30 (±0.45%)	2a	529.5	531.8	1.14	1.41	32.9	67.1	2.0 (±0.8)
35b	32 (±0.45%) #1	2b	529.5	531.7	1.15	1.35	36.0	64.0	2.1 (±0.8)
35c	32 (±0.45%) #2	2c	529.5	531.6	1.18	1.42	35.6	64.4	2.5 (±0.8)
35	31 (±0.75%)	2e	529.7	531.9	1.16	1.39	34.9	65.1	1.8 (±1.0)
37	34 (±0.75%)	2f	529.5	531.5	1.27	1.38	39.5	60.5	1.5 (±1.0)

<sup>a</sup>See preparation section in text

<sup>b</sup>Corrected to zero X-ray exposure time. Uncertainty for each species is ±0.6%

<sup>c</sup>Uncertainty includes both compositional uncertainty (in mol%) and uncertainty in BO% (see text)

BO%” is used because the intercepts represent the true BO% of the sample prior to analysis. An estimate of the experimental uncertainty in BO% is provided by the scatter of measured BO% around the quadratic fits of Figure 3.4a – 3.4d. This uncertainty can be quantified as shown in Figure 3.4e which is a plot of the differences between measured BO% ( $BO_{meas}$ ) and BO% values from the quadratic fits ( $BO_{fit}$ ) taken at the same time as a function of exposure time. The standard deviation  $\sigma = 0.203$  ( $n = 65$ ) and the 95% confidence interval is  $\sim 0.40$  mol%. This value is increased arbitrarily to  $\pm 0.60$  mol% (50% increase) as a way of accounting for any error associated with the adoption of the intercept as the “corrected BO%”. The same error of  $\pm 0.60$  mol% is applied to the corrected BO% values in Table 3.2 and all BO% from Sawyer et al., (2012).  $NBO + O^{2-}$ % is calculated as the difference between the total O% and the BO% and has the same uncertainty associated with it.

The uncertainties associated with  $O^{2-}$  abundances are dependent on the uncertainties associated with BO mol% values and glass compositions ( $X_{K2O}$ ). The root mean squared of the errors associated with each independent variable is required to evaluate  $O^{2-}$  uncertainties (Mosteller et al., 1961). The BO mol% error for all samples is  $\pm 0.60$  mol% and the error assigned to the compositions of samples 35a, 35b and 35c is  $\pm 0.45$  mol%. The uncertainty in  $O^{2-}$  mol% is then  $\pm 0.75$  mol% for these three samples (rounded up to  $\pm 0.80$  mol% in Table 3.2). For all other samples, the error associated with  $X_{K2O}$  is  $\pm 0.75$  mol% so that the error in  $O^{2-}$  mol% is  $\pm 0.96$  mol% (rounded up to  $\pm 1.0$  mol%). These error estimates are conservative in nature and are included with the mol% of  $O^{2-}$  values in the last column of Table 3.2.

### 3.3.4. Other Contributions to Uncertainty

There are three other contributions to the uncertainties related to the accuracy of BO% measurements: (i) peak asymmetry, (ii) the existence of surface peaks on both BO and  $NBO + O^{2-}$  peaks and (iii) potential OH contamination (Nesbitt et al., 1998; Harmer et al., 2009). These issues have been discussed in detail in a review by Nesbitt and Bancroft (2014), but they are worth summarizing here for context. A small peak asymmetry is expected due to the vibrational broadening mechanism that affects the O 1s spectra of all silicates (Bancroft et al., 2009; Nesbitt and Bancroft, 2014). This asymmetry is most evident in the O 1s spectrum of vitreous  $SiO_2$  (Nesbitt et al., 2011). There is no noticeable asymmetry in the O 1s spectra of the potassium silicate glasses (Figure 3.3) and the absence of asymmetry negates the need for more

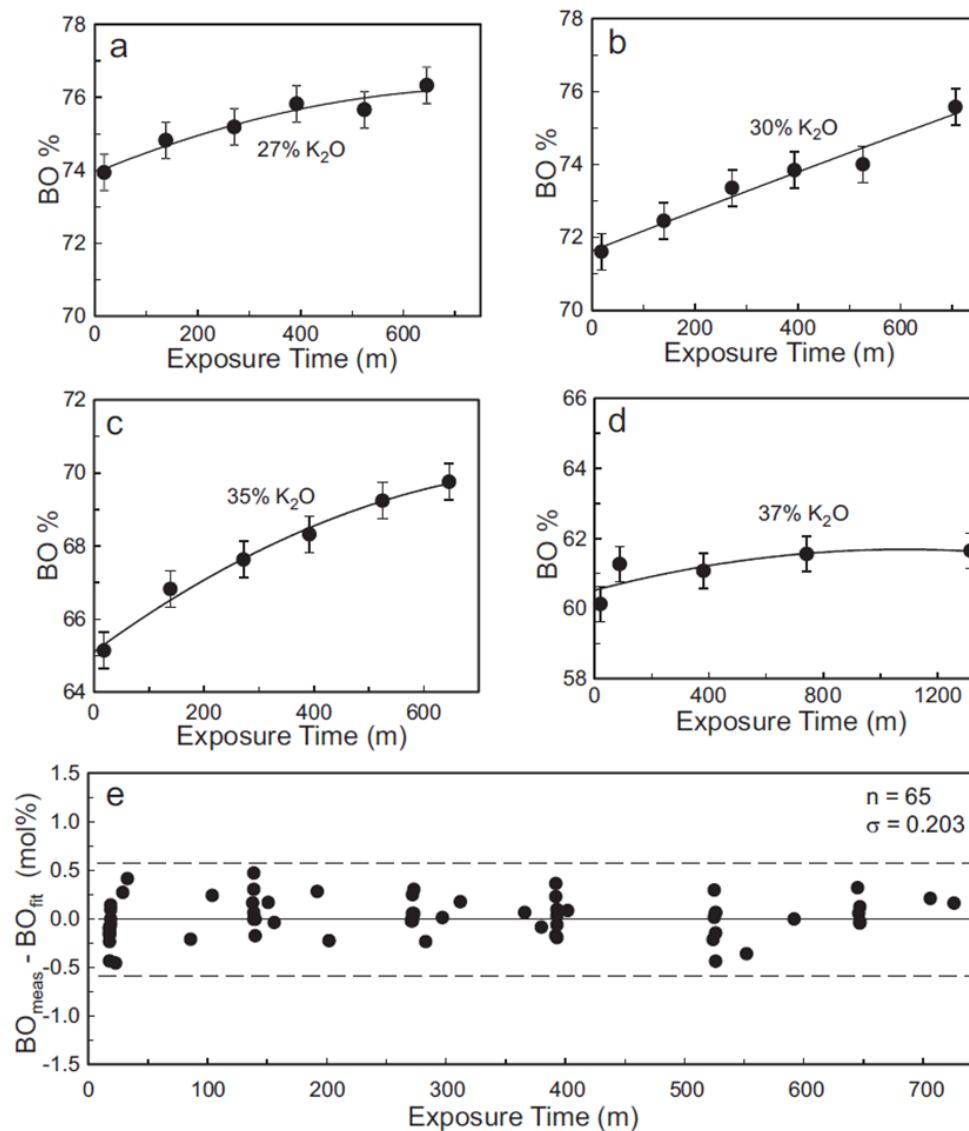


Figure 3.4: (a-d) Plots illustrating the changes to BO% as a function of time of exposure to the X-ray beam. A least squares quadratic fit to each set of data is included in these plots and its extrapolation to zero exposure yields the best estimate of BO% in the glass (see text). (e) Variation of BO% about the least squares quadratic fits (e.g., those in Figures 3.4a-d). The variations have been plotted in Figure 3.4e as a function of exposure time to obtain an estimate of the uncertainty associated with the BO% quoted in Table 3.2. The dashed curves represent  $\pm 3\sigma$  (see text).

complicated fitting procedures. Symmetric peaks introduce minimal uncertainty to BO mol% and NBO + O<sup>2-</sup> mol% values. XPS synchrotron studies of Cu<sub>2</sub>O indicate that surface contributions account for a small percentage (2%-5%) of the total O 1s signal at 1486 eV photon energy (Harmer et al., 2009). Surface signals present for the BO and NBO peaks will cancel each other out during peak fitting and so it cannot be argued that surface contributions preferentially enhance BO signals relative to NBO signals (Nesbitt and Bancroft, 2014). Molecular dynamics (MD) simulations and X-ray Absorption Fine Structure (XAFS) results show that fracture surfaces of alkali silicate glasses will be NBO-rich relative to the bulk sample (Greaves, 2000; Greaves et al., 1981). These results are reasonable since the K-O bond dissociation energy is 239 kJ mol<sup>-1</sup> compared to that of the Si-O bond which is 798 kJ mol<sup>-1</sup> (Speight, 2005). The NBO presence at the fracture surface will be enhanced relative to the BO presence because the weaker K-O bond is more likely to rupture during fracture. Thus, surface contributions do not enhance BO% values.

The OH peak overlaps with the BO peak and the adsorption of OH<sup>-</sup> on the fracture surface of the sample could lead to overestimates of BO%. However, bulk OH<sup>-</sup> in laboratory synthesized glasses is only about 0.1 wt% (~0.2 mol%) which is well within the assigned uncertainties (Le Losq et al., 2012; Le Losq et al., 2013). The ultrahigh vacuum conditions (near 10<sup>-10</sup> Torr) of the XPS instrument and the fact that the O 1s spectrum is collected first within a few minutes of fracture should minimize potential OH<sup>-</sup> accumulation. Extrapolation of BO% to zero exposure time (Figure 3.4a-3.4d) effectively removes the effect that any continued adsorption of OH<sup>-</sup> might have during analysis.

### 3.3.5. Oxygen Speciation from O 1s XPS Spectra

The NBO + O<sup>2-</sup> peak contains a small free oxide contribution which overlaps with the NBO signal, but the BO peak is well resolved (Nesbitt et al., 2011; Sawyer et al., 2012; Dalby et al., 2007). Figure 3.2 illustrates that as K<sub>2</sub>O content increases, the NBO + O<sup>2-</sup> signal increases in intensity relative to the BO signal. The two peaks were fitted and X<sub>BO</sub> values were obtained directly from the fitted areas. The BO and O<sup>2-</sup> mol% values are listed in Table 3.2. The NBO mol% is obtained by subtracting the O<sup>2-</sup> mol% from the NBO + O<sup>2-</sup> mol% of Table 3.2. The BO mol% was calculated from X<sub>BO</sub> values and plotted in Figure 3.5 as shaded and open circles. The results show a clear trend. A previous XPS study by Matsumoto et al. (1998) of two potassium



silicate glasses reported results from which  $X_{BO}$  values were calculated and plotted in Figure 3.5 as crosses. The samples underwent at least one melting and their compositions were corrected by 0.01 in  $X_{K_2O}$  (1 mol%  $K_2O$ ) to reflect this. These data are consistent with the results obtained here and by Sawyer et al. (2012). This consistency verifies the reproducibility of the XPS results. The open squares and shaded triangles are derived from  $^{29}Si$  MAS NMR studies, and those data are subject of further discussion.

Figure 3.5 shows that all XPS data for  $X_{K_2O} > 0.25$  plotted above the short-dashed curve. This indicates that  $X_{BO}$  values are in excess of those expected if Reaction 3.1 goes to completion. Clearly Reaction 3.1 does not go to completion and therefore unreacted  $O^{2-}$  is present and an essential constituent of the glasses.  $X_{O_2-}$  values were calculated for the glasses from the excess  $X_{BO}$  values. They are plotted at the bottom of Figure 3.5 (small circles) and straddle the dash-dotted curve. The XPS results show that  $K_1$  is finite and there are two consequences of this: (i)  $O^{2-}$  is present at low levels in these siliceous glasses and (ii) all three oxygen species are present across the entire binary as required by the mass action equation, though concentrations of some species may be too low to detect directly.

The mole fractions of all three species of oxygen ( $BO$ ,  $NBO$  and  $O^{2-}$ ) were calculated for  $K_1 = 8.0$  and plotted in Figure 3.5 as solid, dashed and dash-dotted curves. The value for  $K_1$  does not represent a best fit for the data but was calculated to satisfy one datum point (sample 35b). The XPS results provide strong indirect evidence for mol% levels of  $O^{2-}$  in potassium silicate glasses containing more than 25 mol%  $K_2O$ . These free oxide estimates are lower than previously reported by Sawyer et al. (2012) due to correction to the glass compositions but are unmistakably present.

### 3.4. OXYGEN SPECIATION FROM $^{29}Si$ MAS NMR SPECTRA

#### 3.4.1. Q-species Signals and Lineshapes

It has been noted elsewhere that there is disagreement between XPS (Nesbitt et al., 2011; Sawyer et al., 2012) and  $^{29}Si$  MAS NMR (Maekawa et al., 1991; Malfait et al., 2007) results regarding oxygen speciation and the presence of  $O^{2-}$ . To address these discrepancies, it is necessary to discuss the relevant NMR results in some detail. To facilitate discussion, three previously published spectra are reproduced. Gaussian peaks are used to fit  $^{29}Si$  MAS NMR spectra and

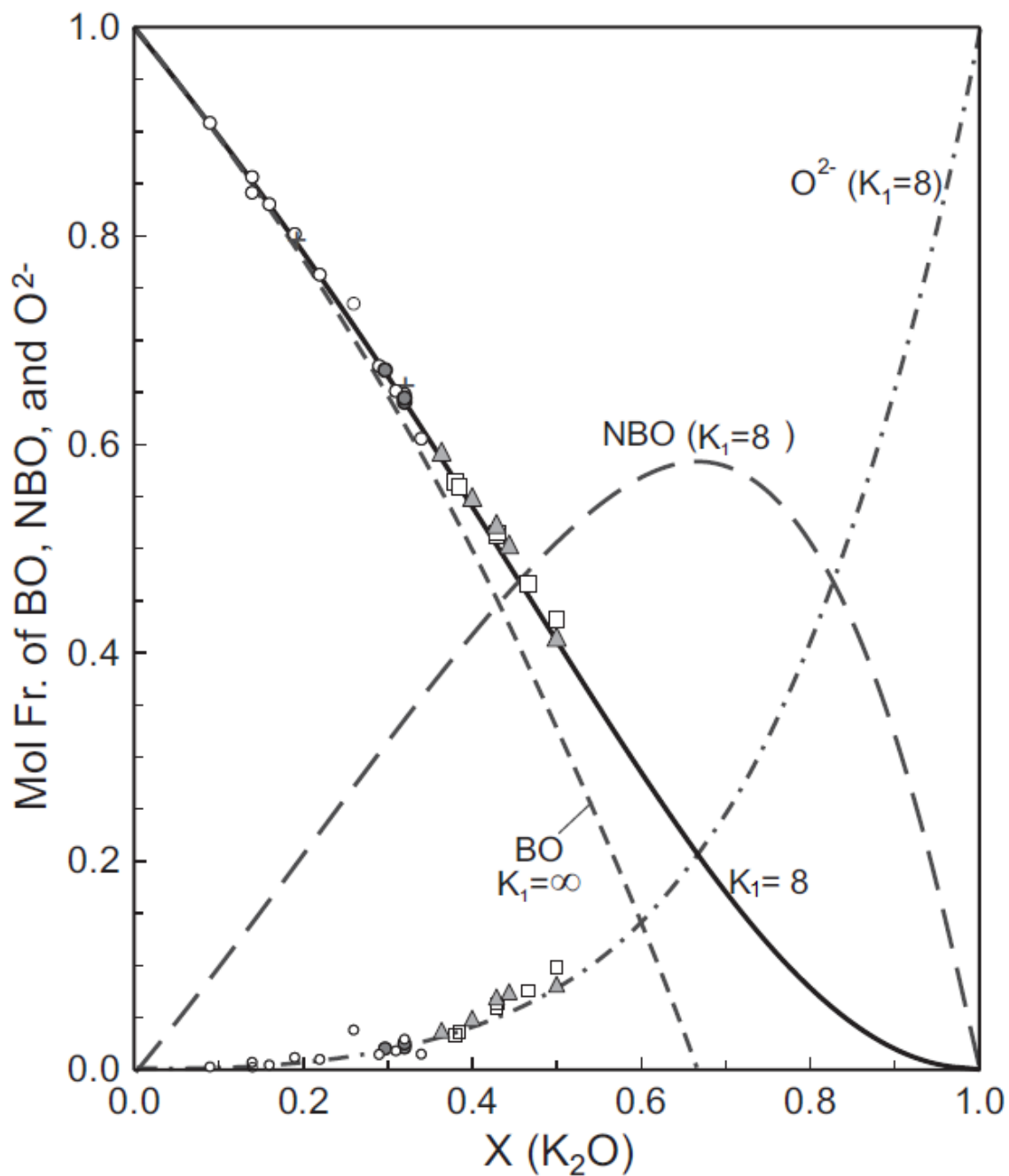


Figure 3.5: Plot of BO mole fraction versus mole fraction MO (or  $M_2O$ ) illustrating relationships among the oxygen species and experimentally determined  $X_{BO}$  values from O 1s XPS and  $^{29}Si$  MAS NMR spectra.  $X_{O_2^-}$  values are plotted and have been derived from experimental  $X_{BO}$  values (see text for calculations). The shaded circles represent experimentally determined  $X_{BO}$  values derived from XPS spectra of Figures 3.2a, 3.2b and 3.2c. The corresponding  $X_{O_2^-}$  values are plotted as small, shaded circles and they straddle the dash-dotted

curve labelled  $K_1 = 8.0$ . The open circles are  $X_{BO}$  values previously reported (Sawyer et al., 2012) and the corresponding  $X_{O_2^-}$  values are plotted as small open circles. The crosses represent  $O\ 1s$  XPS results obtained from a separate laboratory (Matsumoto et al., 1998) Large open squares and large shaded triangle represent  $X_{BO}$  values derived from  $^{29}\text{Si}$  NMR experiments (Maekawa et al., 1991; Malfait et al., 2007) (see Appendix A) and the corresponding  $X_{O_2^-}$  values are plotted as smaller squares and triangles.  $BO$ ,  $NBO$  and  $O^{2-}$  curves labelled  $K_1 = 8.0$  were calculated from mass action Equation 3.2. The short-dashed curve illustrates  $X_{BO}$  where Reaction 3.1 goes to completion (i.e.,  $K_1 = \infty$ ).

individual Q-species are generally derived per peak fit. This approach assumes that each Q-species provides a symmetric and distinct contribution to the NMR spectrum. However, this assumption is not true for crystalline  $K_2Si_2O_5$  (potassium disilicate) and so this approach may not be applicable to potassium disilicate glasses (de Jong et al., 1998). Information from X-ray Diffraction (XRD) and  $^{29}Si$  MAS NMR indicates that only  $Q^3$  species are present in crystalline potassium disilicate (de Jong et al., 1998). Figure 3.6 shows that the  $Q^3$  signals are bimodally distributed rather than being symmetrically distributed with respect to chemical shift. If one broad Gaussian peak were used to fit the envelope of  $Q^3$  peaks, as is done for glasses, the fit obtained would be poor. Better fits could be obtained using two Gaussian peaks or an asymmetric peak. Two peaks would be required to fit this distribution if it were also present in a glass even though only one Q-species was being fit. As will be discussed, two  $Q^2$  species have been used to fit the spectra of potassium silicate glasses in the studies of Maekawa et al. (1991) and Malfait et al. (2007). The use of two Gaussian peaks to fit one Q-species contribution should be considered as evidence for asymmetric Q-species lineshapes or bimodal distribution of signals (e.g., Figure 3.6). As a result, such Q-species assignments should be treated with caution.

It is possible to explain either the bimodal distribution of signals or asymmetric lineshapes through the relationship of Si-O-Si bond angles with each Q-species. The XRD data for crystalline  $K_2Si_2O_5$  from de Jong et al. (1998) shows a close and almost linear relationship between Si-O-Si bond angle and chemical shift of the  $Q^3$  units shown in Figure 3.6. These bond angles range from  $\sim 138^\circ$  to  $\sim 150^\circ$  with the associated chemical shifts being  $\sim 92$  ppm and  $\sim 95$  ppm. These results imply that chemical shifts are primarily determined by Si-O-Si bond angle. An asymmetric distribution of Si-O-Si bond angles in potassium disilicate glass would result in a bimodal or asymmetric lineshape which would mean that the use of a single Gaussian peak to fit each Q-species would not be possible. In order to fit one Gaussian peak per Q-species, it should first be demonstrated that there is a symmetric distribution of Si-O-Si bond angles in the glass for each Q-species if possible. Incorrect spectral assignments and interpretations may result in  $^{29}Si$  MAS NMR spectra due to the asymmetric Si-O-Si bond angle distribution in potassium silicate glasses producing asymmetric Q-species signals.

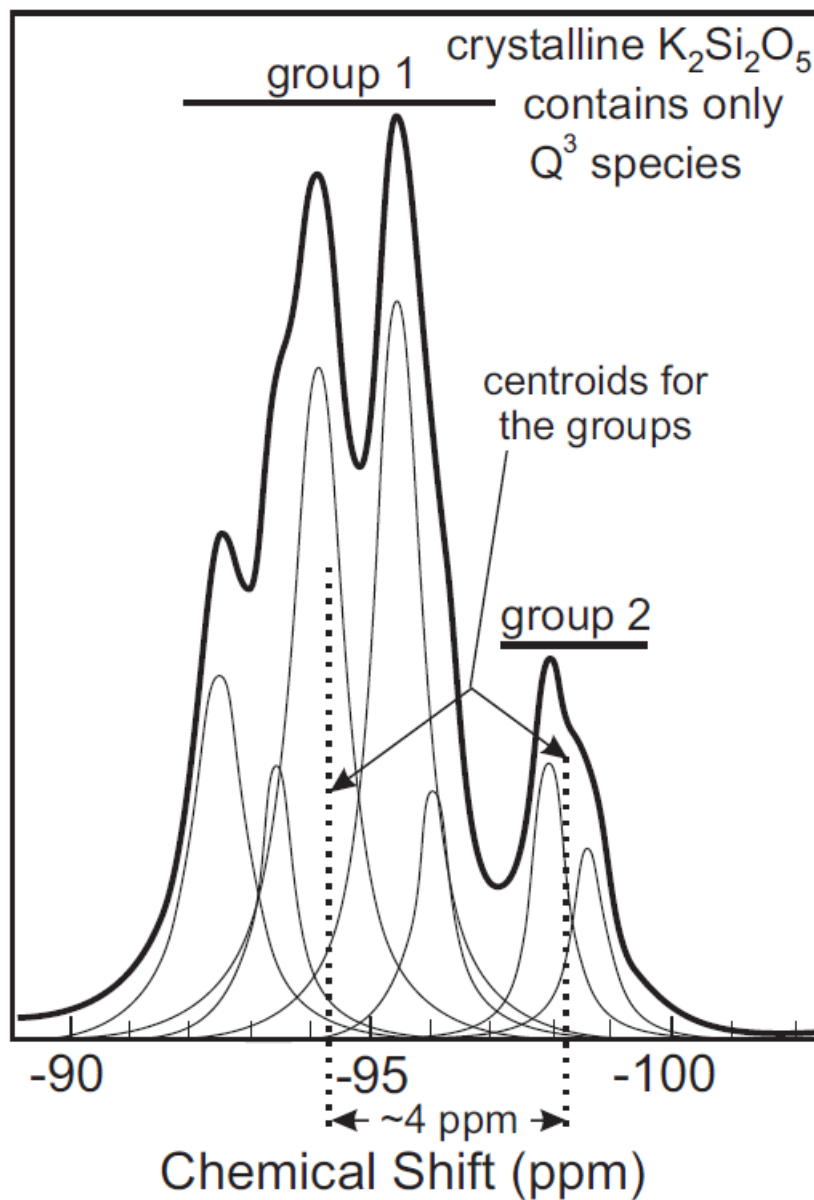


Figure 3.6: Reproduction of the  $^{29}\text{Si}$  MAS NMR spectrum of crystalline  $\text{K}_2\text{Si}_2\text{O}_5$  from de Jong *et al.*, (1998) illustrating the  $\text{Q}$ -species distribution. The spectrum includes seven peaks. A small peak at  $\sim -93.5$  ppm is extraneous (see de Jong *et al.*, (1998) for explanation). The centroids of groups 1 and 2 have been estimated at the half-height for each group and are indicated by the dotted lines.

### 3.4.2. Two Q<sup>2</sup> Species Peaks in Potassium Silicate Glasses

Figure 3.7 shows two reproduced <sup>29</sup>Si MAS NMR spectra from a suite of alkali silicate glasses studied by Maekawa et al. (1991). The potassium metasilicate spectra in Figure 3.7a displays four peaks while the sodium metasilicate spectra in Figure 3.7b displays only three peaks. There was uncertainty regarding the peak assignments for the potassium silicate glass and they presented several possible interpretations. The four peaks were initially assigned as Q<sup>0</sup> to Q<sup>3</sup> and then, as shown in Figure 3.7a, they were assigned as Q<sup>1</sup> to Q<sup>3</sup>. These peak assignments led to NBO/Si ratios of 2.44 and 1.44 for the K-metasilicate and Na-metasilicate, respectively. Both values were different from the expected NBO/Si ratio of 2.0 in which Reaction 3.1 goes to completion and K<sub>1</sub> for Equation 3.2 is infinite. To obtain a fit where NBO/Si = 2.0, Maekawa et al. (1991) assigned a Q<sup>1</sup>, two Q<sup>2</sup> and a Q<sup>3</sup> species to the four peaks even though they noted there was no experimental evidence or expectation for the presence of two types of Q<sup>2</sup> species in potassium silicate glasses. The peak assignment was adopted solely on the basis that it led to an expected NBO/Si value of 2.0. This NBO/Si value presumes that X<sub>O2</sub> = 0.0. There is no experimental or theoretical basis for the assumption that NBO/Si = 2.0 for a metasilicate glass since NBO/Si values and Q-species distributions can change upon melting of the crystalline phases via the polymerization reaction (Nesbitt et al., 2011; Sawyer et al., 2014; Fincham and Richardson, 1954; Toop and Samis, 1962):



(the reverse of Reaction 3.1) which changes NBO/Si to values other than 2.0. Upon melting, disproportionation reactions do not change NBO/Si values:



When assigning Q-species to <sup>29</sup>Si MAS NMR spectra, these have been the only reactions considered by Maekawa et al. (1991) and Malfait et al. (2007). The assumption that NBO/Si = 2.0 in a metasilicate glass was introduced by Maekawa et al. (1991) and there has been no verification of this assumption before or since the publication of their work.

Another concern is that equilibrium between the two Q<sup>2</sup> species was not considered in the study of Maekawa (1991). For the conversion of one Q<sup>2</sup> species to another (i.e., Q<sup>2</sup>'), the mass action equation is

$$K_{Q2} = [Q^2]/[Q^{2'}], \quad (3.5)$$

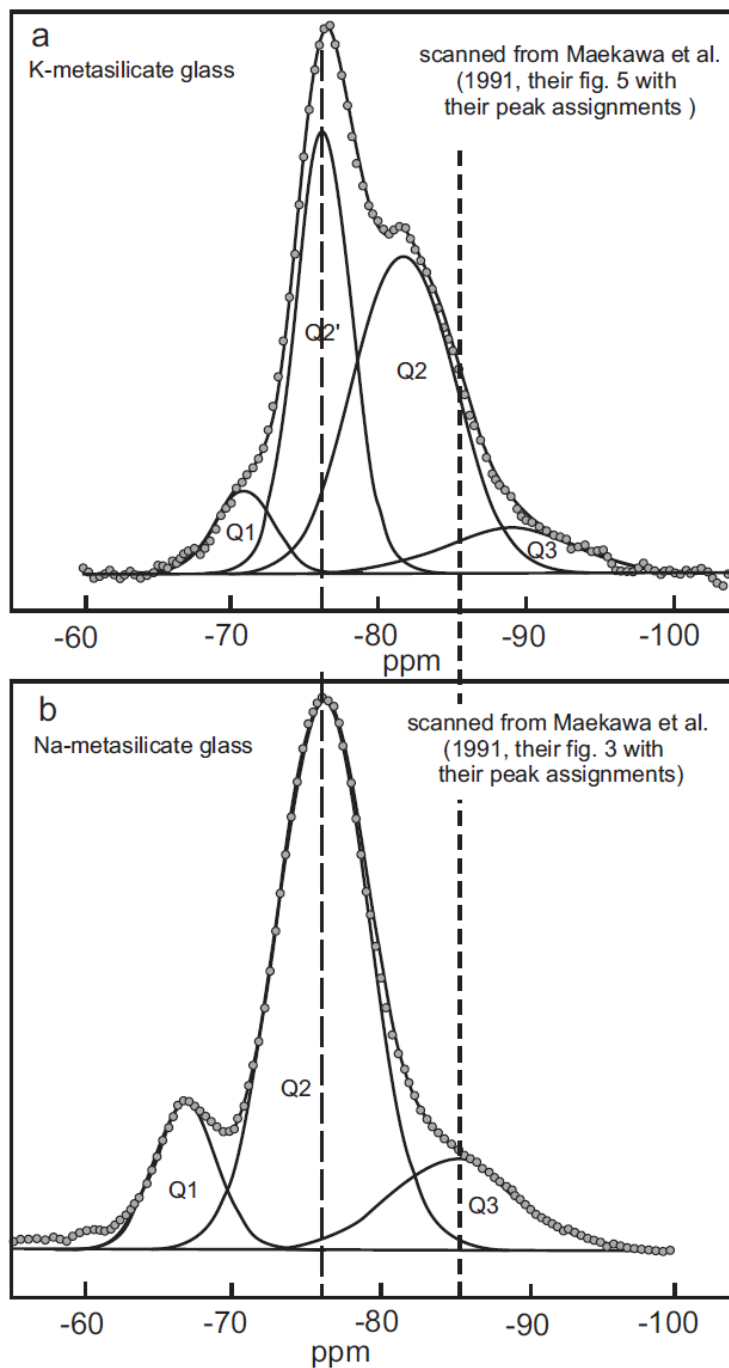


Figure 3.7: (a)  $^{29}\text{Si}$  MAS NMR spectrum of potassium metasilicate glass after Maekawa et al. (1991) and (b) reproduction of the  $^{29}\text{Si}$  MAS NMR spectrum of sodium metasilicate glass from Maekawa et al. (1991) along with their original spectral peak assignments. The differences in the spectra make Q-species assignments uncertain for the potassium metasilicate glass.

where  $K_{Q2}$  is the equilibrium constant, and the brackets represent activities of species. A conditional equilibrium constant can be obtained through substituting mole fractions for activities.  $K_{Q2}$  should remain constant over the compositional range where two  $Q^2$  species were used to fit the spectra, according to equilibrium considerations. In using the  $Q^2$  and  $Q^{2'}$  abundances from Maekawa et al. (1991), the value for  $K_{Q2}$  varies by a factor of  $\sim 5$  in the compositional range where  $X_{K2O}$  is 0.33 to 0.50. The assumption that two  $Q^2$  species are present is problematic because their distribution is inconsistent with thermodynamic considerations.

### 3.4.3. Test for Two $Q^2$ Species

A more recent study of potassium silicate glasses by Malfait et al. (2007) allows for a test of the hypothesis that two  $Q^2$  species are present. The authors performed free fits on their  $^{29}\text{Si}$  MAS NMR spectra and following Maekawa et al. (1991), they assigned a  $Q^1$ , two  $Q^2$  and a  $Q^3$  species to glasses where  $X_{K2O} > 0.333$ .  $X_{BO}$  values were calculated from the reported Q-species abundances (Appendix A) and were plotted in Figure 3.1 as shaded circles. All the data except for the point at  $X_{K2O} = 0.50$  plot below the  $K_1 = \infty$  curve. This means that the freely fit Q-species abundances are physically impossible and as a result, the Q-species assignments are suspect. Underestimation of  $Q^3$  and  $Q^4$  species abundances is the result of these impossibly low  $X_{BO}$  values. It is evident from the analysis in the study of Malfait et al. (2007) that the  $^{29}\text{Si}$  MAS NMR spectra of the potassium silicate glasses where  $X_{K2O} < 0.50$  are not resolved sufficiently enough to obtain accurate estimates of Q-species abundances using free fits. Malfait et al. (2007) noted that their Q-species abundances were inconsistent with those of Maekawa et al. (1991). They adjusted their results by using two assumptions so that they could achieve consistency with the previous results and obtain a value of  $\text{NBO/Si} = 2.0$ . These adjustments assumed the absence of  $O^{2-}$  in the glasses and so oxygen speciation cannot be evaluated from the reported Q-species abundances. To gain additional insight into the nature and distribution of Q-species in potassium silicate glasses, it is necessary to turn to other studies. Davis et al., (2010) found no evidence for two  $Q^2$  species in a highly detailed 2D  $^{29}\text{Si}$  magic angle flipping NMR spectrum of potassium disilicate glass.



### 3.4.4. Two Q<sup>3</sup> Peaks in Potassium Silicate Glasses

The notion that two Q<sup>3</sup> species are possibly present in alkali silicate glasses has existed since at least 1983 (Matson et al., 1983). A study by de Jong et al. (1998) indicated that the NMR spectrum of potassium disilicate glass can be reasonably fitted with two broad Q<sup>3</sup> signals if the ~1 ppm crystalline linewidths (Figure 3.6) are replaced by the broader glass linewidths of Figure 3.7. A 2D and 1D <sup>29</sup>Si MAS NMR study of sodium disilicate glass provided evidence for two Q<sup>3</sup> signals but they could not be resolved in the 1D spectra (Duer et al., 1995). A <sup>29</sup>Si NMR and Raman spectroscopy study of Na<sub>2</sub>Si<sub>3</sub>O<sub>7</sub> and K<sub>2</sub>Si<sub>3</sub>O<sub>7</sub> glasses by Schaller et al. (1999) indicated that a second Q<sup>3</sup> signal developed with the addition of La<sub>2</sub>O<sub>3</sub> to the glasses and was particularly evident in the Raman spectra. A detailed Raman study by Matson et al. (1983) indicated a strong Q<sup>3</sup> band at 1100 cm<sup>-1</sup> with a shoulder at ~1150 cm<sup>-1</sup> in glasses with alkali oxide contents ranging from a few mol% to 30 mol%. They postulated that the shoulder at 1150 cm<sup>-1</sup> was caused by a separate Q<sup>3</sup> signal that was distinct structurally and vibrationally from the main Q<sup>3</sup> signal located at 1100 cm<sup>-1</sup>. The implications of these results being that there is the possibility of the presence of two Q<sup>3</sup> species in alkali silicate glasses with silica-rich compositions.

Another Raman study of potassium disilicate glass showed a strong Q<sup>3</sup> band at 1104 cm<sup>-1</sup>, observing a slight asymmetry in the peak on the low frequency side which they suggested could be an unresolved component under the Q<sup>3</sup> band profile (McMillan et al., 1992). A Raman study by Fukumi et al. (1990) confirmed the findings of Matson et al. (1983) and McMillan et al. (1992). These findings were subsequently reaffirmed by McMillan and Wolfe (1995). All of these experiments indicate the presence of two Q<sup>3</sup> peaks in potassium disilicate glasses. If equilibrium among Q-species exists, then two Q<sup>3</sup> signals must occur in potassium silicate glasses of other compositions.

### 3.4.5. Test for Two Q<sup>3</sup> Signals

In order to test for two Q<sup>3</sup> signals, the following peak assignments were made to the potassium metasilicate spectrum of Figure 3.7a: Q<sup>1</sup> at -70.8 ppm, Q<sup>2</sup> at -76.2 ppm and two Q<sup>3</sup> at -81.7 ppm and -89.0 ppm (i.e., their Q<sup>2'</sup> = our Q<sup>2</sup>, their Q<sup>2</sup> = our Q<sup>3</sup> and their Q<sup>3</sup> = our second Q<sup>3</sup>). These reassignments were applied to all potassium silicate glasses where two Q<sup>2</sup> peaks in the studies of Maekawa et al. (1991) and Malfait et al. (2007). X<sub>BO</sub> values were then calculated (Appendix A)

and plotted in Figure 3.5 as large, shaded triangles and diamonds. These results plot above the curve where  $K_1 = \infty$  and are consistent with the XPS results and with  $K_1 \sim 8.0$ . When two distinct  $Q^3$  signals are used to fit the  $^{29}\text{Si}$  MAS NMR spectra of Maekawa et al. (1991) and Malfait et al. (2007), the results are consistent with those from XPS.

### 3.5. $^{17}\text{O}$ NMR OF POTASSIUM DISILICATE GLASS

#### 3.5.1. Standard Interpretation

Maekawa et al. (1996) fitted a  $^{17}\text{O}$  NMR spectrum of crystalline  $\text{K}_2\text{Si}_2\text{O}_5$  with an NBO peak and a BO peak, but the results did not give the expected NBO:BO ratio of 2:3 based on stoichiometry. To obtain the expected NBO:BO value, they fit a second BO peak. A subsequent XRD study by de Jong et al. (1998) in addition to other studies observed two types of BO signals in crystalline  $\text{K}_2\text{Si}_2\text{O}_5$ : a BO bonded to only two silicon atoms and a BO-K signal where the BO atom is bonded to two silicon atoms and at least one potassium atom (Ching et al., 1983; Cormack et al., 2003; Mead and Mountjoy, 2005; Mead and Mountjoy, 2006; Tilocca and de Leeuw, 2006; Kargl et al., 2006; Machacek et al., 2010; Mountjoy, 2007; de Jong et al., 1998; Maekawa et al., 1996; Greaves et al., 1997; Clarke et al., 2001; Vermillion et al., 1998). The XRD study by de Jong et al. (1998) confirmed the presence of two BO contributions and justified the fit of Maekawa et al. (1996). To fit a  $\text{K}_2\text{Si}_2\text{O}_5$  glass spectrum, Maekawa et al. (1996) used only one BO and one NBO peak. Once again, the results did not give the expected NBO:BO ratio. However, they make no mention of adding a second BO peak to improve the fit as was done with the crystalline sample. The study of Maekawa et al. (1996) demonstrates that the number of BO signals contributing to the  $^{17}\text{O}$  NMR spectra of potassium silicate glasses and crystals must be known before a proper fit can be performed.

#### 3.5.2. Oxygen Coordination and Chemical Shifts

A recent  $^{17}\text{O}$  NMR study by Stebbins and Sen (2013) of a potassium silicate glass with  $X_{\text{K}_2\text{O}} = 0.34\%$  concluded that there was no evidence for  $\text{O}^{2-}$  above 0.1-1.0 mol% levels in the absence of any directly observable  $\text{O}^{2-}$  peak in the spectrum. They calculated a peak position for  $\text{O}^{2-}$  at  $290 \pm 10$  ppm for crystalline  $\text{K}_2\text{O}$ , but that value cannot be verified by experiment due to the instability of  $\text{K}_2\text{O}$  (Huhey, 1983; Cotton and Wilkinson, 1988). However, the calculated value is reasonable (Turner et al., 1985). The chemical shift for  $\text{O}^{2-}$  in the glass was assumed to have a

similar value and the absence of a peak at 290 ppm led to the conclusion that no free oxide was present. Some comments about these assumptions must be made. First, it is unlikely that free oxide atoms will have a similar coordination environment in glass as they do in crystalline  $\text{K}_2\text{O}$  where the oxygen coordination is to eight potassium atoms (Wells, 1984). Mountjoy (2007) found that in alkali and alkaline earth silicate glasses, coordination numbers of BO and NBO vary greatly (from 1 to over 4) and are dependent on the glass composition. It is reasonable to assume that the coordination of  $\text{O}^{2-}$  in these glasses varies to a similar degree and is also dependent on composition. Kohara et al. (2004, 2011) reported  $\text{O}^{2-}$  in magnesium silicate glasses. They did not mention  $\text{O}^{2-}$  coordination numbers but their diagrams (e.g., Figure 3 in Kohara et al., 2004) indicated 2 and 3 coordinated  $\text{O}^{2-}$ . It has been shown that some of these moieties, in particular those moieties with low coordination numbers, will have large second-order quadrupolar shifts and very large electric field gradients (Ashbrook et al., 2005). One example of this is a recent study by Thompson et al. (2012) which observed a large chemical shift of  $\sim 30$  ppm between the “free oxide” in CaO and the “free oxide” in crystalline  $\text{Ca}_3\text{SiO}_5$  where oxygen is sixfold coordinated in both phases. A study by Ashbrook et al. (2005) showed that the free oxide peak position varied greatly with NMR field strength for a magnesium silicate sample. It is likely that there would be shifts of more than 100 ppm for the free oxide peak position in silica-rich potassium silicate glasses compared to crystalline oxides. These shifts should vary with NMR field strength.

### 3.5.3. Search for $\text{O}^{2-}$

$\text{O}^{2-}$  cannot be detected directly with certainty in  $^{17}\text{O}$  NMR spectra yet. In the study by Stebbins and Sen (2013), their broadscan spectra of the 40 mol%  $\text{K}_2\text{O}$  glass taken at 14.1 T showed other small peaks at  $\sim 140$  ppm and  $\sim -20$  ppm (their Figure 2c, 2d) which went unmentioned. These peaks do not appear in their spectra taken at 9.4 T. This can be explained by large second-order quadrupolar shifts for a species like low coordinated  $\text{O}^{2-}$  which would have a large quadrupolar coupling. It may indeed be that the definitive presence of  $\text{O}^{2-}$  in  $^{17}\text{O}$  NMR spectra may not be established until methods are devised to calculate chemical shifts of oxygen as a function of coordination number.

There is the possibility that the  $\text{O}^{2-}$  signal is located under either the NBO or BO peaks of the  $^{17}\text{O}$  NMR spectra. If this is the case, then the  $\text{O}^{2-}$  signal should be reflected in the NBO:BO area

ratio value. In the study by Stebbins and Sen (2013), they fit one symmetric (Gaussian) NBO peak to their  $^{17}\text{O}$  NMR spectrum and subtracted the peak area from the total spectral area to obtain the NBO:BO ratio. The spectrum of the 34 mol%  $\text{K}_2\text{O}$  glass (their Figure 3) is asymmetric in the region of the BO contribution. This asymmetry makes it impossible to obtain an accurate NBO:BO value using their method of peak subtraction because it is not known how the asymmetric BO signal overlaps the NBO signal. To obtain an accurate NBO:BO value it is necessary to perform a complete fit to the spectrum, which the asymmetry disallows. An incomplete fit increases the uncertainty associated with the NBO:BO ratio to a degree larger than reported (>1%). The large uncertainty associated with the value makes it impossible to accurately assess the presence or absence of  $\text{O}^{2-}$ . Despite all these issues,  $^{17}\text{O}$  NMR is likely the most sensitive technique available to detect  $\text{O}^{2-}$ . Accurate calculations of peak positions combined with highly resolved and carefully fit spectra should provide good results. Such results also require knowledge of the number of BO species in the spectra and the reaction rates involving  $\text{O}^{2-}$  (which is highly ionic) must not exceed NMR sampling times (Farnan and Stebbins, 1990).

### 3.6. $\text{O}^{2-}$ ABUNDANCES AND KINETICS OF DISSOLUTION OF GASES IN MELTS

#### 3.6.1. Oxygen Speciation and Thermodynamic Considerations

There is no doubt as to the presence of  $\text{O}^{2-}$  in melts of high MO content as BO, NBO and  $\text{O}^{2-}$  are considered to all exist in ultramafic magmas (Eggler and Rosenhauer, 1978) and  $\text{O}^{2-}$  has been detected by  $^{17}\text{O}$  NMR in highly mafic glasses (Nasikas et al., 2012). Yet at compositions greater than the orthosilicate ( $X_{\text{SiO}_2} > 0.33$ ),  $\text{O}^{2-}$  is considered absent in most alkaline earth and alkali silicate melts and glasses (Thompson et al., 2012; Eggler and Rosenhauer, 1978). The apparent absence of  $\text{O}^{2-}$  in these glasses and melts can be investigated by considering studies done on  $\text{CaO-SiO}_2$  binary melts. Studies have measured the activity of CaO in these melts (Elliot, 1955; Darken and Gurry, 1953). The equilibrium distribution of BO, NBO and  $\text{O}^{2-}$  and the equilibrium constant ( $K_1$ ) have been evaluated based on the assumptions that CaO dissociates entirely and that the Tempkin model holds in the binary (Fincham and Richardson, 1954; Toop and Samis, 1962; Masson, 1968; Ottonello, 2005). Each study employed different methods to obtain values

for  $K_1$ , but all values were finite. Since silicate melts are homogeneous solutions, by thermodynamic principles a finite  $K_1$  at one composition of a binary melts requires  $K_1$  to be finite at all compositions of the binary system. This means that BO, NBO and  $O^{2-}$  must be present at all compositions though in highly siliceous melts,  $O^{2-}$  will be low and perhaps too low to be detected by conventional spectroscopic methods. Nevertheless,  $O^{2-}$  has a specific activity and mole fraction for each composition across the binary. Many molecular dynamics simulation studies have found free oxide in melts (Cormack et al., 2003; de Koker et al., 2009; Martin et al., 2009; Karki, 2010; Karki et al., 2010). If free oxide is present in highly basic homogenous melts, it must be present in more siliceous melts. Arguments to the contrary go against equilibrium thermodynamic principles.

In most thermodynamic treatments, complete dissociation of the MO (e.g., CaO) component of binary silicate melts is assumed (i.e.  $CaO \rightarrow Ca^{2+} + O^{2-}$ ) so that, for example,  $X_{CaO} = X_{O^{2-}}$ . The associated mass action equation is  $K_2 = \{[O^{2-}][Ca^{2+}]\}/[CaO]$  where  $K_2$  is the equilibrium constant of dissociation. Complete dissociation requires  $K_2$  to be infinite. In homogeneous systems, dissociation reactions generally do not go to completion, so an infinite value for  $K_2$  seems unlikely in a homogenous melt. In an aqueous solution, such as NaCl and water for example, the dissociation constant for NaCl is finite and strong association occurs at high temperatures (Helgeson, 1969). For the metal oxide dissociation reaction in silicate melts, the value for  $K_2$  is also likely finite (Fraser, 1977). The available evidence and thermodynamic considerations support the notion that  $O^{2-}$  is present in most alkali, alkaline earth and 3d metal oxide – silicate binary melts and that where present and at any concentration,  $O^{2-}$  is available to react with reagents introduced into the melts.

### 3.6.2. Kinetic and Thermodynamic Aspects of Gas Dissolution in Melts

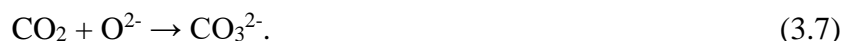
The presence of  $O^{2-}$  has been established and quantified in potassium silicate glasses and because of that, the implications of its presence can be considered in the context of some important reactions that pertain to geochemical processes. The uptake of water,  $CO_2$  and sulfur in silicate glasses and magmas has been well noted and quantified due to their importance to magmatic and volcanic processes (Fine and Stöpler, 1985; Fine and Stöpler, 1986; Iacovino et al., 2013; Seifert et al., 2013; Morizet et al., 2013a,b; Duncan and Dasgupta, 2014; Le Losq et al., 2012; Le Losq et al., 2013; Stöpler, 1982; Cody et al., 2005; Xue and Kanzaki, 2004; Baker and Moretti, 2011).

The reaction of CO<sub>2</sub> with oxygen species in melts will be considered because the uptake of CO<sub>2</sub> has been well documented. An early study by Eggler and Rosenhauer (1978) showed that gaseous CO<sub>2</sub> dissolved in melts and exists as CO<sub>2</sub> and CO<sub>3</sub><sup>2-</sup>. There is general agreement that the overall stoichiometric reaction for the uptake of CO<sub>2</sub> is:



(Fine and Stopler, 1985; Fine and Stopler, 1986; Iacovino et al., 2013; Seifert et al., 2013; Morizet et al., 2013; Duncan and Dasgupta, 2014; Le Losq et al., 2012; Le Losq et al., 2013; Chen et al., 2012; Bodor et al., 2013; Mysen and Virgo, 1980; Brooker et al., 2001). There exists, however, a degree of ambiguity concerning the mechanism of CO<sub>2</sub> uptake. CO<sub>2</sub> has been considered as the “solubility mechanism” (Mysen and Virgo, 1980) and for several decades, NBO has been considered as the reactive oxygen species. The ambiguity exists because Equation 3.6 is a third order reaction, making it unlikely that it is an elementary reaction. Many kinetics textbooks state that reactions which are larger than second order reaction often involve two or more lower order elementary reactions since third-order reactions require three species to interact at the same time (Frost et al., 1961; Laidler, 1965; Lasaga, 1981). This aspect was emphasized by Lasaga (1981) using Fenton’s reaction for oxidation of Fe<sup>2+</sup> by H<sub>2</sub>O<sub>2</sub> in an aqueous solution. For the overall reaction to proceed, it is necessary for five reactants to collide at the same time. Fenton’s reaction involves second order elementary reactions (Lasaga, 1981). In a similar sense, Equation 3.6 is more than likely the sum of two or more second order elementary reactions. It is even more unlikely that Equation 3.6 is an elementary reaction from steric considerations. Potassium silicates have large bond lengths compared with C-O bond lengths in CO<sub>2</sub> (de Jong et al., 1998). It is unlikely that two NBO atoms separated by ~4 Å could attack at once the carbon in CO<sub>2</sub> where the C-O bond length is 1.16 Å.

Two obvious pairs of bimolecular reactions, when added together, give Equation 3.6 and are as follows. The first reaction, which is also the most probable, involves the direct reaction of CO<sub>2</sub> with O<sup>2-</sup> (if it is present) (Pearce et al., 1964; Fine and Stopler, 1985; Fine and Stopler, 1986; Eggler and Rosenhauer, 1978):



This reaction was recognized over 40 years ago by Eggler and Rosenhauer (1978) who stated that it “involves no rearrangement of the silicate network and will be strongly favoured (over Equation 3.6), if such oxides are present”. The reactant O<sup>2-</sup> would be consumed if this reaction

were to occur. The  $O^{2-}$  reactant would be regenerated through the buffering action of the polymerization reaction according to Le Chatelier's Principle, which gives the second reaction:



Thus, more  $CO_3^{2-}$  would form than the amount of  $O^{2-}$  that was present in the melt before the reaction. The sum of Equations 3.7 and 3.8 gives the stoichiometry of Equation 3.6. Equations 3.7 and 3.8 are also second order reactions so they are likely to proceed more rapidly than Equation 3.6. It is possible that Equations 3.7 and 3.8 are elementary reactions given that the XPS experimental results (Figure 3.5) and the results of other described above demonstrate that  $O^{2-}$  is present in numerous binary silicate glasses.

There is also the possibility that  $CO_2$  could react with two NBO in sequence in two second order reactions:



Equations 3.9 and 3.10 also result in Equation 3.6 when summed. However, Equations 3.7 and 3.8 are likely to be more favourable for at least two reasons. First, Egglar and Rosenhauer (1978) suggested that  $O^{2-}$  is a much stronger base than NBO for nucleophilic attack of the centre carbon in  $CO_2$ . This makes Reaction 3.7 more favourable than Reaction 3.9. This idea has been confirmed by experimental studies which have shown that CaO is much more reactive than NBO or BO to  $CO_2$  in silicate minerals like diopside ( $CaMgSiO_6$ ) (Chen et al., 2012; Bodor et al., 2013). Second, Equation 3.8 can involve any NBOs within the volume accessible for  $O^{2-}$  migration while Equation 3.10 requires reaction of an adjacent NBO. Thus, Reaction 3.8 should proceed at a faster rate than Reaction 3.10. It should be noted that the second NBO for Equation 3.10 could attack either the carbon centre or the silicon centre (where the NBO of  $CO_2 \cdot NBO^-$  is attached). If the second NBO attacked the silicon centre, the intermediate silicate moiety would be fivefold coordinated which, from a study by Corriu (1990), is quite common.

Equations 3.7 and 3.8 are likely important elementary reactions since it has been demonstrated that  $O^{2-}$  is present in silicate glasses. The discussion moves to the small amount of  $O^{2-}$  necessary to produce the amounts of  $CO_3^{2-}$  that is observed in reactions of  $CO_2$  with silicate melts in general (Fine and Stopler, 1985; Fine and Stopler, 1986; McMillan et al., 1992; Matson et al., 1983; Dalby et al., 2007; Iacovino et al., 2013; Le Losq et al., 2012; Le Losq et al., 2013). Mass

balances associated with the formation of  $\text{CO}_3^{2-}$  in silica-rich melts are concordant with low initial values for  $\text{O}^{2-}$  (Fine and Stöpler, 1985). In low  $\text{CO}_2$  pressure experiments,  $\text{CO}_3^{2-}$  is below 1 wt% (~0.5 mol%) in a  $\text{NaAlSi}_2\text{O}_6$  (16 mol%  $\text{Na}_2\text{O}$ ) melt and below 0.1 wt% (~0.05 mol%) in a  $\text{NaAlSi}_4\text{O}_{10}$  (10 mol%  $\text{Na}_2\text{O}$ ) melt (Fine and Stöpler, 1985). From Equation 3.7, the  $\text{CO}_3^{2-}$  amounts require only 0.5 and 0.05 mol%  $\text{O}^{2-}$  to convert dissolved  $\text{CO}_2$  to  $\text{CO}_3^{2-}$  in the Na-aluminosilicate melts described above. These low amounts of  $\text{CO}_2$  required have been confirmed by similar studies of natural and synthesized silicate melts (Fine and Stöpler, 1986; Iacovino et al., 2013; Seifert et al., 2013; Morizet et al., 2013a; Duncan and Dasgupta, 2014; Le Losq et al., 2012; Le Losq et al., 2013). The regeneration of the small initial amounts of  $\text{O}^{2-}$  via Reaction 3.8 (according to Le Chatelier's Principle) allows for the low amounts described above to be achieved.

Estimates of  $[\text{CO}_3^{2-}]/[\text{CO}_2]$  ratios as a function of glass MO or  $\text{M}_2\text{O}$  content can be obtained given the relationship that exists between the mole fractions and activities of BO, NBO,  $\text{O}^{2-}$ ,  $\text{CO}_2$  and  $\text{CO}_3^{2-}$  from mass action equations. The mass action for Equation 3.6, where square brackets represent activities, is:

$$K_6 = \{[\text{BO}][\text{CO}_3^{2-}]\}/\{[\text{NBO}]^2[\text{CO}_2]\}. \quad (3.11)$$

By rearranging Equation 3.2, we obtain:

$$[\text{O}^{2-}] = \{[\text{NBO}]^2/[\text{BO}]\}/K_1. \quad (3.12)$$

And by substituting Equation 3.11 into Equation 3.12, we get:

$$K_1K_6[\text{O}^{2-}] = [\text{CO}_3^{2-}]/[\text{CO}_2]. \quad (3.13)$$

$[\text{O}^{2-}]$  and thus,  $X_{\text{O}_2}$ , in melts is determined from Equation 3.12 by  $[\text{NBO}]^2/[\text{BO}]$ . This ratio buffers  $[\text{O}^{2-}]$  and  $X_{\text{O}_2}$  in melts where there is an excess of BO and NBO over  $\text{O}^{2-}$ . A lower  $[\text{NBO}]^2/[\text{BO}]$  ratio reflects low abundances of  $X_{\text{O}_2}$  and conversely, a higher ratio reflects much greater concentrations in melts with higher and lower silicon contents respectively. Equation 3.13 shows the direct relationship between  $[\text{O}^{2-}]$  (hence  $X_{\text{O}_2}$ ) and the  $[\text{CO}_3^{2-}]/[\text{CO}_2]$  ratio. As above, lower  $[\text{O}^{2-}]$  in highly siliceous melts will result in lower  $[\text{CO}_3^{2-}]/[\text{CO}_2]$  ratios where the converse is true where  $[\text{O}^{2-}]$  is high. These relationships have been observed experimentally by Fine and Stöpler (1985) for sodium-aluminosilicate glasses. They found that at low  $\text{CO}_2$  pressures, the  $[\text{CO}_3^{2-}]/[\text{CO}_2]$  ratio varies greatly, as expected from theory, from 0.2 in a  $\text{NaAlSi}_4\text{O}_{10}$  (10 mol%  $\text{Na}_2\text{O}$ ) melt to 1.6 in a  $\text{NaAlSi}_2\text{O}_6$  (16 mol%  $\text{Na}_2\text{O}$ ) melt (Fine and Stöpler, 1985).



The polymerization reaction (Equation 3.8) buffers  $O^{2-}$  at an effectively constant value in siliceous melts of specified melt compositions. The  $[CO_3^{2-}]$  ratio will be an effectively constant value as well, from Equation 3.13, regardless of the partial pressure of  $CO_2$  over the melt (for example, Figure 3.1 of Fine and Stopler, 1985).  $K_1$  has been determined and is known for binary potassium and sodium silicate glasses and so  $CO_2$  solubility experiments on these systems would allow for a way to evaluate  $K_6$ . Such studies would be beneficial in advancing our understanding of the behaviour of  $CO_2$  in melts. It is possible that these experiments would be the best way to determine the nature of the critical oxygen species in the process that converts  $CO_2$  to  $CO_3^{2-}$ . The kinetics and mechanism of this conversion process could be evaluated.

### 3.7. CONCLUSIONS

It is clear from the O 1s spectra of six potassium silicate glasses with compositions ranging from 27 to 37 mol%  $K_2O$  that free oxide is present in the glasses in all cases at a few mol%. Three glasses were analyzed carefully using a special EPMA technique that allowed for more refined uncertainty and error analysis. A reinterpretation of previously published  $^{29}Si$  NMR spectra of potassium silicate glasses between the disilicate and metasilicate compositions was presented, using two  $Q^3$  peaks instead of two  $Q^2$  peaks. These reinterpretations were justified based on previous experimental and theoretical considerations and they yielded free oxide amounts that are consistent with XPS, Raman and XRD results. The abundance of  $O^{2-}$  in these glasses is high enough to react with  $CO_2$  in natural and synthesized melts. From the kinetics and thermodynamics arguments presented, it is suggested that  $O^{2-}$  is the critical reactive species that converts  $CO_2$  to  $CO_3^{2-}$  in natural and synthetic magmas.

### 3.8. REFERENCES

- Ashbrook, S. E., Berry, A. J., Hibberson, W. O., Steuernagel, S., and Wimperis, S., (2005) High resolution  $^{17}O$  MAS NMR spectroscopy of forsterite ( $\alpha$ - $Mg_2SiO_4$ ), wadsleyite ( $\beta$ - $Mg_2SiO_4$ ) and ringwoodite ( $\gamma$ - $Mg_2SiO_4$ ). *American Mineralogist* **90**, 1861-1870.
- Baker, D. R. and Moretti, R., (2011) Modeling the solubility of sulfur in magmas: A 50-year old geochemical challenge. *Reviews in Mineralogy and Geochemistry* **73**, 167-213.
- Bancroft, G. M., Nesbitt, H. W., Ho, R., Shaw, D. M., Tse, J. S., and Biesinger, M. C., (2009) Toward a comprehensive understanding of solid-state core-level XPS linewidths:

- Experimental and theoretical studies on the Si 2p and O 1s linewidths in silicates. *Physical Review B* **80**, 075405-1-13.
- Bodor, M., Santos, R. M., Kriskova, L., Elsen, J., Vlad, M., and Van Gerven, T., (2013) Susceptibility of mineral phases of steel slags towards carbonation: Mineralogical, morphological and chemical assessment. *European Journal of Mineralogy* **25**, 533-549.
- Brooker, R. A., Kohn, S. C., Holloway, J. R., and McMillan, P. F., (2001) Structural controls on the solubility of CO<sub>2</sub> in silicate melts Part I: Bulk solubility data. *Chemical Geology* **174**, 225-239.
- Brown, G. E., Farges, F., and Calas, G., (1995) X-ray scattering and X-ray spectroscopy studies of silicate melts. *Reviews in Mineralogy and Geochemistry* **32**, 317-410.
- Chen, C., Yang, S.-T., and Ahn, W.-S., (2012) Calcium oxide as high temperature CO<sub>2</sub> sorbent: Effects of textural properties. *Materials Letters* **75**, 140-142.
- Ching, W. Y., Murray, R. A., Lam, D. G., and Veal, B. W., (1983) Comparative studies of electronic structures of sodium metasilicate and  $\alpha$  and  $\beta$  phases of sodium disilicate. *Physical Review B* **28** (8), 4724-4735.
- Clarke, T. M., Grandinetti, P. J., Florian, P., and Stebbins, J. F., (2001) An <sup>17</sup>O NMR investigation of crystalline sodium metasilicate: Implications for the determination of local structure in alkali silicates. *Journal of Physics and Chemistry B* **105**, 12257-12265.
- Cody, G. D., Mysen, B. O., and Lee, S. K., (2005) Structure vs. composition: A solid-state <sup>1</sup>H and <sup>29</sup>Si NMR study of quenched glasses along the Na<sub>2</sub>O-SiO<sub>2</sub>-H<sub>2</sub>O join. *Geochimica et Cosmochimica Acta* **69** (9), 2373-2384.
- Cormack, A. N., Du, J., and Zeitler, T. R., (2003) Sodium ion migration mechanisms in silicate glasses probed by molecular dynamics simulations. *Journal of Non-Crystalline Solids* **323**, 147-154.
- Cormier, L., and Cuello, G. J., (2013) Structural investigation of glasses along the MgSiO<sub>3</sub>-CaSiO<sub>3</sub> join: Diffraction studies. *Geochimica et Cosmochimica Acta* **122**, 498-510.
- Corriu, R. J. P., (1990) Hypervalent species of silicon: Structure and reactivity. *Journal of Organometallic Chemistry* **400**, 81-106.
- Cotton, F. A. and Wilkinson, G., (1988) *Advanced Inorganic Chemistry*, 5th edition. John Wiley and Sons, New York, 1455 p.
- Dalby, K. N., Nesbitt, H. W., Zakaznova-Herzog, V. P., and King, P. L., (2007) Resolution of

- bridging oxygen signals from O 1s spectra of silicate glasses using XPS: Implications for O and Si speciation. *Geochimica et Cosmochimica Acta* **71**, 4297-4313.
- Darken, L. S. and Gurry, R. W., (1953) *Physical Chemistry of Metals*. McGraw-Hill: New York, 535 p.
- Davis, M. C., Kaseman, D. C., Parvani, S. M., Sanders, K. J., Grandinetti, P. J., Massiot, D., and Florian, P., (2010) Q<sup>(n)</sup> species distribution in K<sub>2</sub>O-2SiO<sub>2</sub> glass by <sup>29</sup>Si magic angle flipping NMR. *Journal of Physics and Chemistry A* **114**, 5503-5508.
- Davis, M. C., Sanders, K. J., Grandinetti, P. J., Gaudio, S. J., and Sen, S., (2011) Structural investigations of magnesium silicate glasses by <sup>29</sup>Si 2D magical angle flipping NMR. *Journal of Non-Crystalline Solids* **357**, 2787-2795.
- de Jong, B. H. W. S., Super, H. T. J., Spek, A. L., Veldman, N., Nachtegaal, G., and Fischer, J. C., (1998) Mixed alkali systems: Structure and <sup>29</sup>Si MAS NMR of Li<sub>2</sub>Si<sub>2</sub>O<sub>5</sub> and K<sub>2</sub>Si<sub>2</sub>O<sub>5</sub>. *Acta Crystallographica B* **54**, 568-577.
- de Koker, N. P., Stixrude, L., and Karki, B. B., (2009) Thermodynamics, structure, dynamics and freezing of Mg<sub>2</sub>SiO<sub>4</sub> liquid at high pressure. *Geochimica et Cosmochimica Acta* **72**, 1427-1441.
- Dingwell, D.B., (2006) Transport properties of magmas: Diffusion and rheology. *Elements* **2**, 281-286.
- Du, J., and Cormack, A. N., (2004) The medium range structure of sodium silicate glasses: A molecular dynamics simulation. *Journal of Non-Crystalline Solids* **349**, 66-79.
- Duer, M. J., Elliot, S. R., and Gladden, L. F., (1995) An investigation of the structural units in sodium disilicate glass: A 2D <sup>29</sup>Si NMR study. *Journal of Non-Crystalline Solids* **189**, 107-117.
- Duncan, M., and Dasgupta, R., (2014) CO<sub>2</sub> solubility and speciation in rhyolitic sediment partial melts at 1.5-3.0 GPa: Implications for carbon flux in subduction zones. *Geochimica et Cosmochimica Acta* **124**, 328-347.
- Eggler, D. H. and Rosenhauer, M., (1978) Carbon dioxide in silicate melts: II. Solubilities of CO<sub>2</sub> and H<sub>2</sub>O in CaMgSi<sub>2</sub>O<sub>6</sub> (diopside) liquids and vapors at pressures to 40 kb. *American Journal of Science* **278**, 64-94.
- Elliott, J. F., (1955) Activities in the iron oxide-silica-lime system. *Journal of Metals* **7**, 485-488.
- Farnan, I. and Stebbins, J. F., (1990) High-temperature <sup>29</sup>Si NMR investigation of solid and

- molten silicates. *Journal of the American Chemical Society* **112**, 32-39.
- Fincham, C. F. B. and Richardson, F. D., (1954) The behaviour of sulphur in silicate and aluminate melts. *Proceedings of the Royal Society of London: Series A* **223**, 40-62.
- Fine, G. and Stolper, E., (1985) The speciation of carbon dioxide in sodium aluminosilicate glasses. *Contributions to Mineralogy and Petrology* **91**, 105-121.
- Fine, G. and Stolper, E., (1985/86) Dissolved carbon dioxide in basaltic glasses: Concentrations and speciation. *Earth and Planetary Science Letters* **76**, 263-278.
- Fraser, D. G., (1977) Thermodynamic properties in silicate melts. *In: Thermodynamics in Geology* (ed. D. G. Fraser). D. Riedel Publ. Co., Dordrecht, pp. 301–326.
- Frost, A. A. and Pearson, R. G., (1961) *Kinetics and Mechanism*, 2nd edition. John Wiley and Sons, New York, 432 p.
- Fukumi, K., Hayakawa, J., and Komiyama, T., (1990) Intensity of Raman band in silicate glasses. *Journal of Non-Crystalline Solids* **119**, 297-302.
- Greaves, G. N., (2000) Structure and ionic transport in disordered silicates. *Mineralogical Magazine* **64**, 441-446.
- Greaves, G. N., Fontaine, A., Lagarde, P., Raoux, D., and Gurman, S. J., (1981) Local structure of silicate glasses. *Nature* **293**, 611-616.
- Greaves, G. N., Smith, W., Giulotto, E., and Pantos, E. J., (1997) Local structure, microstructure and glass properties. *Journal of Non-Crystalline Solids* **222**, 13-24.
- Harmer, S. L., Skinner, W. M., Buckley, A. N., and Fan, L.-J., (2009) Species formed at cuprite fracture surfaces: Observation of O 1s surface core level shift. *Surface Science* **603**, 537-545.
- Helgeson, H. C., (1969) Thermodynamics of hydrothermal systems at elevated temperatures and pressures. *American Journal of Science* **267**, 729-804.
- Helgeson, H. C., Delaney, J. M., Nesbitt, H. W., and Bird, D. K., (1978) Summary and critique of the thermodynamic properties of rock forming minerals. *American Journal of Science* **278-A**, 1–234.
- Henderson, G. S., (2005) The structure of silicate melts: A glass perspective. *Canadian Mineralogist* **43**, 1921-1958.
- Henderson, G. S., Calas, G., and Stebbins, J. F., (2006) The structure of silicate glasses and melts. *Elements* **2**, 269-273.

- Hess, P. C., (1980) Polymerization model for silicate melts. *In: Physics of Magmatic Processes* (ed. R. B. Hargraves). Princeton University Press, Princeton pp. 3–25.
- Huhey, J. E., (1983) *Inorganic Chemistry: Principles of Structure and Reactivity*, 3rd edition. Harper and Row, New York, 936 p.
- Iacovino, K., Moore, G., Roggensack, K., Oppenheimer, C., and Kyle, P., (2013) H<sub>2</sub>O-CO<sub>2</sub> solubility in mafic alkaline magma: Applications to volatile sources and degassing behaviour at Erebus volcano, Antarctica. *Contributions to Mineralogy and Petrology* **166**, 845-860.
- Kargl, F., Meyer, A., Koza, M. M., and Schober, H., (2006) Formation of channels for fast-ion diffusion in alkali silicate melts: A quasielastic neutron scattering study. *Physical Review B* **74**, 014304-1-5.
- Karki, B. B., (2010) First-principles molecular dynamics simulations of silicate melts: Structural and dynamic properties. *Reviews in Mineralogy and Geochemistry* **71**, 355-389.
- Karki, B. B., Bhattarai, D., Mookherjee, M., and Stixrude, L., (2010) Visualization-based analysis of structural and dynamical properties of simulated hydrous silicate melt. *Physics and Chemistry of Minerals* **37**, 103-117.
- Kohara, S., Suzuya, K., Takeuchi, K., Loong, C.-K., Grimstitch, M., Weber, J. K. R., Tangeman, A., and Key, S., (2004) Glass formation at the limit of insufficient network formers. *Science* **303**, 1649-1652.
- Kohara, S., Akola, J., Morita, H., Suzuya, K., Weber, J. K. R., Wilding, M. C., and Benmore, C. J., (2011) Relationship between topological order and glass forming ability in densely packed enstatite and forsterite composition glasses. *Proceedings of the National Academy of Sciences of the United States of America* **108 (36)**, 14780-14785.
- Kracek, F. C., Bowen, N. L., and Morley, G. W., (1937) Equilibrium relations and factors influencing their determination in the system K<sub>2</sub>SiO<sub>3</sub>-SiO<sub>2</sub>. *Journal of Physical Chemistry* **41 (9)**, 1183-1193.
- Laidler, K.J., (1965) *Chemical Kinetics*. McGraw-Hill, New York, 566 p.
- Lasaga, A. C., (1981) Rate laws of chemical reactions. *In: Volume 8: Kinetics of Geochemical Processes* (eds. A. C. Lasaga and R. J. Kirkpatrick). Reviews in Mineralogy, Mineralogical Society of America, Washington D.C., pp. 1–68.
- Le Losq, C., Moretti, R., and Neuville, D.R., (2013) Speciation and amphoteric behaviour of

- water in aluminosilicate melts and glasses: High temperature Raman spectroscopy and reaction equilibria. *European Journal of Mineralogy* **25**, 777-790.
- Le Losq, C., Neuville, D. R., Moretti, R., and Roux, J., (2012) Determination of water content in silicate glasses using Raman spectroscopy: Implications for the study of explosive volcanism. *American Mineralogist* **97**, 779-790.
- Lee, S. K. and Stebbins, J. F., (2006) Disorder and the extent of polymerization in calcium silicate and aluminosilicate glasses:  $^{17}\text{O}$  NMR results and quantum chemical molecular orbital calculations. *Geochimica et Cosmochimica Acta* **70**, 4275-4286.
- Lee, S. K. and Stebbins, J. F., (2009) Effects of the degree of polymerization on the structure of sodium silicate and aluminosilicate glasses and melts: An  $^{17}\text{O}$  NMR study. *Geochimica et Cosmochimica Acta* **73**, 1109-1119.
- Machacek, J., Gedeon, O., and Liska, M., (2010) The MD study of mixed alkali effect in alkali silicate glasses. *Physics and Chemistry of Glasses – European Journal of Glass Science and Technology Part B* **51**, 65-84.
- Maekawa, H., Florian, P., Massiot, D., Kiyono, H., and Nakamura, M., (1996) Effect of alkali metal oxide on  $^{17}\text{O}$  NMR parameters and Si-O-Si angles of alkali mixed disilicate glasses. *Journal of Physical Chemistry* **100**, 5525-5532.
- Maekawa, H., Maekawa, T., Kawamura, K., and Yokokawa, T., (1991) The structural groups of alkali silicate glasses determined from  $^{29}\text{Si}$  MAS-NMR. *Journal of Non-Crystalline Solids* **127**, 53-64.
- Malfait, W. J., Halter, W. E., Morizet, Y., Meier, B. H., and Verel, R., (2007) Structural control on bulk melt properties: Single and double quantum  $^{29}\text{Si}$  NMR spectroscopy on alkali-silicate glasses. *Geochimica et Cosmochimica Acta* **71**, 6002-6018.
- Martin, G. B., Spera, F. J., Ghiorso, M. S., and Nevins, D., (2009) Structure, thermodynamic and transport properties of molten  $\text{Mg}_2\text{SiO}_4$ : Molecular dynamics simulations and model EOS. *American Mineralogist* **94**, 693-703.
- Masson, C. R., (1968) Ionic equilibria in liquid silicates. *Journal of the American Ceramic Society* **51** (3), 134-143.
- Matson, D. W., Sharma, S. K., and Philpotts, J. A., (1983) The structure of high-silica alkali-silicate glasses: A Raman spectroscopic investigation. *Journal of Non-Crystalline Solids* **58**, 323-352.

- Matsumoto, S., Nanba, T., and Miura, Y., (1998) X-ray photoelectron spectroscopy of alkali silicate glasses. *Journal of the Ceramic Society of Japan* **106** (4), 415-421.
- McMillan, P. F. and Wolfe, G. H., (1995) Vibrational spectroscopy of silicate liquids. In: *Volume 32: Structure, Dynamics and Properties of Silicate Melts* (eds. J. F. Stebbins, P. F. McMillan, and D. B. Dingwell). Reviews in Mineralogy; Mineralogical Society of America, Washington D.C., pp. 247–315.
- McMillan, P., Wolf, G. W., and Poe, B. T., (1992) Vibrational spectroscopy of silicate liquids and glasses. *Chemical Geology* **96**, 351-366.
- Mead, R. N. and Mountjoy, G., (2005) The structure of CaSiO<sub>3</sub> glass and the modified random network model. *Physics and Chemistry of Glasses* **46**, 311-314
- Mead, R. N. and Mountjoy, G., (2006) A molecular dynamics study of the atomic structure of (CaO)<sub>x</sub>(SiO<sub>2</sub>)<sub>1-x</sub> glasses. *Journal of Physical Chemistry B* **110**, 14273-14278.
- Morizet, Y., Brooker, R. A., Iacono-Marziano, G., and Kjarsgaard, B. A., (2013a) Quantification of dissolved CO<sub>2</sub> in silicate glasses using micro-Raman spectroscopy. *American Mineralogist* **98**, 1788-1802.
- Morizet, Y., Paris, M., Di Carlo, I., and Scaillet, B., (2013b) Effects of sulphur on the structure of silicate melts under oxidizing conditions. *Chemical Geology* **358**, 131-147.
- Mosteller, F., Rourke, R. E. K. and Thomas, G. B., (1961) Probability with statistical applications. Addison-Wesley, Reading, MA, 478p.
- Mountjoy, G., (2007) The local atomic environment of oxygen in silicate glasses from molecular dynamics. *Journal of Non-Crystalline Solids* **353**, 1849-1853.
- Mysen, B. O., (2003) Physics and chemistry of silicate glasses and melts. *European Journal of Mineralogy* **15** (5), 781-802.
- Mysen, B. O. and Virgo, D., (1980) Solubility mechanisms of carbon dioxide in silicate melts: A Raman spectroscopic study. *American Mineralogist* **65**, 885-899.
- Nasikas, N. K., Edwards, T. G., Sen, S., and Papatheodorou, G. N., (2012) Structural characteristics of novel Ca-Mg orthosilicate and suborthosilicate glasses: Results from <sup>29</sup>Si and <sup>17</sup>O NMR spectroscopy. *Journal of Physical Chemistry B* **116**, 2696-2702.
- Nesbitt, H. W., and Bancroft, G. M., (2014) Chapter 7: High resolution core- and valence-level XPS studies of the properties (structural, chemical and bonding) of silicate minerals and glasses. In: *Spectroscopic Methods in Mineralogy and Materials Sciences* (eds. G. S.

- Henderson, D. R. (Neuville, R.T. Downs) Reviews in Mineralogy and Geochemistry **78**, pp. 271-330
- Nesbitt, H. W., Bancroft, G. M., Davidson, R., McIntyre, N. S., and Pratt, A. R., (2004) Minimum XPS core-level line widths of insulators, including silicate minerals. *American Mineralogist* **89**, 878-882.
- Nesbitt, H. W., Bancroft, G. M., Henderson, G. S., Ho, R., Dalby, K. N., Huang, Y., and Yan, Z., (2011) Bridging, non-bridging and free ( $O^{2-}$ ) oxygen in  $Na_2O-SiO_2$  glasses: An X-ray Photoelectron Spectroscopic (XPS) and Nuclear Magnetic Resonance (NMR) study. *Journal of Non-Crystalline Solids* **357**, 170-180.
- Nesbitt, H. W., Bancroft, G. M., Pratt, A. R., and Scaini, M., (1998) Sulfur and iron surface states on fractured pyrite surfaces. *American Mineralogist* **83**, 1067-1076.
- Nesbitt, H. W., Henderson, G. H., Bancroft, G. M., and Ho, R., (2015) Experimental evidence for Na coordination to bridging oxygen in Na-silicate glasses: Implications for spectroscopic studies and for the modified random network model. *Journal of Non-Crystalline Solids* **409**, 139-148.
- Ottonello, G., (2005) Chemical interactions and configurational disorder in silicate melts. *Annals of Geophysics* **48 (4/5)**, 561-581.
- Park, J. H., (2013a) Effect of silicate structure on thermodynamic properties of calcium silicate melts: Quantitative analysis of Raman spectra. *Metals and Materials International* **19 (3)**, 577-584.
- Park, J. H., (2013b) Structure-property relationship of CaO-MgO-SiO<sub>2</sub> slag: Quantitative analysis of Raman spectra. *Metallurgical and Materials Transactions B* **44B**, 938-947.
- Park, J.-H. and Rhee, P. C.-H., (2001) Ionic properties of oxygen in slag. *Journal of Non-Crystalline Solids* **282**, 7-14.
- Pearce, M. L., (1964) Solubility of carbon dioxide and variation of oxygen ion activity in soda-silica melts. *Journal of the American Ceramic Society* **47**, 342-347.
- Retsinas, A., Kalamounias, A. G., and Papatheodorou, G. N., (2014) Reaching the ionic limit in the  $(1-X)[Ca_{0.5}Mg_{0.5}]O-XSiO_2$  pseudo binary glass system with  $0.5 < X < 0.27$ : Glass formation and structure. *Journal of Non-Crystalline Solids* **383**, 38-43.
- Sawyer, R., Nesbitt, H. W., and Secco, R. A., (2012) High resolution X-ray Photoelectron



- Spectroscopy (XPS) study of K<sub>2</sub>O-SiO<sub>2</sub> glasses: Evidence for three types of O and at least two types of Si. *Journal of Non-Crystalline Solids* **358**, 290-302.
- Schaller, T., Stebbins, J. F., and Wilding, M. C., (1999) Cation clustering and formation of free oxide ions in sodium and potassium lanthanum silicate glasses: Nuclear magnetic resonance and Raman spectroscopic findings. *Journal of Non-Crystalline Solids* **243**, 146-157.
- Seifert, R., Malfait, W. M., Lerch, P., and Sanchez-Valle, C., (2013) Partial molar volume and compressibility of dissolved CO<sub>2</sub> in glasses with magmatic compositions. *Chemical Geology* **358**, 119-130.
- Sen, S., Maekawa, H., and Papatheodorou, G. N., (2009) Short-range structure of invert glasses along the pseudo-binary join MgSiO<sub>3</sub>-Mg<sub>2</sub>SiO<sub>4</sub>: Results from <sup>29</sup>Si and <sup>25</sup>Mg MAS NMR spectroscopy. *Journal of Physical Chemistry B* **113**, 15243-15248.
- Sen, S. and Tangeman, J., (2008) Evidence for anomalously large degree of polymerization in Mg<sub>2</sub>SiO<sub>4</sub> glass and melt. *American Mineralogist* **93**, 946-949.
- Shirley, D. A., (1972) High resolution x-ray photoelectron spectrum of the valence band of gold. *Physical Review B* **5** (12), 4709-4714.
- Speight, J. G., (2005) Lange's Handbook of Chemistry (70th Anniversary Edition). McGraw-Hill Standard Handbook, New York, pp. 4.41-4.51.
- Stebbins, J. F., (1995) Dynamics and structure of silicate and oxide melts: Nuclear magnetic resonance studies. *Reviews in Mineralogy and Geochemistry* **32**, 191-246.
- Stebbins, J. F., and Sen, S., (2013) Oxide ion speciation in potassium silicate glasses: New limits from <sup>17</sup>O NMR. *Journal of Non-Crystalline Solids* **368**, 17-22.
- Stebbins, J. F., Wu, J., and Thompson, L. M., (2013) Interactions between network cation coordination and non-bridging oxygen abundance in oxide glasses and melts: Insights from NMR spectroscopy. *Chemical Geology* **346**, 34-46.
- Stolper, E., (1982) Water in silicate glasses: An infrared spectroscopic study. *Contributions to Mineralogy and Petrology* **81**, 1-17.
- Thompson, L. M., McCarty, R. J., and Stebbins, J. F., (2012) Estimating accuracy of <sup>17</sup>O NMR measurements in oxide glasses: Constraints and evidence from crystalline and glassy calcium and barium silicates. *Journal of Non-Crystalline Solids* **358**, 2999-3006.
- Tilocca, A. and de Leeuw, N. H., (2006) Structural and electronic properties of modified sodium

- and soda-lime silicate glasses by Car-Parrinello molecular dynamics. *Journal of Materials Chemistry* **16**, 1950-1955.
- Toop, G. W., and Samis, C. S., (1962) Activities of ions in silicate melts. *Transactions of the Metallurgical Society of America* **224**, 878-887.
- Turner, G. L., Chung, S. E., and Oldfield, E., (1985) Solid state  $^{17}\text{O}$  Nuclear Magnetic Resonance spectroscopic study of the Group II oxides. *Journal of Magnetic Resonance* **64**, 316-324.
- Vermillion, K. E., Florian, P., and Grandinetti, P. J., (1998) Relationships between bridging oxygen  $^{17}\text{O}$  quadrupolar coupling parameters and structure in alkali silicates. *Journal of Chemical Physics* **108**, 7274-7285.
- Wells, A. F., (1984) Structural Inorganic Chemistry. Clarendon Press, Oxford, 1382 p.
- Xue, X. and Kanzaki, M., (2004) Dissolution mechanisms of water in depolymerized silicate melts: Constraints from  $^1\text{H}$  and  $^{29}\text{Si}$  NMR spectroscopy and ab initio calculations. *Geochimica et Cosmochimica Acta* **68 (24)**, 5027-5057.
- Zakaznova-Herzog, V.P. Nesbitt, H.W. Bancroft, G.M. Tse, J.S. Gao, X Skinner, W., (2005) High-resolution valence-band XPS spectra of the nonconductors quartz and olivine. *Phys. Rev. B* **72**, 205113-1-13.
- Zhang, P., Grandinetti, P. J., and Stebbins, J. F., (1997) Anionic species determination in  $\text{CaSiO}_3$  glass using two-dimensional  $^{29}\text{Si}$  NMR. *Journal of Physic Chemistry B* **101**, 4004-4008.

## Chapter 4

### 4.0 DISSOLUTION OF $\text{Al}_2\text{O}_3$ IN K-SILICATE MELTS, WITH IMPLICATIONS FOR THE STABILITY OF Al-BEARING SILICATE MELTS<sup>3</sup>

#### 4.1. INTRODUCTION

Kinetic studies on the dissolution of refractory oxides, such as  $\text{Al}_2\text{O}_3$ , in silicate melts have primarily focused on the mechanism controlling the rates of dissolution (e.g., Schwerdtfeger, 1966; Monaghan et al., 2004; Shaw, 2004; Shaw et al., 2018). The findings of these studies show that the dissolution rates of solids are controlled by diffusion, except during the initial stage of dissolution where reaction rates are the controlling mechanism. Lasaga and Gibbs (1990) observed that an understanding of the structure and dynamics of mineral surfaces must be the foundation for quantitative studies of heterogeneous kinetics. Despite this observation, these kinetic studies do not address the processes by which Al is removed from the bulk solid surface and incorporated into the melt. Chemical reactions must cause the removal of Al from the  $\text{Al}_2\text{O}_3$  surface in a process where Al-O bonds are ruptured, releasing Al into the melt. This chapter is concerned with the reactions that occur at the solid-melt interface and within the melt during dissolution of  $\text{Al}_2\text{O}_3$ .

X-ray Photoelectron Spectroscopy (XPS) of the O 1s orbital is employed to study the effects of dissolution of aluminum in K-silicate and K-Al-silicate glasses. Changes in binding energy (BE) of the O 1s signal reflect changes in electron densities on bridging oxygen (BO) and non-bridging oxygen (NBO) atoms. A lower BE of the NBO atom indicates a greater electron density on that atom than on the BO atom. The O 1s spectra are useful in that oxygen is the common structural unit that is bonded to Si, Al and K. The binding energies of the O 1s XPS signals of fused silica and quartz (Si-O-Si moieties) are similar at ~533.2 eV and ~532.8 eV whereas the Al-O-Al moiety of  $\text{NaAlO}_2$ , is located at ~530.5 eV (Barr, 1991). There are no XPS

---

<sup>3</sup> This chapter is an early draft of a paper that was subsequently published as “Sawyer, R., Nesbitt, H.W., Bancroft, G.M., Secco, R.A. and Henderson, G.S., 2022. Congruent dissolution of  $\text{Al}_2\text{O}_3$  in a K-disilicate melt, with constraints on the reaction mechanism. *Journal of Non-Crystalline Solids*, 586, p.121565. doi:10.1016/j.jnoncrysol.2022.121565”

data for  $K_2O$  due to its instability but from the BE of the NBO peak (Si-O-K moiety) in Figure 3.8 at  $\sim 529.7$  eV the effect of K on BE is evident. It decreases the O 1s XPS signal to still lower values. The BE of the  $O^{2-}$  contribution (K-O-K moiety) should be still lower. The metal-oxygen bond strengths decrease in the order of Si-O > Al-O > K-O (798 kJ/mol > 512 kJ/mol > 239 kJ/mol) (Speight, 2005). These relationships prove useful in evaluating the stability relationships among the various chemical species in potassium aluminosilicate glasses and melts. The relationships between electron density and bond strength have been observed in other melts (Dalby et al., 2007; Nesbitt et al., 2011; Sawyer et al., 2012; Sawyer et al., 2015).

BO abundances have been observed to increase with the introduction of Al to melts at the expense of NBO abundances (Brückner et al., 1980; Miura et al., 2000). Observed changes in  $Q^n$  species ( $Q$  = Si tetrahedron and  $n$  = number of BO atoms associated with the Si tetrahedron) have also shown that for alkali silicates, the addition of Al promotes the formation of Si-O-Si moieties at the expense of Si-O-M ( $M$  = metal cation) moieties (Mysen, 1990; Mysen et al., 2003). The changes resulting from addition of  $Al_2O_3$  to melts have implications for the stability of melts and their effects on the generation of the crust of the earth. Aluminum is a major constituent of silicate melts and is a major component of the minerals composing the granodioritic crust. This is evidenced by the fact that the minerals plagioclase and K-feldspar, along with quartz, make up approximately 75% of all minerals in the crust and through studies which show that  $SiO_2$  (at  $\sim 65$  wt.%) and  $Al_2O_3$  (at  $\sim 15$  wt.%) are the most abundant oxides in the crust's bulk composition (Shaw et al., 1967; Wedepohl, 1969; Taylor and McLennan, 1981; Nesbitt and Young, 1984).  $Al^{3+}$  substitutes for  $Si^{4+}$  on tetrahedral sites in common silicate minerals even though Al is  $\sim 33\%$  larger than Si, has a greater effective ionic radius (0.53 Å, compared to 0.40 Å for Si) and a different formal charge. Si and Al are also tetrahedrally coordinated in melts (Mysen and Richet, 2005). Given these stark differences between Al and Si, it is surprising that silicate melts with high Al content have a high degree of stability in the upper mantle and crust. This chapter will discuss the effects that dissolved Al has on melt stability in silicate melts and in particular, will offer an explanation for the stability of Al-rich silicate melts.

## 4.2. BACKGROUND AND EXPERIMENTAL ASPECTS

### 4.2.1. Background

Two recent studies have shown that it's possible to obtain highly resolved O 1s XPS spectra of K-silicate glasses and these glasses have been well characterized (Sawyer et al., 2012; Sawyer et al., 2015). This study used small amounts of Al<sub>2</sub>O<sub>3</sub> to avoid any issues that may result with Al-O-Al speciation and incongruent dissolution (Bates, 1987; Dubinsky and Stebbins, 2006; Shaw et al., 2018). It has been observed that K<sup>+</sup> atoms interact weakly with the O atoms of silicate tetrahedra in comparison to K<sup>+</sup> interactions with the O atoms of Al tetrahedra (Navrotsky et al., 1982; Navrotsky et al., 1985; Wilding and Navrotsky, 1998; Morishita et al., 2004). Because of this we use a starting sample with a constant composition of 33 mol % K<sub>2</sub>O – 67 mol% SiO<sub>2</sub> (a K-disilicate melt).

### 4.2.2. Lewis Acids and Bases

Lewis bases donate electrons and Lewis acids accept them to form bonds. In the context of the study of silicate glasses, Si and Al are Lewis acids whereas NBO and BO are Lewis bases. Lewis acids are known as electrophiles, while Lewis bases are known as nucleophiles in the chemical kinetics literature (e.g., Laidler, 1965; Laidler, 1988; House, 1997). A Lewis base's strength is based on its tendency to donate electrons to a Lewis acid thus forming a chemical bond. The NBO<sup>-</sup> moiety is the strongest nucleophile in siliceous alkali silicate glasses. It reacts with Si and Al to produce Si-O and Al-O bonds in melts (Farnan and Stebbins, 1994; Nesbitt et al., 2017a; Nesbitt et al., 2020). The dissociation of an NBO-M bond (where M is an alkali metal) produces the NBO<sup>-</sup> moiety and in alkali silicate crystals, the dissociation of Si-NBO-Na and Si-NBO-K bonds begins at ~770 K (Nesbitt et al., 2017a). Nesbitt et al. (2017a) demonstrate this through examination of the Raman spectra of Na<sub>2</sub>SiO<sub>3</sub> from Richet et al. (1996). Only a Q<sup>2</sup> signal is present in the spectra up until ~770 K where a Q<sup>3</sup> band appears and increases within the premelting region. There are no Q<sup>1</sup> bands observed below ~1200 K and so the only way to produce Q<sup>3</sup> species without producing an equal amount of Q<sup>1</sup> species is through a polymerization reaction involving two Q<sup>2</sup> species. The resulting products of the reaction are itinerant Na<sup>+</sup> and O<sup>2-</sup>; a strong nucleophile (Nesbitt et al., 2017a). The degree of dissociation

increases with temperature (Nesbitt et al., 2017a; Nesbitt et al., 2017b). The dissociation reaction is promoted by temperature through thermal agitation and proceeds according to:



The associated mass action equation is:

$$K_1 = (\text{X}_{\text{Si-NBO}^-})(\text{X}_{\text{M}^+})/(\text{X}_{\text{Si-NBO-M}}), \quad (4.2)$$

where  $K_1$  is the equilibrium constant, and  $X$  is mole fraction.  $K_1$  is a conditional equilibrium constant since mole fractions are used. Where  $K_1$  is finite and equilibrium pertains, all three species of Eq. (4.1) must be present at finite concentrations in melts.

#### 4.2.3. Sample Preparation

A bulk starting mixture of nominally K-disilicate composition was made from which glasses were prepared following the sample preparation methods of Sawyer et al. (2015). Homogeneity was achieved through repeated coning and grinding. The mixture was ground under anhydrous ethanol for 1 hour and dried under an IR lamp. This process was repeated four times in order to ensure homogeneity. Three samples were prepared from the bulk. One containing no  $\text{Al}_2\text{O}_3$  (KS glass), one containing 1 mol% of  $\text{Al}_2\text{O}_3$  (KAS1) and one containing 3 mol%  $\text{Al}_2\text{O}_3$  (KAS3). The  $\text{K}_2\text{O}:\text{SiO}_2$  ratio was kept constant for all three samples. K 2p, Si 2p and O 1s spectra were collected and analyzed. Al spectra were not analyzed due to the low concentrations of  $\text{Al}_2\text{O}_3$ .

After grinding, each sample was sintered at  $\sim 200^\circ\text{C}$  below the melting point based on the  $\text{K}_2\text{O}-\text{SiO}_2-\text{Al}_2\text{O}_3$  phase diagram (Fig. 4 of Schairer and Bowen, 1955). The samples were ground again and melted in a platinum crucible at  $1230^\circ\text{C}$  for four hours. In the temperature range  $200^\circ\text{C}$  below and above the liquidus, the temperature was increased at  $20^\circ\text{C}$  intervals. Glasses were quenched by dipping the bottom of the crucible in ice water. The samples were then crushed, ground and melted again. Each sample underwent the melting procedure three times to ensure homogeneity. The samples were then placed in a desiccator.

#### 4.2.4. XPS Analysis

Glass pieces  $\sim 1 \text{ cm}^2$  were cut, notched and placed in copper sample holders for analysis. The structure of the glasses is probably representative of that of the melt near the fictive temperature ( $T_f$ ) which is  $\sim 700 \text{ K}$  for a K-disilicate glass (MacDonald et al., 1985). It is unknown the extent to which  $T_f$  increases with the addition of small amounts of  $\text{Al}_2\text{O}_3$ . The XPS experiments were

conducted at ambient temperatures using a Kratos Axis Ultra X-ray Photoelectron Spectrometer with an Al K $\alpha$  X-ray source (Nesbitt et al., 2004). Samples were placed in the introduction chamber and held there until vacuum pressure reached  $\sim 10^{-7}$  torr. The samples were then placed into the transfer chamber (vacuum pressure  $\sim 10^{-9}$  torr) where they were fractured to obtain a pristine surface. After fracture, the samples were transferred to the analysis chamber (vacuum pressure  $\sim 10^{-10}$  torr) and analyzed. Charge compensation was provided by the Kratos Axis Ultra's magnetic charge confinement system. At the beginning and end of each analysis, broadscans (survey scans) were collected using a 0.3 eV step size, a 60 ms dwell time and a pass energy of 160 eV. Narrow scans of the O 1s, Si 2p, Al 2p, K 2p and C 1s orbitals were also collected. For the O 1s spectra of the KAS1 sample a 0.025 eV step size, 68 ms dwell time and 10 eV pass energy were used. The same conditions were used for the KAS3 sample, except for the dwell time which was 100 ms. The Si 2p and Al 2p spectra were collected using a 0.025 eV step size, a 115 ms dwell time and a pass energy of 10 eV. The C 1s and K 2p spectra were collected with a 0.025 eV step size, 86 ms dwell time and 10 eV pass energy. CasaXPS software was used to analyze the spectra. A Shirley background was used to fit all spectra (Shirley, 1972). All spectra were fit with a 70:30 Gaussian:Lorentzian lineshape using a Voight sum function (Hesse et al., 2007).

#### 4.2.5. XPS Results

The spectra were standardized to the C 1s peak at 285.0 eV binding energy (BE). This peak represents adventitious carbon common to all samples and resulting from its presence in the analysis chamber. The preparation technique of Sawyer et al. (2015) was used where they demonstrate that the technique causes  $\sim 2$  mol% loss of K with 2-3 fusions. The base glass KS had nominal composition K<sub>2</sub>O:SiO<sub>2</sub>  $\sim 33.3:66.7$  (molar ratio) with nominal proportions of K:Si:O 22:22:56. We estimate the KS glass contains  $\sim 31$  mol% K<sub>2</sub>O based on the findings of Sawyer et al. (2015) and indeed the XPS broadscan analysis of the KS glass indicates molar proportions of 21:22:57 K:Si:O. This confirms the KS glass contains  $\sim 31$  mol% K<sub>2</sub>O. This glass (and melt) will be referred to as the KS or K-dsilicate glass (or melt) in this text.

The Al 2p peak of the sample KAS1 (containing 1 mol% Al<sub>2</sub>O<sub>3</sub>) was too weak to obtain a reasonable fit, but the peak maximum was at  $\sim 74.5$  eV BE. The sample KAS3 (3 mol% Al<sub>2</sub>O<sub>3</sub>) was resolved sufficiently that a meaningful fit could be obtained. The peak maximum was at

74.4 ( $\pm 0.3$ ) eV BE and the full width at half maximum (FWHM) was 1.4 eV. For the Si 2p peak of the KS glass, the maximum was at 101.8 ( $\pm 0.2$ ) eV BE and the FWHM was 1.27 eV. The Si 2p peak of the KAS1 glass had a BE of 101.6 ( $\pm 0.2$ ) eV and a FWHM of 1.21 eV, whereas the KAS3 glass had a BE of 102.1 ( $\pm 0.2$ ) eV and a FWHM of 1.54 eV. The addition of 1 mol% Al<sub>2</sub>O<sub>3</sub> does not significantly change the BE of the Si 2p peak maximum or FWHM, but the addition of 3 mol% Al<sub>2</sub>O<sub>3</sub> makes the peak broader and shifts the peak maximum to a higher BE.

In Figures 4.1a, 4.1b and 4.1c, the fitted NBO peak maxima are 529.7 eV, 529.5 eV and 529.8 eV respectively and for the BO are 531.9 eV, 531.7 eV and 532.0 eV. The intensities of the NBO and BO peaks change with the addition of Al<sub>2</sub>O<sub>3</sub>. The FWHM of the NBO peaks do not change significantly in the three samples, but that of the BO peaks increases systematically from 1.36 eV in the KS glass to 1.60 in the KAS3 glass (Fig. 4.1). These increases indicated substantial changes to the BO spectral contributions with the addition of small amounts of Al<sub>2</sub>O<sub>3</sub>. Taking difference spectra makes these changes most apparent. The spectrum of the KS glass (Fig. 4.1a) is subtracted from the spectra of the glasses containing 1 and 3 mol% Al<sub>2</sub>O<sub>3</sub> (Figs. 4.1b and 4.1c) with the results showing the changes in spectral contributions. First, the standardization of binding energies and the normalization of spectral intensities must be performed. All three spectra are fit. The BE maxima of the fitted NBO peaks of the KAS1 and KAS3 glasses were standardized to the BE maximum of the fitted NBO peak of the KS glass (Fig. 4.1a). Two adjustments are required to the peak intensities (the y-axis of Fig. 4.1). The first is the subtraction of backgrounds, and a Shirley background used to fit the spectra was subtracted from each. The second involves the normalization of the spectral intensity to the same number of oxygen atoms (i.e., obtaining intensity per mole of oxygen; see Table 4.1 for O<sub>Total</sub>). The shaded circles and crosses of Figs. 4.2a and 4.2b show the standardized and normalized spectra. Difference spectra were obtained by subtracting the KS spectrum from the KAS1 and KAS3 spectra (Fig. 4.2, black dots).

### 4.3. INTERPRETATION OF DATA

#### 4.3.1. O 1s XPS Spectra

Figure 4.1 shows that the O 1s XPS spectra of the glasses display two peaks: a BO peak and an NBO peak. The peaks were fit and the residuals (Figs. 4.1b, 4.1d and 4.1e) indicate that the fits



Table 4.1: Calculation of BO% and NBO% in Al-bearing K silicate melts

Composition			Total Moles			KAlO <sub>2</sub> Formation			Q <sup>3</sup> →Q <sup>4</sup>		%O Species	
1	2	3	4	5	6	7	8	9	10	11	12	13
K <sub>2</sub> O mol%	SiO <sub>2</sub> mol%	AlO <sub>1.5</sub> mol%	O <sub>Tot</sub> moles	K <sub>Tot</sub> moles	Al <sub>Tot</sub> moles	K <sub>NBO</sub> <sup>1</sup> moles	NBO <sup>2</sup> moles	BO <sup>2</sup> moles	NBO <sup>3</sup> moles	BO <sup>3</sup> moles	NBO <sup>4</sup> mol%	BO <sup>4</sup> mol%
31.0	69.0	0.0	169.0	62.0	0.0	62.0	62.0	107.0			36.7	63.3
30.4	67.6	2.0	168.6	60.8	2.0	58.8	58.8	109.9	56.8	111.9	33.7	66.3
29.1	64.9	6.0	167.9	58.3	6.0	52.3	52.3	115.6	46.3	121.6	27.6	72.4

1 –  $K_{NBO}$  = Amount of K available to react with BO of Si-O-Si moieties to produce the Si-NBO-K moieties. This assumes that K of KAlO<sub>2</sub> is unavailable to react with BO.

2 – Assumes  $K_{NBO}$  (column 7) reacts with Si-BO-Si to produce Si-NBO-K moieties. With NBO calculated, moles of BO are evaluated by the difference ( $O_{Tot}$ -NBO).

3 – Assumes Reaction 4.3 proceeds: NBO of Q<sup>3</sup> (Reaction 4.1) is converted to BO, with the amount of NBO converted being equal to the moles of Al dissolved in the melt.

4 – NBO and BO values and columns 10 and 11 are recalculated to 100%

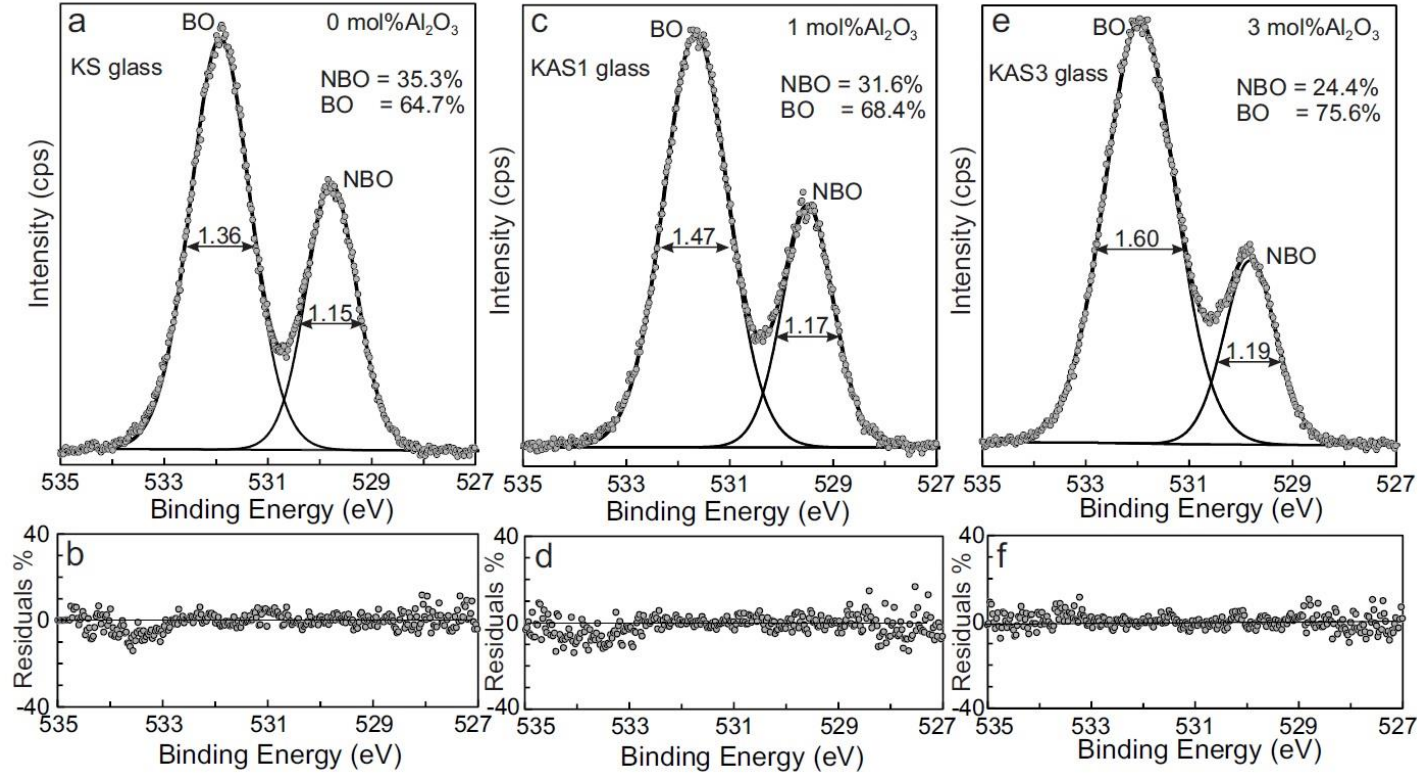


Figure 4.1: O 1s XPS spectra, fits and residuals for K-silicate glasses containing 0, 1 and 3 mol%  $\text{Al}_2\text{O}_3$ . All fits were performed using a Voigt sum function (Hesse et al., 2007). Full widths at half maximum (FWHM) of the fitted peaks are indicated by the double-headed lines. (a) A two-peak fit to the KS glass ( $\sim 33$  mol%  $\text{K}_2\text{O}$ ). (b) Residuals of the fit shown in Fig. 4.1a. (c) A two-peak fit to the KAS1 glass (1 mol%  $\text{Al}_2\text{O}_3$ ). (d) Residuals of the fit shown in Fig. 4.1c. (e) A two-peak fit to KAS3 glass (3 mol%  $\text{Al}_2\text{O}_3$ ). (f) Residuals of the fit shown in Fig. 4.1e.

reproduce the spectra well. The FWHM of the NBO peaks of the three spectra range from 1.15 to 1.19 eV. These values are similar to those obtained from other high resolution XPS glass studies (Dalby et al., 2007; Nesbitt et al., 2011; Nesbitt et al., 2017a; Nesbitt et al., 2017c; Sawyer et al., 2015;) and also conform to the theoretical and practical considerations of Bancroft et al. (2009). The FWHM of the BO peaks in Figure 4.1 range from 1.36 eV to 1.60 eV. The BO peaks are broader than the NBO peaks. They are also broader than the BO peaks of vitreous silica (FWHM = 1.25 eV, Nesbitt et al., 2015). The FWHM of the BO and NBO peaks for all crystalline and vitreous silicates should be ~1.2-1.3 eV, as demonstrated by Bancroft et al., 2009. The reason is because the FWHM are controlled by same final state vibrational broadening and phonon broadening contributions (Nesbitt et al., 2004; Bancroft et al., 2009; Nesbitt and Bancroft, 2014). Thus, the only explanation for the broader BO spectra is new contributions to spectra envelope. Since each glass has the same effective K<sub>2</sub>O content, these new contributions cannot be associated with potassium. Instead, they are related to the presence of Al<sub>2</sub>O<sub>3</sub>. Since these contributions are contained within the BO peak and cannot be resolved, the difference spectra technique can be used as a way of quantifying them and gaining information about them.

#### 4.3.2. Difference Spectra

Difference spectra are plotted in Figs. 4.2a and 4.2b as solid dots. Also plotted are the standardized and normalized spectra from which these spectra were derived. The NBO region the difference spectra display negative values with a maximum negative value at ~529.8 eV. This indicates that NBO has been lost from the spectrum with the addition of Al<sub>2</sub>O<sub>3</sub> and that more Al<sub>2</sub>O<sub>3</sub> causes a greater loss of NBO.

The BO peak broadens with the addition of Al<sub>2</sub>O<sub>3</sub> to the K silicate melt and the difference spectra show that the broadening is due to two BO contributions at the extremities of the BO envelope. One contribution (Peak A) is centered at ~531 eV and the other (Peak B) is centered at ~532.8 eV. The intensities of Peaks A and B increase from the KAS1 sample (Fig. 4.2a) to the KAS3 sample (Fig 4.2b), demonstrating a sympathetic relationship between the intensities of these peaks and Al<sub>2</sub>O<sub>3</sub> content. Furthermore, the absolute difference between the areas (counts) under Peaks A and B (+24112) and the negative NBO peak (-23977) is 0.6%, demonstrating that the addition of Al<sub>2</sub>O<sub>3</sub> results in a mole-per-mole conversion of NBO to BO. The result also indicates that the standardization and normalization techniques applied to the spectra create no

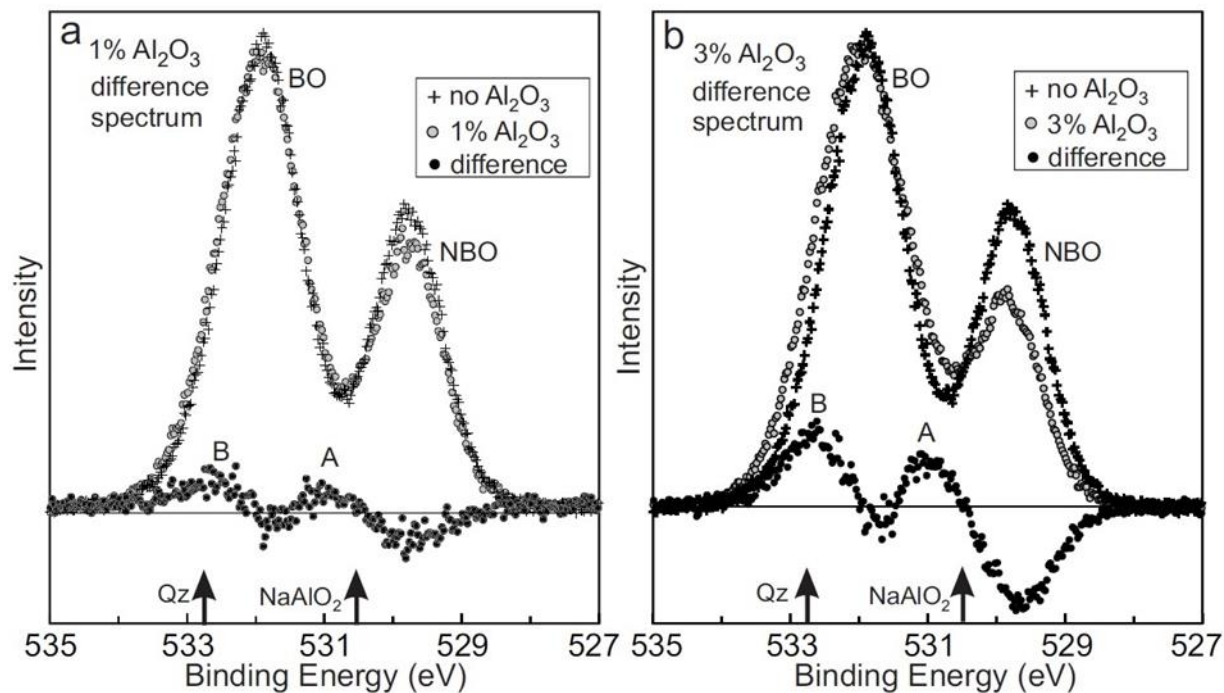


Figure 4.2: O 1s XPS spectra of the K-silicate glasses where the BEs have been standardized to a common value and the intensities have been normalized to obtain intensity per mole of O. Difference spectra are indicated by the solid dots in each diagram. (a) The standardized and normalized KS and KAS1 spectra. The difference spectra obtained by the subtraction of the KS spectrum from the KAS1 spectrum. (b) The standardized and normalized KS and KAS3 spectra. The difference spectrum is obtained by subtracting the KS spectrum from the KAS3 spectrum. The arrows indicate the BEs of vitreous SiO<sub>2</sub> (Nesbitt et al., 2015) and of crystalline NaAlO<sub>2</sub> (Barr, 1991). Both phases contain only BO atoms.

distortions. Peaks A and B and the negative NBO peak have FWHM between  $\sim 1$ - $1.5$  eV which are reasonable and expected for O 1s spectral peaks. The areas of Peaks A, B and the NBO peak of Fig. 4.2b are approximately three times greater than the areas of the same peaks of Fig. 4.2a. This relationship is expected considering the  $\text{Al}_2\text{O}_3$  contents.

### 4.3.3. Interpretation of Peaks A and B

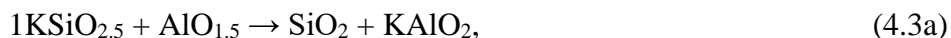
The arrows on Fig. 4.2 show the position of the O 1s peak maxima for crystalline  $\text{NaAlO}_2$  and quartz (Barr, 1991; Nesbitt et al., 2015). These indicate similarities to the peak maxima of Peaks A and B. In  $\text{NaAl}_2\text{O}_4$ , aluminum is tetrahedrally coordinated with oxygen and forms Al-O-Al moieties by bridging to other  $\text{AlO}_4$  tetrahedra. This results in a network of corner linked  $\text{AlO}_4$  tetrahedra (Kaduk and Pei, 1995). In kyanite, Al-O-Si and Al-O-Al moieties are present in a 4:1 ratio (Ohuchi et al., 2006). Ohuchi et al. (2006) show in their O 1s XPS spectra of kyanite that the BO peak of the Al-O-Si moiety is located at  $\sim 531.4$  eV and the BO peak of the Al-O-Al moiety is located at  $\sim 530.6$  eV. Nsimama et al. (2010) presented an O 1s XPS spectra of  $\text{SrAl}_2\text{O}_4$  with a BO peak maximum of  $\sim 530.8$  eV. All these values span the binding energy range of Peak A. Clearly Peak A represents BO of an  $\text{AlO}_4$  anionic framework species. In this study, the low concentrations of Al make the likelihood that significant Al-O-Al moieties are present very small. It is likely that the BOs of  $\text{AlO}_4$  are bonded to Si and form Al-O-Si moieties. This finding is consistent with the Al avoidance rule and many studies (e.g. Dubinsky and Stebbins, 2006).

The BE peak maximum of Peak B is  $\sim 532.6$  eV (Fig. 4.2). BO-K distances in crystalline  $\text{K}_2\text{Si}_2\text{O}_5$  led Nesbitt et al. (2017e) to argue for three types of BO atoms in K-disilicate glasses, related to the number of K atoms coordinated to BO. BO atoms coordinated to 0-1 potassium were located at  $\sim 532.9$  eV. Those coordinated to 1-2 potassium were located at  $\sim 532.0$  eV. Finally, those coordinated to 2-3 potassium were located at  $\sim 531.5$  eV (see Figure 1 of Nesbitt et al., 2017e). The peak maximum for Peak B is  $\sim 532.6$  eV (Fig. 4.2) which indicates that the BO atoms are coordinated to 0-1 potassium. The BE of Peak B is also similar to that of vitreous silica and quartz (Nesbitt et al., 2015). This similarity is consistent with Peak B representing the signal of a  $\text{Q}^4$  species.

## 4.4. STOICHIOMETRIC DISSOLUTION REACTIONS

### 4.4.1. Al<sub>2</sub>O<sub>3</sub> Dissolution Reaction

The way in which Al<sub>2</sub>O<sub>3</sub> dissolves in the KS melt is constrained by the above interpretations of Peaks A and B. The intensity of the NBO signal is 35 mol% in the KS glass and decreases to 24 mol% in the KAS3 glass as Al<sub>2</sub>O<sub>3</sub> increases from 0 to 3 mol% (Figs. 4.1a, 4.1c, 4.1e). This relationship requires the consumption of NBO with the dissolution of Al<sub>2</sub>O<sub>3</sub>, thus NBO is a reactant during dissolution of Al<sub>2</sub>O<sub>3</sub>. BO increases in proportion to the amount of Al<sub>2</sub>O<sub>3</sub> which makes it a reaction product of the dissolution of Al<sub>2</sub>O<sub>3</sub>. The difference spectra in Fig. 4.2 indicate that the BO reaction product produces two melt species: a Q<sup>4</sup> species (Peak B) and a KAlO<sub>2</sub> species (Peak A). For K-disilicate glass, Maekawa et al. (1991) reported Q-species abundances of 7% Q<sup>2</sup>, 86% Q<sup>3</sup> and 7% Q<sup>4</sup>. The Q<sup>3</sup> species contains an NBO and its high abundance means that it is likely the dominant reactant species. The stoichiometric composition of the Q<sup>3</sup> species is KSiO<sub>2.5</sub>. The dissolution reaction is then



where AlO<sub>1.5</sub> represents the solid where all O atoms are BOs (i.e. Al-O-Al moieties). The reaction can be written in Q-species notation where, considering the Si-NBO-K moiety of Q<sup>3</sup>, the Q<sup>3</sup> species is represented by K-Q<sup>3</sup>:



Reaction 4.3 is a polymerization reaction that allows for the conversion of NBO to BO (Fig. 4.1) and the production of Peaks A (KAlO<sub>2</sub>) and B (SiO<sub>2</sub>) of Fig. 4.2. The reaction also produces SiO<sub>2</sub> and KAlO<sub>2</sub> in equal amounts. While Peak B is slightly more intense than Peak A, the difference in intensities might be the result of interference of the negative NBO peak (loss) with Peak A (gain) which would make the area of Peak A less intense.

The abundances of NBO and BO as a function of Al content can be calculated and is a test of the validity of Reaction 4.3. Table 4.1 lists the three glass compositions of Fig. 4.1 (columns 1-3) and the total moles of O, K and Al (columns 4-6). It is assumed that for the KS glass each mole of K is associated with a mole of NBO (as Si-NBO-K species). In the K<sub>2</sub>O-SiO<sub>2</sub>-Al<sub>2</sub>O<sub>3</sub> melt, the K of the KAlO<sub>2</sub> moiety is associated with the BO of that moiety and is not related to NBO production. Thus, the amount of K available to react with SiO<sub>2</sub> to produce Si-NBO-K can be found by subtracting the amount of K associated with KAlO<sub>2</sub> from K<sub>TOT</sub> (column 5). K:Al is 1:1

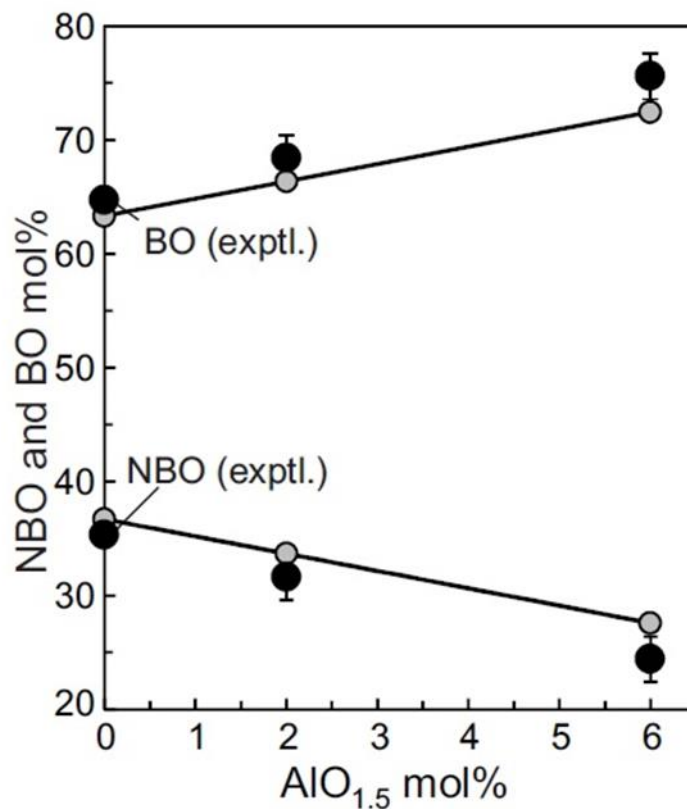


Figure 4.3: NBO and BO abundances measured and calculated as a function of dissolved  $AlO_{1.5}$  in K-disilicate glass. The large, filled circles are experimental results from Fig. 4.1 ( $\pm 2\%$  uncertainty). The small, shaded circles represent calculated values of Table 4.1 (columns 12 and 13). The solid lines indicate the trends of the calculated results. The calculations are provided in section 4.4.1.

in  $\text{KAlO}_2$ , thus the amount of K available to react with BO of Si-O-Si moieties is equal to  $\text{K}_{\text{Tot}} - \text{Al}_{\text{Tot}}$ . These values are labelled  $\text{K}_{\text{Si}}$  and listed in column 7. Every mole of  $\text{K}_{\text{Si}}$  produces an equal number of moles of NBO when reacted with BO (column 8). The BO abundances of column 9 are calculated as the difference between the  $\text{O}_{\text{Tot}}$  values of column 4 and the NBO values of column 8.

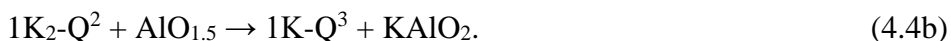
NBO and BO abundances are also affected by Reaction 4.3 (Table 4.1, columns 10-13) which converts some NBO to BO ( $\text{Q}^3$  to  $\text{Q}^4$  conversion), the extent of which is in direct proportion to the amount of Al present in the melt. According to Reaction 4.3, each mole of Al causes one mole of NBO (of  $\text{Q}^3$  species) to be consumed and one mole of BO (as  $\text{SiO}_2$  or  $\text{Q}^4$  species) to be produced. Column 10 of Table 4.1 lists the NBO values of column 8 corrected for the  $\text{Q}^3$ - $\text{Q}^4$  conversion of Reaction 4.3, which depends on the amount of Al in the melt. Columns 12 and 13 list the NBO and BO values recalculated to 100%. These values are plotted on Fig. 4.3 as shaded circles. The agreement between calculation and experiment of Fig. 4.3 provides strong evidence for several claims. First, Reaction 4.3 proceeds during the dissolution of  $\text{Al}_2\text{O}_3$  and its stoichiometry is correct. Also,  $\text{KAlO}_2$  is a distinct chemical species of the melt. Finally, the K of  $\text{KAlO}_2$  does not promote the formation of NBO.

#### 4.4.2. Another reaction

It is possible that the  $\text{Q}^2$  species ( $\text{K}_2\text{SiO}_3$ ) of the K disilicate melt may be a reactant during dissolution of  $\text{Al}_2\text{O}_3$  according to the reaction:



Reaction 4.4a can be expressed using Q-species notation as the following, where  $\text{K}_2\text{-Q}^2$  and  $\text{K-Q}^3$  represent  $\text{Q}^2$  and  $\text{Q}^3$  respectively:



Reaction 4.4 is qualitatively similar to Reaction 4.3. Both are polymerization reactions where a reactant  $\text{Q}^n$  species is consumed to produce a  $\text{Q}^{n+1}$  species that is more polymerized. Both reactions are likely to occur but the greater abundance of  $\text{Q}^3$  species in the melt means Reaction 4.3 should be dominant.



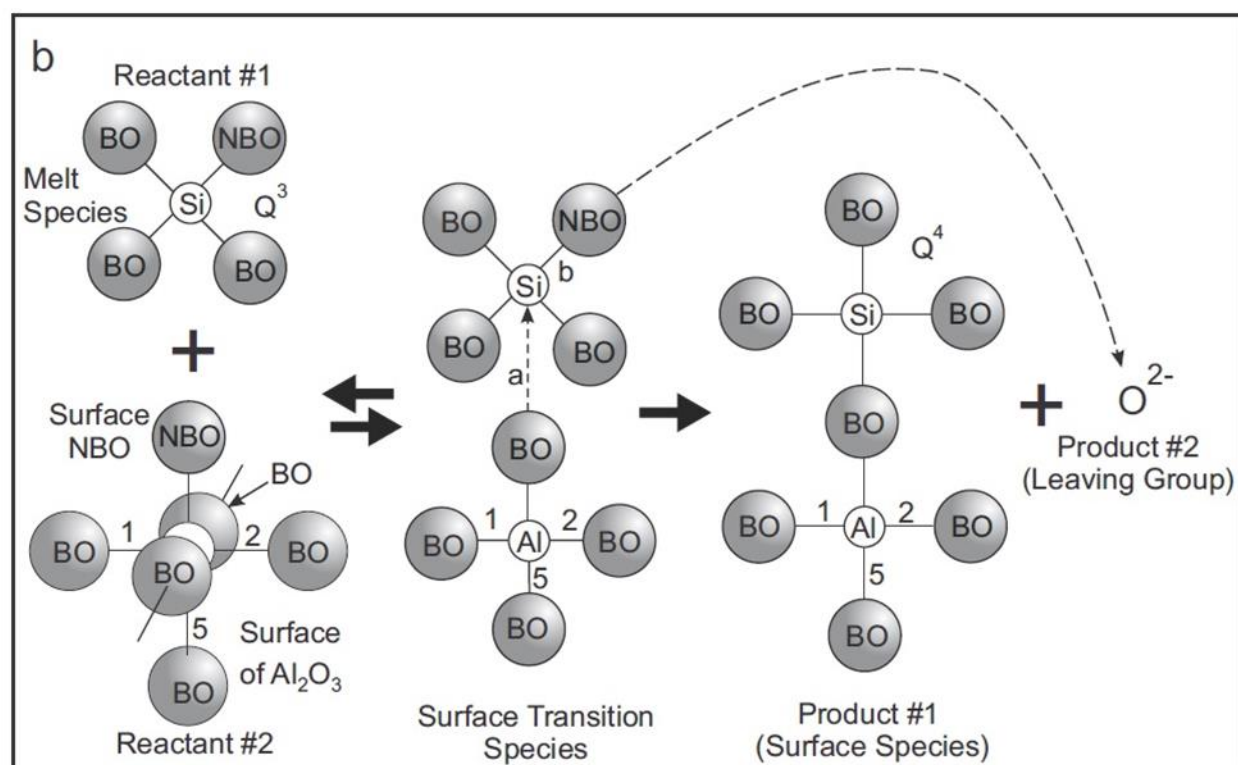
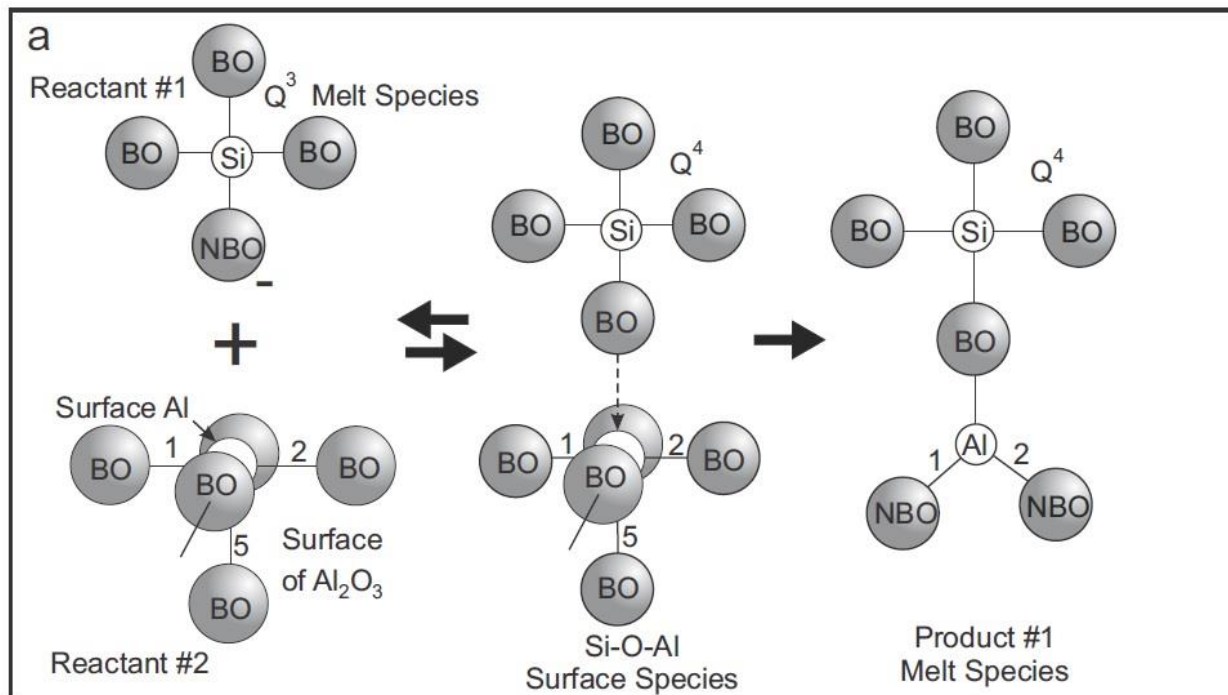


Figure 4.4: Schematic diagram showing the reaction between a  $Q^3$  species of the melt and under-coordinated  $Al^V$  and O atoms at the  $Al_2O_3$  surface. Surface Al sites are strong Lewis acids and surface O sites are strong Lewis bases. (a) illustrates the reaction of a  $Q^3$  melt species (Reactant #1) with a surface  $Al^V$  atom (Reactant #2) to produce a Si-O-Al species attached to the  $Al_2O_3$  surface. Three Al-O bonds numbered 1, 2 and 5 are labelled. Bonds 3 and 4 are directed along the x-axis and are not shown. (b) illustrates the reaction between a  $Q^3$  species of the melt (Reactant #1) and a surface NBO species (Reactant #2). A surface transition species containing  $Si^V$  is produced. The reactant NBO becomes a BO in the transition species. The transition species may decompose to either the original reactants (double arrow) or to a surface Si-O-Al species and a  $Q^2$  melt species (single arrow). Detachment of the surface species produces a Si-O-Al melt species.

## 4.5. REACTIONS AT THE MELT- $\text{Al}_2\text{O}_3$ INTERFACE AND IN MELTS

In a K-disilicate melt,  $\text{Al}_2\text{O}_3$  will dissolve congruently (i.e., directly or homogeneously) at 200-250K above the liquidus, provided that no more than ~6 mol% is dissolved (Schairer and Bowen, 1955; Kim et al., 2018). Incongruent dissolution occurs in instances where greater amounts of  $\text{Al}_2\text{O}_3$  are dissolved (e.g., Oishi et al., 1965; Bates, 1987; Zhang et al., 2000; Shaw et al., 2018). The experiments on the Ca-Al-Si-O system conducted by Shaw et al. (2018) provide insight into way in which  $\text{Al}_2\text{O}_3$  dissolves in silicate melts. They observed that dissolution rates during the first ~30 minutes of melting were controlled by the reactions which occur at the melt- $\text{Al}_2\text{O}_3$  interface, after which time the dissolution rates were controlled by diffusion through the melt. The dissolution of  $\text{Al}_2\text{O}_3$  in silicate melts is rapid compared with diffusion-controlled dissolution.

Understanding the state of the surface of crystalline  $\text{Al}_2\text{O}_3$  provides insight into its dissolution. Digne et al. (2004) identified six reactive Lewis acidic sites (under-coordinated surface Al atoms) and Lewis basic sites (under-coordinated surface O atoms) from density functional theoretical studies on the (100), (110) and (111) surfaces. The most acidic of the Lewis acid sites were the surface  $\text{Al}^{\text{III}}$ ,  $\text{Al}^{\text{IV}}$  and  $\text{Al}^{\text{V}}$  sites. A highly stylized representation of  $\text{Al}^{\text{V}}$  and O atoms at the surface of  $\text{Al}_2\text{O}_3$  is presented in Figure 4.4.

### 4.5.1. Al (Lewis Acid) surface sites

Reaction 4.1 produces the strong Lewis base  $\text{Si-NBO}^-$  through thermal agitation in high temperature alkali silicate melts (e.g., Nesbitt et al., 2017a; Nesbitt et al., 2017b; Nesbitt et al., 2020). According to the measurements of Maekawa et al. (1991), K-disilicate melts contain ~86 mol%  $\text{Q}^3$  species where  $\text{Si-NBO}^-$  mostly resides. Figure 4.4a shows  $\text{Si-NBO}^-$  attacking acidic Al sites at the  $\text{Al}_2\text{O}_3$  surface. In a successful attack,  $\text{NBO}^-$  is consumed to produce a BO Si-O-Al moiety attached to the surface of the  $\text{Al}_2\text{O}_3$  solid. As a result, the reactant  $\text{Q}^3$  becomes a  $\text{Q}^4$  species which is part of the Si-O-Al surface species. Peak B of Fig. 4.2 arises in part due to this process. The surface species' lifetime is unknown, and it may decompose into the original reactants or detach from the surface to produce a Si-O-Al melt species. The latter process requires some Al-O bonds of the solid to be ruptured. Fig. 4.4a illustrates this. Originally the surface Al atom was five-fold coordinated, but detachment causes only bonds 1 and 2 to remain

intact. The result is a Si-O-Al melt species that contains an under-coordinated Al<sup>III</sup> atom (Fig. 4.4a, product #1).

When the Si-O-Al surface species is formed, electron densities within the near surface should be perturbed. These perturbations likely weaken some of the Al-O bonds that bind Al to the bulk solid. If weakened sufficiently, surface Al and possibly some O atoms will be removed and incorporated into the bulk melt. This process will create Si-O-Al melt species (Fig. 4.4a, product #1). Some O atoms bonded to the surface Al atom may remain with the solid when the Al atom is detached causing a decrease in the coordination number of the Al atom. Figure 4.4a illustrates this concept. A surface Al atom is bonded to 5 O atoms (reactant #2) but with detachment from the surface some O atoms remain, and the coordination number of the Al atom is reduced to 3 (product #1).

#### 4.5.2. Reactions in melts

Upon detachment from the solid surface, Al atoms may not be 4-fold coordinated and so reactions within the melt must convert them to 4-fold coordination. In an instance where an Al atom detaches to produce a 3-fold coordinated Al melt species (such as in Fig. 4.4a, product #1), it can be converted to 4-fold coordination by the reaction shown in Figure 4.5. In Figure 4.5, the NBO of a Q<sup>3</sup> species (labelled reactant #1) attacks the Al<sup>III</sup> centre which forms a Si-O-Al bond and produces an Al-centred tetrahedron bonded to two BOs and two NBOs (labelled product). This reaction converts an NBO to a BO. There may be other reactions which occur that depend on the coordination number of the detached Al atom.

Figure 4.5 shows an Al<sup>IV</sup> product species which incorporates two NBOs produced by Al-O bond rupture during detachment from the Al<sub>2</sub>O<sub>3</sub> surface. In Figure 4.1, the BEs of Peak A indicate that Al is only bonded to BOs. Thus, the Al tetrahedra must undergo NBO-to-BO conversion in the melt for the Al atom to acquire four BOs such as the conversion illustrated in Figure 4.5. Greater electron density will be present on O atoms bonded to Si than on ones bonded to Al since Si is more electronegative than Al. Therefore, the electron densities on NBO of Si-NBO will be greater than on NBO of Al-NBO. This makes the NBO of the Al-NBO moiety the stronger nucleophile and more reactive towards electrophiles such as the Si centres of tetrahedra. Figure 4.6 illustrates a transition species that is produced from successful nucleophilic attack of the Al-

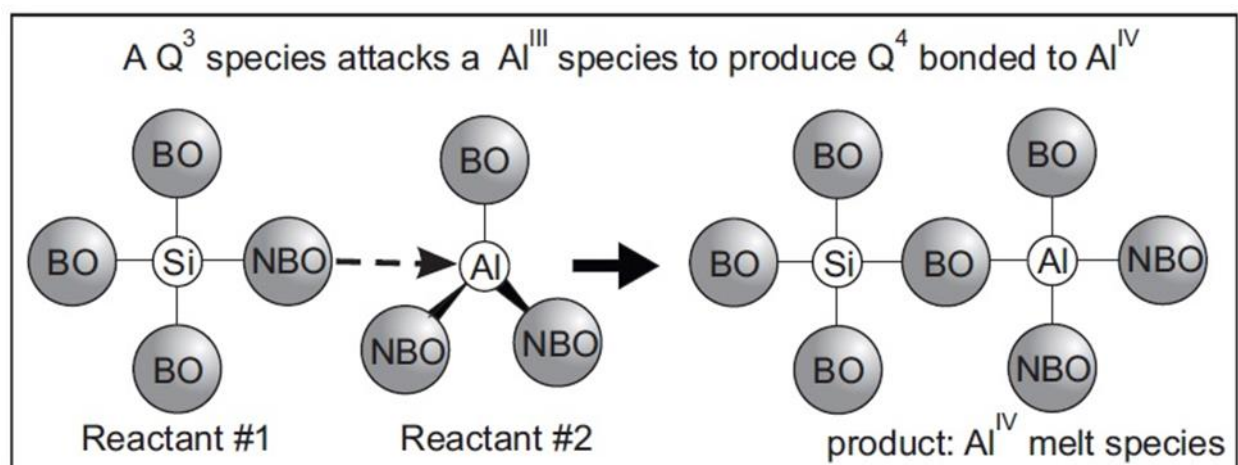


Figure 4.5: The conversion of an  $Al^{III}$  melt species (Reactant #2) to an  $Al^{IV}$  species by reaction with a  $Q^3$  species bearing an  $NBO^-$  (Reactant #1). The  $NBO^-$  is converted to  $BO$  by the reaction, which increases the number of  $BO$ s bonded to the  $Al$  moiety by one. The reaction occurs in the melt.

NBO moiety (reactant #1) on a  $Q^3$  species (bonded to a second  $Q^3$ ). This is an  $S_N$  reaction (Nesbitt et al., 2021). According to transition state theory, the transition species may decompose to the original reactants (double arrow of Fig. 4.6) or decompose to new products (single arrow of Fig. 4.6). The new products will be an Al-O-Si melt species where the number of BO bonded to the Al tetrahedron has increased by one. Another reaction would produce an Al tetrahedron where all the O atoms are BOs. This explains the process that results in Peak A of Figure 4.1 It is possible that some Al may not be associated with K (i.e., some Al could be in octahedral coordination and would not require charge compensation).

Figure 4.6 also indicates that a  $Q^2$  species is produced as a leaving product in the process described above. The abundance of  $Q^2$  species should increase with the conversion of Al-NBOs to Al-BOs and thus should increase with Al dissolution. The results of Mysen (1990, his Fig 7) confirm this prediction. The Raman spectra of Mysen (1990) indicate that the addition of Al to alkali tetrasilicate melts increases the spectral intensity at  $\sim 950\text{ cm}^{-1}$  which is the same frequency as the  $Q^2$  symmetric stretch (McMillan, 1984). The Raman spectroscopic results are explained by the conversion of NBOs to BOs on Al tetrahedral melt species.

## 4.6. DISCUSSION

### 4.6.1. Stoichiometric and elementary reactions

Reaction 4.3 is a stoichiometric reaction, and it incorporates at least three elementary reactions (chemical reactions with single reaction steps and single transition states). At the melt-solid interface, one reaction involves surface Lewis acidic (Al) sites, and one involves surface Lewis basic (NBO) sites. Elementary reactions also occur within the melt to produce tetrahedrally coordinated Al bonded to 4 BOs. It is likely that the reactions within the melt proceed via  $S_N$  reaction mechanisms where transition species (activated complex) are formed in which Si is five-fold coordinated (Frost and Pearson, 1961; Laidler, 1965; Farnan and Stebbins, 1994; Atkins, 1998; Laidler, 1998; Nesbitt et al., 2017c; Nesbitt et al., 2020). There is also the possibility that  $S_N$  reaction mechanisms involve Al melt species where transition species contain  $Al^V$ . The presence of  $Al^V$  in  $Na_3AlSi_7O_{17}$  glass at  $\sim 1\%$  of dissolved Al supports this claim (Allwardt et al., 2005; Florian et al., 2018). To better understand the elementary reactions and their relationship

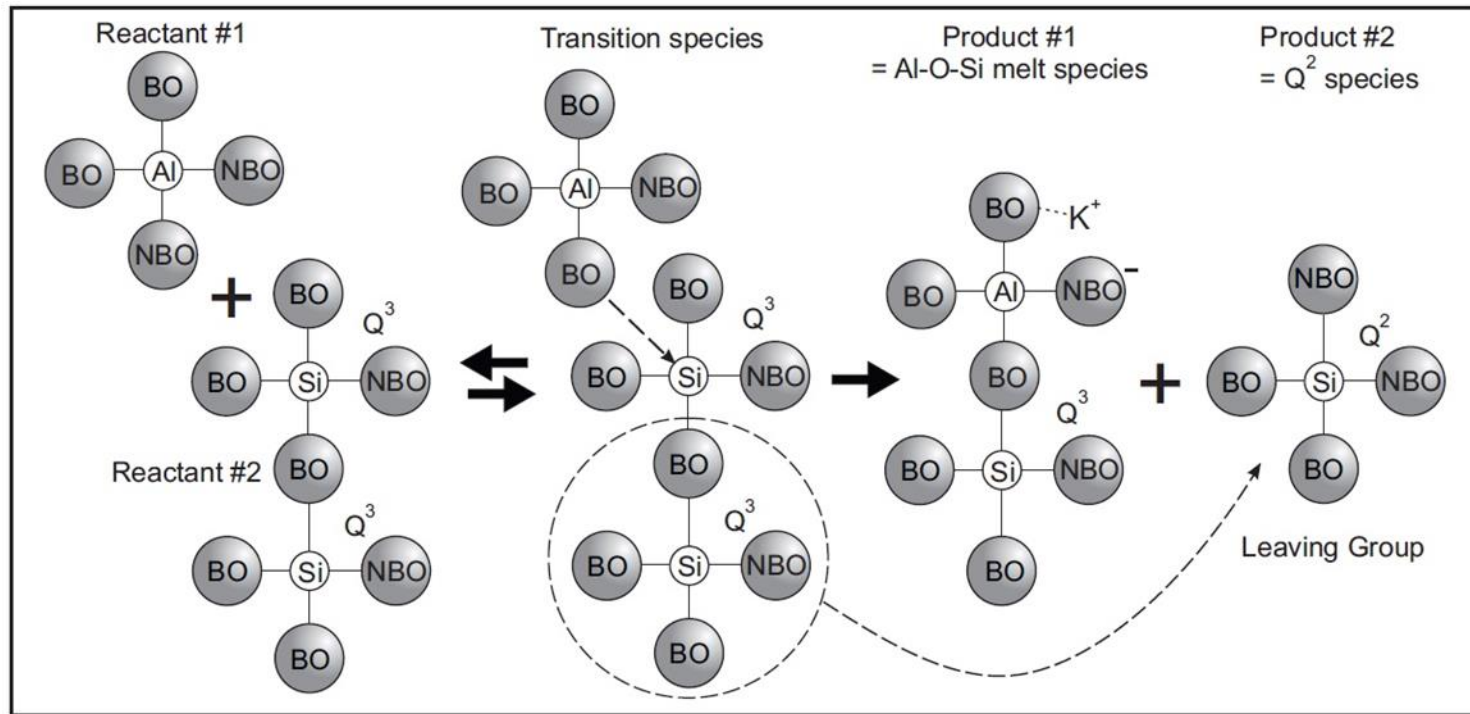


Figure 4.6: Schematic showing the replacement of NBOs for BOs on the aluminate species by attack of a  $Q^3$  species containing an NBO. The NBO is converted to BO with formation of the transition species. With successful reaction, the number of BOs on the product moiety ( $AlO_4$ ) increases by one. When the reaction is repeated, it may yield an  $AlO_4$  moiety consisting of only BOs. The reaction follows a  $S_N$  reaction mechanism with the transition species in which Al is five-fold coordinated.

to the stoichiometric reaction (Reaction 4.3), kinetic studies, molecular dynamic simulations and density functional theoretical calculations are needed.

From the O 1s XPS experimental results and the oxygen mass balances, it is clear that the Al of  $\text{KAlO}_2$  is bonded primarily to BOs (Fig. 4.2b, Peak A) and yet the  $\text{KAlO}_2$  species may be more complex than presented here. Aluminate tetrahedra incorporating Al-NBO moieties have been detected in Na and Ca peralkaline melts, albeit with greater Al contents than the ones studied here (Mysen and Toplis, 2007). The extent to which the observations of Mysen and Toplis (2007) apply to K-silicate melts is unknown, as K-Al-O interactions are stronger than Na-Al-O or Ca-Al-O interactions (Navrotsky et al., 1985; Wilding and Navrotsky, 1998).

#### 4.6.2. Stability of Al-bearing melts

From a simplistic perspective, Al dissolution should decrease the stability of silicate melts because Al-O bonds are weaker than Si-O bonds (Speight, 2005). However, other reactions mitigate this effect. In Reaction 4.3, the reactant  $\text{Q}^3$  species is consumed to produce a  $\text{Q}^4$  species and  $\text{KAlO}_2$  species. The  $\text{Q}^3$  species contains a Si-NBO bond which is the weakest of the Si-BO, Al-BO and Si-NBO bonds (Speight, 2005, Fig. 2), thus the enthalpy of formation of the melt should decrease, making the melt more stable as  $\text{Q}^3$  is consumed and  $\text{Q}^4$  is produced. In addition, K sequestration by Al to produce  $\text{KAlO}_2$  species decreases the NBO content of the melt. The introduction of Al via Reaction 4.3 results in the Al-bearing melt being more stable than the binary K-disilicate melt. This stability is due to the formation of Al melt species and the effects of Reaction 4.3. Based on this observation it can be concluded that Al-rich melts are more stable in natural environments than binary silicate melts with little or no Al. Without the stabilizing effects of Si-NBO consumption and Si-BO production, natural melts would probably be less aluminous than observed. Additionally, the composition of the crust and its evolution would be different from what it is at present.

The dissolution of Al affects the reactivity (kinetics) of melts towards reagents. Nesbitt et al. (2017d) showed that in alkali silicate glasses the O 2p valence band contributions to BO located 2-6 eV lower in the valence band (higher BE) than the O 2p NBO contributions. A consequence of this is that the O 2p BO orbitals are less energetic than the O 2p NBO orbitals. The O 2p NBO orbitals are among the highest energy orbitals of the valence band occupying molecular



orbitals. The conversion of NBOs to BOs via Reaction 4.3 decreases the electron density at the top of the valence band and diminishes the reactivity of Al-bearing melts relative to those with no Al.

#### 4.7. CONCLUSIONS

From high resolution O 1s XPS spectra it was determined that NBO decreases and BO increases in a manner directly proportional to the amount of Al<sub>2</sub>O<sub>3</sub> dissolved (up to 3 mol% in this study) in K-disilicate melts. With dissolution of Al<sub>2</sub>O<sub>3</sub>, two fully polymerized melt species are formed, Q<sup>4</sup> and KAlO<sub>2</sub>, where Si and Al are only bonded to BO atoms. By fitting the O 1s XPS spectra, proportions of NBO and BO in the glass were obtained from which the stoichiometric reaction by which Al<sub>2</sub>O<sub>3</sub> dissolves in the melt was determined (Reaction 4.3). Reaction 4.3 contains many elementary reactions. Two of these reactions are surface reactions that occur at the melt-Al<sub>2</sub>O<sub>3</sub> solid interface. Other elementary reactions occur in the melt after Al is detached from the surface. The primary method of Al<sub>2</sub>O<sub>3</sub> dissolution is probably through the attack of the nucleophile Si-NBO<sup>-</sup> (Lewis base) on Al (Lewis acid) centres of the Al<sub>2</sub>O<sub>3</sub> surface. As Si-O-Al bonds form at the surface, attacking NBO<sup>-</sup> will be converted to BO and a Q<sup>3</sup> to a Q<sup>4</sup> species. This process may also weaken Al-O-Al bonds within the bulk solid, causing Al surface atoms to detach and be taken into the melt. Although the coordination numbers of Al atoms produced by dissolution may vary and although Al atoms may be bonded to NBO atoms, reactions to form tetrahedrally coordinated Al bonded only to BO (e.g., KAlO<sub>2</sub>) must occur within the melt. These reactions likely proceed via a S<sub>N</sub> reaction mechanism. To better understand these types of reactions, further experimental studies and theoretical and molecular dynamic simulations are needed.

The dissolution of Al<sub>2</sub>O<sub>3</sub> in K-disilicate melts acts to stabilize the melts by eliminating Si-NBO-K moieties and in turn forming Si-BO and Al-BO moieties. The stabilizing effects of aluminosilicate melts contributes to their being the dominant melts in the crust and upper mantle. In the absence of this stabilization, the crust and its evolution would be different from what is observed at present.

#### 4.8. REFERENCES

Allwardt, J.R., Poe, B.T., and Stebbins, J.F., (2005) The effect of fictive temperature on Al

- coordination in high-pressure (10 GPa) sodium aluminosilicate glasses. *American Mineralogist* **90**, 1453-1457.
- Atkins, P.W., (1998) *Physical Chemistry* (6th ed.), Oxford Univ. Press, Oxford, 1014 p.
- Bancroft, G.M., Nesbitt, H.W., Ho, R., Shaw, D.M., Tse, J.S., and Biesinger, M.C., (2009) Toward a comprehensive understanding of solid-state core-level XPS linewidths: Experimental and theoretical studies on the Si 2p and O 1s linewidths in silicates. *Physical Review B* **80**, 075405-1-13.
- Barr, T.L., (1991) Recent advances in x-ray photoelectron spectroscopy studies of oxides. *Journal of Vacuum Science and Technology A* **9**, 1793-1805.
- Bates, J.L., (1987) Heterogeneous dissolution of refractory oxides in molten calcium-aluminum silicate. *Journal of the American Ceramic Society* **70**, C-55 – C-57.
- Brückner, R., Chun, H.-U., Goretzki, H., and Sammet, M., (1980) XPS measurements and structural aspects of silicate and phosphate glasses. *Journal of Non-Crystalline Solids* **42**, 49-60.
- Dalby, K.N. Nesbitt, H.W. Zakaznova-Herzog, V.P., and King, P.L., (2007) Resolution of bridging oxygen signals from O 1s spectra of silicate glasses using XPS: Implications for O and Si speciation. *Geochimica et Cosmochimica Acta* **71**, 4297-4313.
- Digne, M., Sautet, P., Raybaud, P., Euzen, P., and Toulhoat, H., (2004) Use of DFT to achieve a rational understanding of acid–basic properties of  $\gamma$ -alumina surfaces. *Journal of Catalysis* **226**, 54-68.
- Dubinsky, E., and Stebbins, J.F., (2006) Quench rate and temperature effects on framework ordering in aluminosilicate melts. *American Mineralogist* **91**, 753-761.
- Farnan, I., and Stebbins, J.F., (1994) The nature of the glass transition in a silica-rich oxide melt. *Science* **265**, 1206-1209.
- Florian, P., Novikov, A., Drewitt, J.W.E., Hennet, L., Sarou-Kanian, V., Massiot, D., Fischer, H.E., and Neuville, D.R., (2018) Structure and dynamics of high-temperature strontium aluminosilicate melts. *Physical Chemistry Chemical Physics* **20**, 27865-27877.
- Frost, A.A., and Pearson, R.G., (1961) *Kinetics and Mechanism* (2nd ed.), John Wiley and Sons, Inc. New York, 405p.
- Hesse, R., Streubel, P., and Szargan, R., (2007) Product or sum: comparative tests of Voigt, and product or sum of Gaussian and Lorentzian functions in the fitting of synthetic Voigt

- based X-ray photoelectron spectra. *Surface and Interface Analysis* **39**, 381-391.
- House, J. E., (1997) Principles of Chemical Kinetics. Wm. C. Brown Publishing, 244p.
- Kaduk, J.A., and Pei, S., (1995) The crystal structure of sodium aluminate,  $\text{NaAlO}_2 \cdot 5/4\text{H}_2\text{O}$ , and its dehydration product. *Journal of Solid State Chemistry* **115**, 126-139.
- Kim, D.-G., Konar, B., and Jung, I.-H., (2018) Thermodynamic optimization of the  $\text{K}_2\text{O}-\text{Al}_2\text{O}_3-\text{SiO}_2$  system. *Ceramics International* **44**, 16712-16724.
- Laidler, K.J., (1965) Chemical Kinetics. McGraw-Hill, New York, 566 p.
- Laidler, K.J., (1988) Just what is a transition state. *Journal of Chemical Education* **65**, 540-542.
- Lasaga, A.C., and Gibbs, G.V., (1990) Ab-initio quantum mechanical calculations of water-rock interactions: adsorption and hydrolysis reactions. *American Journal of Science* **290**, 263-295.
- MacDonald, W.M., and Anderson, A.C., (1985) Low-temperature behavior of potassium and sodium silicate glasses. *Physical Review B* **31**, 1090-1101.
- Maekawa, H., Maekawa, T., Kawamura, K., and Yokokawa, T., (1991) The structural groups of alkali silicate glasses determined from  $^{29}\text{Si}$  MAS-NMR. *Journal of Non-Crystalline Solids* **127**, 53-64.
- McMillan, P., (1984) Structural studies of silicate glasses and melts – applications and limitations of Raman spectroscopy. *American Mineralogist* **69**, 622-644.
- Miura, Y., Matsumoto, S., Nanba, T., and Akazawa, T., (2000) X-ray photoelectron spectroscopy of sodium aluminosilicate glasses. *Physics and Chemistry of Glasses* **41**, 24-31.
- Monaghan, B.J., Nightingale, S.A., Chen, L., and Brooks, G.A., (2004) The dissolution behaviour of selected oxides in  $\text{CaO}-\text{SiO}_2-\text{Al}_2\text{O}_3$  slags. VII International Conference on Molten Slags Fluxes and Salts, South African Institute of Mining and Metallurgy 585-594.
- Morishita, M., Navrotsky, A., and Wilding, M.C., (2004) Direct measurement of relative partial molar enthalpy of  $\text{SiO}_2$  in  $\text{SiO}_2-\text{M}_2\text{O}$  ( $\text{M}=\text{Li}, \text{Na}, \text{K}, \text{Cs}$ ) binary and  $\text{SiO}_2-\text{CaO}-\text{Al}_2\text{O}_3$  ternary melts. *Journal of the American Ceramic Society* **87**, 1550-1555.
- Mysen, B.O., (1990) Role of Al in depolymerized, peralkaline aluminosilicate melts in the systems  $\text{Li}_2\text{O}-\text{Al}_2\text{O}_3-\text{SiO}_2$ ,  $\text{Na}_2\text{O}-\text{Al}_2\text{O}_3-\text{SiO}_2$ , and  $\text{K}_2\text{O}-\text{Al}_2\text{O}_3-\text{SiO}_2$ . *American Mineralogist* **75**, 120-134.
- Mysen, B. O., and Richet, P., (2005) Silicate Glasses and Melts: Properties and Structure.

- Elsevier, Amsterdam, 544 p.
- Mysen, B.O., and Toplis, M., (2007) Structural behavior of  $\text{Al}^{3+}$  in peralkaline, metaluminous, and peraluminous silicate melts and glasses at ambient pressure. *American Mineralogist* **92**, 933-946.
- Mysen, B.O., Lucier, A., and Cody, G.D., (2003) The structural behavior of  $\text{Al}^{3+}$  in peralkaline melts and glasses in the system  $\text{Na}_2\text{O}-\text{Al}_2\text{O}_3-\text{SiO}_2$ . *American Mineralogist* **88**, 1668-1678.
- Navrotsky, A., Peraudeau, G., McMillan, P., and Coutures, J-P., (1982) A thermochemical study of glasses and crystals along the joins silica-calcium aluminate and silica-sodium aluminate. *Geochimica et Cosmochimica Acta*. **46**, 2039-2047.
- Navrotsky, A., Geisinger, K.L., McMillan, P., and Gibbs, G.V., (1985) The Tetrahedral Framework in Glasses and Melts-Inferences from Molecular Orbital Calculations and Implications for Structure, Thermodynamics, and Physical Properties. *Physics and Chemistry of Minerals* **11**, 284-298.
- Nesbitt, H.W., Bancroft, G.M., Davidson, R., McIntyre, N.S., and Pratt, A.R., (2004) Minimum XPS core-level line widths of insulators, including silicate minerals. *American Mineralogist* **89**, 878–882.
- Nesbitt, H.W., Bancroft, G.M., Henderson, G.S., Ho, R., Dalby, K.N., Huang, Y., and Yan, Z., (2011) Bridging, non-bridging and free ( $\text{O}^{2-}$ ) oxygen in  $\text{Na}_2\text{O}-\text{SiO}_2$  glasses: An X-ray Photoelectron Spectroscopic (XPS) and Nuclear Magnetic Resonance (NMR) study. *Journal of Non-Crystalline Solids* **357**, 170–180.
- Nesbitt, H.W., and Bancroft, G.M., (2014). High resolution core- and valence-level XPS studies of the properties (structure, chemical and bonding) of silicate minerals and glasses: Chapter 7. (Eds. G.S. Henderson, D.R. Neuville and R.T. Downs), Spectroscopic Methods. Reviews in Mineralogy and Geochemistry **78**, pp. 271–330.
- Nesbitt, H.W., Henderson, G.S., Bancroft, G.M., and Ho, R., (2015) Experimental evidence for Na coordination to bridging oxygen in Na-silicate glasses: Implications for spectroscopic studies and for the modified random network model. *Journal of Non-Crystalline Solids* **409**, 139-148.
- Nesbitt, H.W., Bancroft, G.M., Henderson, G.S., Richet, P., and O’Shaughnessy, C., (2017a)

- Melting, crystallization, and the glass transition: Toward a unified description for silicate phase transitions. *American Mineralogist* **102**, 412-420.
- Nesbitt, H.W., Cormack, A.N., and Henderson, G.S., (2017b) Defect contributions to the heat capacities and stabilities of some chain, ring, and sheet silicates, with implications for mantle minerals. *American Mineralogist* **102**, 2220-2229.
- Nesbitt, H.W., Henderson, G.S., Bancroft, G.M., and O'Shaughnessy, C., (2017c) Electron densities over Si and O atoms of tetrahedra and their impact on Raman stretching frequencies and Si-NBO force constants. *Chemical Geology* **461**, 65-74.
- Nesbitt, H.W., Bancroft, G.M., and Ho, R., (2017d) XPS valence band study of Na-silicate glasses: energetics and reactivity. *Surface and Interface Analysis* **49**, 1298-1308.
- Nesbitt, H.W., Henderson, G.S., Bancroft, G.M., Sawyer, R., and Secco, R.A., (2017e) Bridging oxygen speciation and free oxygen (O<sup>2-</sup>) in K-silicate glasses: Implications for spectroscopic studies and glass structure. *Journal of Non-Crystalline Solids* **461**, 13-22.
- Nesbitt, H.W., Bancroft, G.M., and Henderson, G.S., (2020) Polymerization during melting of ortho- and meta-silicates: Effects on Q-species stability, heats of fusion, and redox state of mid-ocean range basalts (MORBs). *American Mineralogist* **105**, 716-726.
- Nesbitt, H.W., Bancroft, G.M., and Henderson, G.S., (2021) Nucleophilic substitution reaction mechanisms: An atomic-molecular perspective on chemical speciation and transport properties in silicate melts. *Chemical Geology* **555**, 119818.
- Nesbitt, H.W., and Young, G.M., (1984) Prediction of some weathering trends of plutonic and volcanic rocks based on thermodynamic and kinetic considerations. *Geochimica et Cosmochimica Acta* **48**, 1523-1534.
- Nsimama, P.D., Ntwaeaborwa, O.M., and Swart, H.C., (2010) Auger electron/X-ray photoelectron and cathodoluminescent spectroscopic studies of pulsed laser ablated SrAl<sub>2</sub>O<sub>4</sub>:Eu<sup>2+</sup>,Dy<sup>3+</sup> thin films. *Applied Surface Science* **257**, 512-517.
- Ohuchi, F.S., Ghose, S., Engelhard, M.H., and Baer, D.R., (2006) Chemical bonding and electronic structures of the Al<sub>2</sub>SiO<sub>5</sub> polymorphs, andalusite, sillimanite, and kyanite: X-ray photoelectron- and electron energy loss spectroscopy studies. *American Mineralogist* **91**, 740-746.
- Oishi, Y., Cooper, A.R., and Kingery, W.D., (1965) Dissolution in Ceramic Systems: 111,

- Boundary Layer Concentration Gradients. *Journal of the American Ceramic Society* **48**, 88-95.
- Richet, P., Mysen, B.O., and Andraut, D., (1996) Melting and premelting of silicates, Raman spectroscopy and X-ray diffraction of  $\text{Li}_2\text{SiO}_3$  and  $\text{Na}_2\text{SiO}_3$ . *Physics and Chemistry of Minerals* **23**, 157–172.
- Sawyer, R., Nesbitt, H.W., and Secco, R.A., (2012) High resolution X-ray Photoelectron Spectroscopy (XPS) study of  $\text{K}_2\text{O}$ – $\text{SiO}_2$  glasses: Evidence for three types of O and at least two types of Si. *Journal of Non-Crystalline Solids* **358**, 290-302.
- Sawyer, R., Nesbitt, H.W., Bancroft, G.M., Thibault, Y., and Secco, R.A., (2015) Spectroscopic studies of oxygen speciation in potassium silicate glasses and melts. *Canadian Journal of Chemistry* **93**, 60–73.
- Schairer, J.F., and Bowen, N.L., (1955) The system potassium oxide-alumina-silica, *American Journal of Science* **253**, 681-746.
- Schwerdtfeger, K., (1966) Dissolution of solid oxides in oxide melts. The rate of dissolution of solid silica in  $\text{Na}_2\text{O}$ - $\text{SiO}_2$  and  $\text{K}_2\text{O}$ - $\text{SiO}_2$  melts. *Journal of Physical Chemistry* **70**, 2131-2136.
- Shannon, R.D., (1976) Revised effective ionic radii and systematic studies of interatomic distances in halides and chalcogenides. *Acta Crystallographica* **A32**, 751-767.
- Shaw, C.S., (2004) Mechanisms and rates of quartz dissolution in melts in the CMAS ( $\text{CaO}$ – $\text{MgO}$ – $\text{Al}_2\text{O}_3$ – $\text{SiO}_2$ ) system. *Contributions to Mineralogy and Petrology* **148**, 180-200.
- Shaw, C.S. Klausen, K.B., and Mao, H., (2018) Kinetics of dissolution of sapphire in melts in the  $\text{CaO}$ – $\text{Al}_2\text{O}_3$ – $\text{SiO}_2$  system. *Geochimica et Cosmochimica Acta* **229**, 129-146.
- Shaw D.M., Reilly G.A., Muysson J.R., Pattenden G.E., and Campbell, F.E., (1967) An estimate of the chemical composition of the Canadian Precambrian Shield. *Canadian Journal of Earth Sciences* **4**, 829-853.
- Shirley, D.A., (1972) High resolution X-ray photoemission spectrum of the valence bands of Au. *Physical Review B* **5**, 4709–4714.
- Speight, J.G., (2005) Lange’s Handbook of Chemistry 70th Anniversary Edition, Table 4.11, 4.41–4.51. McGraw Hill, New York.
- Taylor S.R., and McLennan S.M., (1981) The composition and evolution of the continental crust:

- rare earth element evidence from sedimentary rocks. *Philosophical Transactions of the Royal Society of London* **A301**, 381-399.
- Wedepohl, K. H., (1969) The handbook of geochemistry. v. 1, (ed. K. H. Wedepohl), Springer-Verlag, Germany, pp. 247-248.
- Wilding, M.C., and Navrotsky, A., (1998) The dissolution of silica and alumina in silicate melts: in situ high temperature calorimetric studies. *Neues Jahrbuch für Mineralogie – Abhandlungen* **172**, 177-201.
- Zhang, S., Rezaie, H.R., Sarpoolaky, H., and Lee, W.E., (2000) Alumina dissolution into silicate slag. *Journal of the American Ceramic Society* **83**, 897-903.

## Chapter 5

### 5.0. CONCLUSIONS

#### 5.1. Potassium Silicate Glasses

This thesis presents the first detailed study of the potassium silicate glass system using X-ray Photoelectron Spectroscopy. The spectra herein are of the highest resolution so far collected. Previous XPS studies of potassium silicate glasses contained numerous issues such as poor spectral resolution (BO and NBO signals were not resolved), the inability to deal with sample charging issues (e.g., large peak linewidths), and not accounting for sample damage over time from the X-ray source. The results presented here take into consideration all the above-mentioned issues.

The NBO peaks have FWHM which range from 1.16 eV to 1.54 eV. The NBO peak incorporates the NBO and O<sup>2-</sup> contributions, although the latter is a very small percentage of the total peak (less than ~1-2%). The BO peaks incorporate numerous BO contributions one from each of the Q<sup>n</sup> species in the glass. They have FWHM which range from 1.35 eV to 1.53 eV. These values are comparable to the O 1s spectra of quartz and vitreous silica which are comprised of a singular BO contribution with an FWHM of ~1.25 eV. These results provide further confirmation that charge broadening does not contribute to the linewidths of these samples. The linewidths in this study represent an improvement in collecting highly resolved XPS spectra compared to earlier studies mentioned with O 1s linewidths of about 2 eV.

The study has evaluated the damage caused by the X-ray beam to the samples over time. The damage presents itself in the form of alkali migration with the resulting changes to the intensity of the O 1s BO signal. To account for beam damage, several O 1s spectra were taken over the course of the analytical cycle (~800 minutes). BO abundances were measured for all O 1s spectra and then plotted as BO% vs time of exposure to the X-ray beam. The results were fit with a quadratic least-squares equation and extrapolated back to time zero. The extrapolated values represent the BO values prior to exposure to the X-ray beam.



It has been shown that XPS presents a viable alternative to  $O^{17}$  NMR for studying silicate glasses and can also be used as a complementary analysis technique. In the K-silicate system, the BO and NBO contributions often overlap in the  $O^{17}$  NMR spectra and the number of BO contributions to the spectra must be known before fitting for the spectra to obtain reasonable fits. A strength of XPS is that it can provide O 1s spectra with resolution equivalent to the best resolved  $O^{17}$  NMR spectra. Well defined and separated BO and NBO contributions are apparent in Na and K silicate glasses. The BO and NBO peaks are easily identifiable by their binding energies, which are unique. By comparing BO peak linewidths to those of quartz and vitreous silica, additional contributions to the BO peak can be inferred.

Experimentally derived BO abundances were found to be greater than predicted by the Continuous Random Network (CRN) model where:



is assumed to go to completion (where an equilibrium constant,  $K_1$ , for the reaction is infinite). Thermodynamic modeling indicated a finite equilibrium constant indicating the presence of free oxygen ( $O^{2-}$ ) in the binary system, the abundance of which increases with  $K_2O$  content. These findings created a discrepancy with previous NMR studies for the glasses with  $K_2O > 25$  mol%. The amount of  $O^{2-}$  in the  $K_2O$  glasses was greater than that in  $Na_2O$  glasses from a previous XPS study. The greater ionic radius of the K cation was suggested to create larger percolation channels as defined by Greaves et al. (1997) within the glass network and thus a more ionic environment conducive to the formation and stability of  $O^{2-}$  atoms. The breadth of the BO peak was found to be variable and wider than that of the NBO peak whose breadth remains constant. It was suggested that the greater breadth is a possible indication of two (or more) types of BO atoms, one bonded to two Si atoms only, and one bonded to two Si atoms plus a K atom.

The Si 2p peak shapes were highly variable and asymmetric. The peak shape changes considerably as a function of  $K_2O$  content, unlike the Si 2p spectra of Na-silicate glasses. Two spin-orbit split doublet peaks were fit to the Si 2p peaks of these siliceous K-silicate glass spectra and the relative intensities of the two peaks varied sympathetically with  $Q^4$  and  $Q^3$  abundances of  $Q^4$  and  $Q^3$  species obtained from NMR studies of K-silicate glasses. These results imply that XPS may be used to identify  $Q^n$  species in some circumstances where the asymmetric nature of the Si 2p peak suggests more than one contribution.

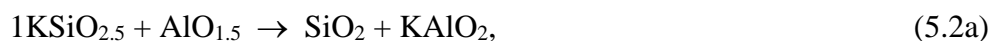
A new interpretation of the NMR data allowed for results consistent with the XPS data. Four new glasses were prepared: three with nominally 35 mol%  $K_2O$  and one with nominally 37 mol%  $K_2O$ . EPMA analysis using a defocused electron beam at 40  $\mu m$  and 8 s counting time provided the best possible conditions to obtain accurate compositions. The three nominally 35 mol% glasses were found to have compositions of 30, 32 and 32 mol % indicating that each melting of the glass sample during synthesis accounts for the loss of about 1 mol%  $K_2O$ . The results for all glasses including the ones from Chapter 2 were adjusted by 1 or 2 mol%  $K_2O$  to reflect this new uncertainty. The mol fractions of BO, NBO and  $O^{2-}$  were calculated for an equilibrium constant value of  $K_1 = 8$ . The  $O^{2-}$  estimated abundances were lower than those reported in Chapter 1 accounting for the new uncertainties. Previous NMR spectra of  $K_2O$  glasses were fit with two  $Q^2$  peaks based on the sole assumption that Reaction 5.1 goes to completion with no other theoretical or experimental evidence (Maekawa et al. 1991; Malfait et al., 2007). Here, it has been demonstrated that two  $Q^3$  peaks fit the previous NMR data and also agreed with the XPS results. Free oxygen, rather than NBO, was suggested to be the critical reactive species to convert  $CO_2$  to  $CO_3^{2-}$  in experimental and natural magmas.

## 5.2. Potassium Aluminosilicate Glasses

The dissolution of  $Al_2O_3$  into a potassium silicate melt and its incorporation into the melt structure was studied with XPS. The same degree of high resolution was achieved with these spectra as with the glass spectra from Chapters 2 and 3. This is the first instance where high resolution XPS spectra of K-aluminosilicate glasses have been presented. It was found that the FWHM of the KS glass (31 mol%  $K_2O$ , no  $Al_2O_3$ ) BO peak was 1.36 eV and increased to 1.47 eV and 1.60 eV with the additions of 1 mol% and 3 mol%  $Al_2O_3$  respectively. The NBO peak FWHM increased from 1.15 eV to 1.17 eV and 1.19 eV. This excellent resolution allowed two distinct chemical species to be identified with the use of difference spectra at  $\sim 531$  eV BE (Peak A) and  $\sim 532.8$  eV BE (Peak B) and a negative NBO peak at  $\sim 529.8$  eV BE. A sympathetic relationship between the increase in the intensities of Peaks A and B and the addition of  $Al_2O_3$  was found. The absolute difference of 0.6% between the positive BO difference spectra peaks and the negative NBO peak demonstrated that the addition of  $Al_2O_3$  results in a mol per mol conversion of NBO to BO. The FWHM of the difference spectra peaks is  $\sim 1.15$  eV which is consistent and expected of O 1s spectral peaks. These results indicate that the difference spectra

technique resulted in no distortions in the data. Peak A was shown to be indicative of a BO contribution in the form of an  $\text{AlO}_4$  framework species due to the similarities in BE with previous studies of kyanite and  $\text{SrAl}_2\text{O}_4$  and thus represents a  $\text{Q}^3$  species contribution. Peak B was identified with a  $\text{Q}^4$  species contribution due to its binding energy being similar to those of quartz and vitreous silica from previous studies.

The dissolution of  $\text{Al}_2\text{O}_3$  in K-silicate glasses results in polymerization of the melt and follows the stoichiometric reaction:



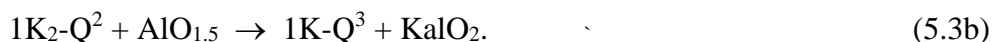
or in Q-species notation:



The reaction accounts for the production of BO at the expense of NBO, and the production of Peak A ( $\text{KAlO}_2$ ) and Peak B ( $\text{Q}^4$ ). A similar reaction may occur during  $\text{Al}_2\text{O}_3$  dissolution where the  $\text{Q}^2$  species ( $\text{K}_2\text{SiO}_3$ ) is present:

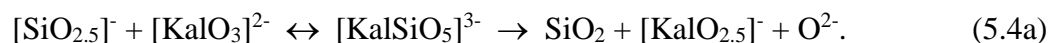


or in Q-species notation where  $\text{K}_2\text{-Q}^2$  represents  $\text{K}_2\text{SiO}_3$  and  $\text{K-Q}^3$  represents  $\text{K}_1\text{SiO}_{2.5}$ :

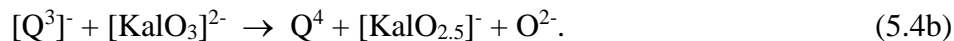


A transition reaction that occurs at the  $\text{Al}_2\text{O}_3$  surface was proposed. The reaction is responsible for converting surface Al to 4-fold coordination where it not already coordinated in that way.

The transition species is 5-fold coordinated Al which may decompose to the original components in the reaction or form a new species  $[\text{KAlO}_{2.5}]^-$  and a leaving species ( $\text{O}^{2-}$ ):



Or ignoring the transition species and writing in Q-species notation:



The  $\text{O}^{2-}$  may be consumed in depolymerization reactions or it may produce Al-NBO surface moieties by attacking and bonding to surface Lewis acid (Al) sites.

### 5.3. Future Directions and Implications

Hindsight is the product of wisdom gained in the search for truth. In few places is this more evident than at the conclusion of a thesis. There are limitations to the work presented here and, if I could go back and do things over, I would like to say I would do things slightly different. The

main limitation of this work is that it relies on a single spectroscopic technique. While I stand by my results and am confident in them, when challenging long-held assumptions concerning an idea, the onus is on the challenger to prove their case. A multi-spectroscopic approach would have greatly benefited this work. Another limitation is in the resolution of the XPS instrument. Further improvements in charge compensation methods will likely yield XPS spectra of better resolution which will in turn allow for better results to be obtained and from that more accurate and precise analyses. The constraints applied to background and peak function (i.e., Shirley background and 70% Gaussian-30% Lorentzian peak function) have been established in our laboratory as providing good fits to the spectra of silicates and sulfides (Nesbitt and Bancroft 2014). Nesbitt and Bancroft (2014) mention that the Lorentzian component creates a slight variation in linewidth but that the overall area of the peak is not affected (See Table 3 in Nesbitt and Bancroft (2014)). The approach taken in fitting the spectra in this thesis was to use as few constraints as possible in order to introduce the minimum amount of uncertainty. My reinterpretations of the NMR spectra, specifically in assigning two  $Q^3$  species to the potassium silicate glasses as a way of resolving the discrepancy with the XPS results, needs more study to be confirmed. Although I am confident in the reassignment, I would perhaps be more confident if I had used my own spectra from my own glasses. The biggest lesson to be learned is stated in Chapter 3: that good results can be obtained through careful fitting procedures and cautious interpretation free of assumptions that the results should conform to a certain model and provided the contributions to the peaks are known.

Additional studies on other alkali and alkaline earth silicate glasses with XPS will be useful in further establishing the technique as one for bulk sample analysis. Compositional analysis with XPS is possible to a certain degree of precision, but more accuracy can be obtained using the EMPA technique described in Chapter 3. The use of XPS in combination with other techniques such as NMR, Raman spectroscopy or molecular dynamic simulations for example, could lead to greater insights regarding the structural role that  $O^{2-}$  occupies in these glasses and the effects it may have on melt properties.

More study is needed with XPS concerning potassium aluminosilicate glasses. This thesis contained only an elementary study but nonetheless yielded some important results. Further modelling of the dissolution reactions of  $Al_2O_3$  into the K-silicate melt and solid surface is

required to understand the related mechanisms and identify the elementary reactions. These goals could be achieved with further XPS study utilizing the difference spectra technique that was presented in addition to molecular dynamics simulations. It would also be interesting to use XPS to study natural glasses, impact glasses, tektites, Libyan desert glass.

These results are part of an exciting debate that is ongoing within the glass community concerning free oxygen. Indeed, one of the aspects that attracted me to the study of glass and continues to sustain my fascination with the material is the lively debates that occur over the most fundamental aspects. The research I have presented is fundamental in nature but has implications for the Earth and planetary sciences. If free oxygen is the major reactive species in melts, its presence in quantities large enough to be significant could change the way we model things like volcanic eruptions and the way we consider geochemical processes that occur in melts.

#### 5.4. References

- Greaves, G. N., Smith, W., Giolotto, E., and Pantos, E., (1997) Local structure, microstructure and glass properties. *Journal of Non-Crystalline Solids* **222**, 13-24.
- Maekawa, H., Maekawa, T., Kawamura, K., and Yokokawa, T., (1991) The structural groups of alkali silicate glasses determined from  $^{29}\text{Si}$  MAS-NMR. *Journal of Non-Crystalline Solids* **127**, 53-64.
- Malfait, W. J., Halter, W. E., Morizet, Y., Meier, B. H., and Verel, R., (2007) Structural control on bulk melt properties: Single and double quantum  $^{29}\text{Si}$  NMR spectroscopy on alkali-silicate glasses. *Geochimica et Cosmochimica Acta* **71**, 6002-6018.
- Nesbitt, H.W., and Bancroft, G.M., (2014). High resolution core- and valence-level XPS studies of the properties (structure, chemical and bonding) of silicate minerals and glasses: Chapter 7. (Eds. G.S. Henderson, D.R. Neuville and R.T. Downs), *Spectroscopic Methods. Reviews in Mineralogy and Geochemistry* **78**, pp. 271–330.

## Appendix A: Calculation of $X_{BO}$ and $X_{O_2^-}$ from Q-species Abundances and from BO%

The data from previously published Raman and  $^{29}Si$  NMR spectra were used to obtain the mole fractions of BO, NBO and  $O^{2-}$  species. Fits to Raman and  $^{29}Si$  NMR spectra of silicate glasses give mole percentages of Q-species. To obtain the moles of BO ( $N_{BO}$ ) and NBO ( $N_{NBO}$ ) associated with Q-species, the following summations can be used since all BO and NBO are bonded to silicon centres:

$$N_{BO} = (4Q^4 + 3Q^3 + 2Q^2 + 1Q^1 + 0Q^0)/2, \quad (A1a)$$

and

$$N_{NBO} = (4Q^0 + 3Q^1 + 2Q^2 + 1Q^3 + 0Q^4), \quad (A1b)$$

where  $Q^n$  ( $n = 0$  to  $4$ ) represents the percentage of each Q-species determined by experiment. It is necessary to divide Equation A1a by two so that each BO atom is not counted twice.  $X_{BO}$  can then be obtained:

$$X_{BO} = N_{BO}/N_{O \text{ total}}, \quad (A2)$$

where  $N_{O \text{ total}}$  is the number of moles of oxygen per atom of silicon. As an example,  $N_{O \text{ total}} = 2.5$ , 3.0 and 4.0 for the disilicate, metasilicate and orthosilicate glass compositions respectively.

There are two ways that  $X_{O_2^-}$  can be calculated. For the first derivation,  $N_{BO}/N_{NBO}$  is

$$N_{BO}/N_{NBO} = x = [(4Q^4 + 3Q^3 + 2Q^2 + 1Q^1)/2]/(1Q^3 + 2Q^2 + 3Q^1 + 4Q^0). \quad (A3)$$

To calculate  $X_{O_2^-}$ , two mass balance equations are required. One equation shows the relationship between the moles of silicon ( $N_{Si}$ ) and the moles of BO and NBO:

$$N_{Si} = N_{BO}/2 + N_{NBO}/4. \quad (A4)$$

By substituting Equation A3 into Equation A4, rearranging and collecting terms, we obtain:

$$N_{NBO} = 4N_{Si}/(1 + 2x). \quad (A5)$$

The second mass balance equation gives the relationship between the oxygen species to  $N_{O \text{ total}}$  in the glass:

$$N_{O \text{ total}} = N_{BO} + N_{NBO} + N_{O_2^-}. \quad (A6)$$

By substituting Equation A3 for  $N_{BO}$  of Equation A6 and collecting the terms we get:

$$N_{O \text{ total}} = (1 + x)N_{NBO} + N_{O_2^-}, \quad (A7)$$

and by substituting Equation A5 for  $N_{NBO}$  in Equation A7 we obtain:

$$N_{O \text{ total}} = 4[(1+x)/(1+2x)] N_{Si} + N_{O_2^-}. \quad (A8)$$

The mole fraction of  $O^{2-}$  ( $X_{O_2}$ ) can be obtained by dividing both sides of Equation A8 by  $N_{O \text{ total}}$ :

$$X_{O_2} = 1.0 - 4[(1 + x)/(1 + 2x)] N_{Si}/N_{O \text{ total}}. \quad (\text{A9a})$$

The value for  $X_{O_2}$  must be zero or positive and a negative value means that Q-species have been assigned incorrectly. It is unknown if this constraint has been used to test Q-species assignments. When  $X_{O_2}$  is found, the mole fractions of BO( $X_{BO}$ ) and NBO( $X_{NBO}$ ) can be calculated from:

$$X_{BO} = [N_{BO}/(N_{BO} + N_{NBO})](1.0 - X_{O_2}), \quad (\text{A9b})$$

$$X_{NBO} = [N_{NBO}/(N_{BO} + N_{NBO})](1.0 - X_{O_2}). \quad (\text{A9c})$$

Although Equation A9b gives the same results as Equation A2, Equations A9b and A9c are important because they show the dependence of the mole fractions of BO and NBO on  $X_{O_2}$ .  $X_{BO}$  and  $X_{NBO}$  can be closely approximated by considering only the terms in the square brackets of Equations A9b and A9c in glasses where  $X_{SiO_2} > 0.3$  since the  $(1.0 - X_{O_2})$  is generally close to 1.0. This was used in Sawyer et al. (2012). Comparison with the results of Sawyer et al. (2012) and the ones presented here show that errors giving an overestimate of XBO can arise in glasses where  $X_{SiO_2} < 0.3$ .

There is a second method to obtain  $X_{O_2}$  where Equations A1a and A1b are substituted directly into Equation A6. We note that  $N_{O_2} = N_{O \text{ total}}X_{O_2}$  and  $N_{BO} + N_{NBO} = N_{Q \text{ total}}$  and rearranging we get:

$$N_{O \text{ total}} = N_{Q \text{ total}} + N_{O \text{ total}}X_{O_2}. \quad (\text{A10})$$

And rearranging the above and solving for  $X_{O_2}$ :

$$X_{O_2} = 1 - (N_{Q \text{ total}}/N_{O \text{ total}}). \quad (\text{A11})$$

Equations A9a and A11 are identical and can be used interchangeably given that  $N_{O \text{ total}}$  is the number of moles of oxygen per silicon atom. Equations A9a, A9b and A9c are very useful however, in that they show the dependence of the mole fractions of BO and NBO on the abundance of  $O^{2-}$  (shown in Equations A9b and A9c).

## Curriculum Vitae

**Name:** Ryan Sawyer

**Post-secondary Education and Degrees:** University of Western Ontario  
London, Ontario, Canada  
2004-2008 B.Sc. Planetary Science

The University of Western Ontario  
London, Ontario, Canada  
2008-2022 Ph.D. Geophysics (Planetary Science)

**Honours and Awards:** Misasa International Student Intern Program  
2008

Robert and Ruth Lumsden Graduate Award in Earth Sciences  
2010

Queen Elizabeth II Graduate Scholarship in Science and Technology  
2012-2013

**Related Work Experience** Teaching Assistant  
The University of Western Ontario  
2008-2013

Volunteer Researcher, Science Team  
Kepler Carbon ReCapture  
2021-Present

Application Scientist  
Sciencetech Inc.  
2022-Present

### **Publications:**

#### First Author

**Sawyer, R.**, Nesbitt, H. W., Bancroft, G. M., Secco, R. A., and Henderson, G. S., (2022)  
Congruent dissolution of  $\text{Al}_2\text{O}_3$  in a K-disilicate melt, with constraints on the reaction mechanism. *Journal of Non-Crystalline Solids* 586, 121565.

**Sawyer, R.**, Nesbitt, H.W., Bancroft, G.M, Thibault, Y., and Secco, R.A., (2015) Spectroscopic studies of oxygen speciation in potassium silicate glasses and melts. *Canadian Journal of Chemistry* 93, 60-73.

**Sawyer, R.**, Nesbitt, H.W., and Secco, R.A., (2012) High resolution X-ray Photoelectron



Spectroscopy (XPS) study of  $K_2O-SiO_2$  glasses: Evidence for three types of O and at least two types of Si. *Journal of Non-Crystalline Solids* 358, 290-302.

#### Co-Author

Nesbitt, H.W., Henderson, G.S., Bancroft, G.M., **Sawyer R.**, and Secco, R.A., (2017) Bridging Oxygen speciation and Free Oxygen ( $O_2^-$ ) in K-silicate glasses: Implications for spectroscopic studies and glass structure. *Chemical Geology* 461, 13-22.

Nesbitt, H.W., Bancroft, G.M., Henderson, G.S., **Sawyer, R.**, and Secco, R.A., (2015) Direct and indirect evidence for Free Oxygen ( $O^{2-}$ ) in MO-silicate glasses and melts (M = Mg, Ca, Pb). *American Mineralogist* 100, 2566-2578.

Nesbitt, H.W., Bancroft, G.M., Thibault, Y., **Sawyer, R.**, and Secco, R.A., (2015) Reply to the comment by Malfait on "Spectroscopic studies of oxygen speciation in potassium silicate glasses and melts". *Canadian Journal of Chemistry* 93, 581-587.

#### In Preparation

Nesbitt, H.W., **Sawyer, R.**, Bancroft, G.M., and Secco, R.A. Molecular orbital interactions at K-silicate glass surfaces resulting from reaction with gaseous HCL.

#### Conference Abstracts

**Sawyer, R.**, Nesbitt, H.W., and Secco, R.A., (2010) Evidence for Free Oxygen ( $O^{2-}$ ) in  $K_2O-SiO_2$  glasses from X-ray Photoelectron Spectroscopic (XPS) Analysis. Canadian Geophysical Union Joint Annual General Meeting with the Canadian Meteorological and Oceanographic Society. Presentation Abstract, ID 3690.

**Sawyer, R.**, Nesbitt, H.W., and Secco, R.A., (2009) The effects of composition, pressure and temperature on the structure of potassium silicate glasses. American Geophysical Union Spring Meeting. Poster Abstract, #MA73A-02.